Fumonisin B_1 aptamer optimization and progress towards mycotoxin nanoaptasensors

by

Nadine Frost

A thesis submitted to the Faculty of Graduate and Postdoctoral Affairs in partial fulfillment of the requirements for the degree of

Master of Science

in

Chemistry

Carleton University
Ottawa, Ontario

Abstract

Fumonisin B_1 (FB_1) and ochratoxin A (OTA) are agriculturally important mycotoxins that have implications in human and animal health. Aptamers are short single-stranded oligonucleotides that can be used as molecular recognition elements for the sensitive and selective detection of mycotoxins. Aptamers for FB_1 and OTA were screened using a novel DNase I footprinting assay to characterize their structure and in-solution affinity. Two minimal binding aptamers for FB_1 were identified that retain high binding affinity in solution and to a bound target. Progress was made towards fluorescence turn-on and turn-off sensors for FB_1, utilizing semiconductor quantum dots and fluorescein in conjunction with metallic- and carbon-based quenchers. A fluorescence nano-aptasensor was developed as a simple paper test, with the capacity to detect OTA with a limit of detection between 10 – 100 nM. Rapid, robust aptasensors for FB_1 and OTA have promising applications for in-field screening of mycotoxin residues on crops.

Acknowledgements

The past two years at Carleton have passed by in a flash,

Filled with long days in the lab and running with friends at the track,

I have received so much encouragement throughout this degree,

This is my chance to thank you all, as it means so much to me.

First and foremost I am in awe of my supervisor Maria,

For her unwavering confidence, boundless energy and ideas,

Thank you for being an inspiring mentor to me along the way,

I am forever grateful for everything I have learned to this day.

To the invigorating professors and staff in the Chemistry department,

Thank you for welcoming me in, and keeping my goals on target,

I would like to thank my committee members for their time and experience,

Dr. Miller, thank you for inspiring me with your knowledge and brilliance.

To my lab mates: if a day without laughter is a day wasted,

Then no days have gone by without endless entertainment,

When the science gets tough, the friendships get tougher,

Thank you to the best lab family for supporting one another.

Thank you -

Emily: for all of your excellent humour and genuine advice,

Erin: for helping me learn the ropes and training me on every device,

Annamaria & McKenzie: for always being reliable, thoughtful, and having the best food,

Eman & Phepa: for your wisdom, strong spirits, and positive moods.

Chris, Velu, Selvan and Josh: for brave men of the lab that is filled with ladies,

Keeping everyone calm and balanced even when we seem crazy,

Monica: my fellow Maritimer, for all of the insightful hallway talks,

Maureen: for your mentorship from far away and helping me think outside the box.

To my parents back at home, my older sisters, and my twin,

Thank you for being my support network through thick and thin,

To Sadig, even through distance you're always just a phone call away,

Thank you for your perspective, love, and making me smile every day.

Table of Contents

List of Tables

List of Figures

List of Appendices

List of Abbreviations

A: adenine

AFB_1: aflatoxin B_1

amSWCNT: acid-modified single walled carbon nanotubes

ATP: adenosine triphosphate

AuNP: gold nanoparticle

AuNR: gold nanorod

BM: benchmark

BSA: bovine serum albumin

C: cytosine

CD: circular dichroism

cDNA: complementary DNA

CdSe: cadmium selenide

CdTe: cadmium telluride

CL: chemiluminescence

CMCT: 1-cyclohexyl-3-(2-morpholino-ethyl)-carbodiimide metho-p-toluenesulfonate

CNT / SWCNT: carbon nanotube / single-walled carbon nanotube

CPG: controlled pore glass

CS: ceramide synthase

CTAB: cetyl trimethylammonium bromide

DMS: dimethylsulfate

DMT: dimethoxytrityl

DNA: deoxyribonucleic acid

DON: deoxynivalenol

dsDNA: double stranded DNA

ECL: electrochemiluminescence

EDC: 1-ethyl-3-(3-dimethylaminopropyl)carbodiimide

EDTA: ethylenediaminetetraacetic acid

EHC: enterohepatic circulation

EIS: electrochemical impedance spectroscopy

ELAA: enzyme-linked aptamer assay

ELEM: equine leukoencephalomalacia

ELISA: enzyme-linked immunosorbent assay

ELONA: enzyme-linked oligosorbent assay

EtBr: ethidium bromide

FAM: fluorescein phosphoramidite

$FB_{1/2/3/4/6}$: fumonisin $B_{1/2/3/4/6}$

FRET: fluorescence resonance energy transfer

G: guanine

GO: graphene oxide

HEPES: 4-(2-hydroyethyl)-1-piperazineethanesulfonic acid

HFB_1: hydrolyzed FB_1

HPLC: high performance liquid chromatography

HPLC-MS/MS –FD: HPLC-mass spectrometry / -fluorescence detector

HRP: horseradish peroxidase

HR-TEM: high resolution transmission electron microscopy

IAC: immunoaffinity column

IARC: International Agency for Research on Cancer

ITC: isothermal titration calorimetry

IUPAC: International Union of Pure and Applied Chemistry

JECFA: Joint FAO/WHO Expert Committee on Food Additives

K_d: dissociation constant

LDR: linear dynamic range

LC-HRMS^2: liquid chromatography high resolution mass spectrometry

LC-MS: liquid chromatography mass spectrometry

LFD: lateral flow device

LIANA: linkage inversion assisted nano-aptasensor

LOD: limit of detection

MB: magnetic bead

MB: methylene blue

MeOH: methanol

MES: 2-(*N*-morpholino)ethanesulfonic acid

MTL: maximum tolerable limit

NIR: near-infrared

NMR: nuclear magnetic resonance

NOEL: no observed effect level

nt: nucleotide

NTD: neural tube defect

OTA: ochratoxin A

μPAD: microfluidic paper-based analytical device

PAGE: polyacrylamide gel electrophoresis

PES: polyethersulfone

PBR: primer binding region

PBS: phosphate buffered saline

PCR: polymerase chain reaction

PPE: porcine pulmonary edema

PMTDI: provisional maximum tolerable daily intake

PTWI: provisional tolerable weekly intake

QCM: quartz crystal microbalance

QD: quantum dot

RCA: rolling circle amplification

RNA: ribonucleic acid

Sa: sphinganine

SAW: surface acoustic wave

SELEX: systematic evolution of ligands by exponential enrichment

SEM: scanning electron microscopy

SG: SYBR Green I

So: sphingosine

SPR: surface plasmon resonance

ssDNA / ssRNA: single stranded DNA / RNA

Sulfo-NHS: N-hydroxysulfonsuccinimide

T: thymine

TBE: tris borate EDTA

TCEP: tris-(2-carboxyethyl)phosphine

TEM: transmission electron microscopy

TEMED: tetramethylethylenediamine

TLC: thin layer chromatography

T_m: melting temperature

UCNP: upconversion nanoparticle

UV-Vis: ultraviolet visible

ZEA: zearalenone

ZnS: zinc sulfide

1.0 Introduction

1.1 Mycotoxins

1.1.1 General Information

Mycotoxins are secondary metabolites produced by fungi that are known to affect human and/or animal health. The ingestion of agriculturally important mycotoxins results in a wide range of acute and chronic toxicities in humans and animals.[1] For many mycotoxins, their toxicities and resulting diseases were known historically before the toxic chemical was isolated. Outbreaks of equine leukoencephalomalacia in the 1890's were understood to be associated with the consumption of mouldy maize, now attributed to fumonisin toxicity.[2]

The fungi that produce mycotoxins include species in the *Aspergillus*, *Penicillium*, and *Fusarium* genus. As secondary metabolites, mycotoxins can be produced both in field and in storage. Toxin production will be higher on stressed plants or under optimal fungal growth conditions, which depend on the interaction of a number of conditions including moisture, temperature, and insect stress.[3] The main mycotoxins are summarized in Table 1.1 below with their associated toxicities and the main crops that are contaminated (Table 1.1).

Table 1.1 Major mycotoxin classes with representative structures, fungal production, and contaminated products.[1] AFB_1 (aflatoxin B_1), OTA (ochratoxin A), FB_1 (fumonisin B_1), DON (deoxynivalenol), ZEA (zearalenone).

Mycotoxin class	Representative structure	Fungal production (genus)	Major contaminated products
Aflatoxins	AFB_1: 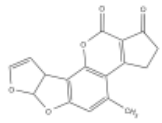	*Aspergillus*	maize groundnuts
Ochratoxins	OTA: 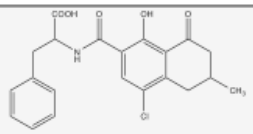	*Aspergillus* *Penicillium*	wheat & cereal crops wine, grapes, fruit, spices
Fumonisins	FB_1: 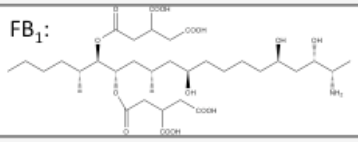	*Fusarium*	maize
Tricothecenes	DON: 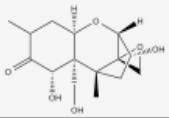	*Fusarium*	wheat & cereal crops maize
Zearalenone	ZEA: 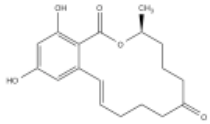	*Fusarium*	wheat & cereal crops maize

Mycotoxin contamination results in both post-harvest loss in crops (productivity, quality, and trade) and negative impacts on human health. Two important mycotoxins, fumonisins and ochratoxins, will be discussed further with regards to their toxicity, detection, and the challenge of risk management and regulation. An emphasis will be placed on fumonisin for introductory purposes, as it is the primary mycotoxin target studied and presented.

1.1.2 Fumonisins

Fumonisins are produced by *Fusarium verticillioides* (formerly *F. moniloforme*), *F. proliferatum, F. fujikuroi* as well as some uncommon species such as *F.anthophilum*, *F. dlamini*, *F. napiforme* and *F. thapsinum.*[4,5] Fumonisins can contaminate rice resulting

from infection by *F. proferatum* and *F. fujikuroi*.[6] However, most fumonisin exposure results from consumption of corn affected by the disease Fusarium Kernel Rot. *Fusarium verticillioides* or *F. proliferatum* occurs systemically in leaves, stems, roots and kernels and can be recovered from virtually all maize kernels worldwide including those that are healthy.[7,8] Fumonsin B_2 and B_4 are produced by *Aspergillus niger*. These toxins have been found in grapes[9] and other dried fruits,[10] notably figs,[11,12] and in wine.[13,14]

Fumonisin B_1 (FB_1) was isolated in 1988 from *F. verticillioides*.[15] FB_1 ($C_{34}H_{59}NO_{15}$) has a molar mass of 721.84 g/mol and the IUPAC designation (2*S*,2'*S*)-2,2'-{[(5*S*,6*R*,7*R*,11*S*,16*R*,18*S*,19*S*)-19-amino-11,16,18-trihydroxy-5,9-dimethylicosane-6,7-diyl]bis[oxy(2-oxoethane-2,1-diyl)]}disuccinic acid. Fumonisins are produced predominantly in warm, dry conditions. Toxin production is also dependent on insect stress. *Bt*-strains of corn with active resistance against lepidopteran pests have shown a decreased risk of contamination when FB_1 production is induced by manual insect stress with European corn borer and Western bean cutworm.[16]

The major fumonisins vary by minor structural variations based on the location of hydroxyl residues (Figure 1.1).

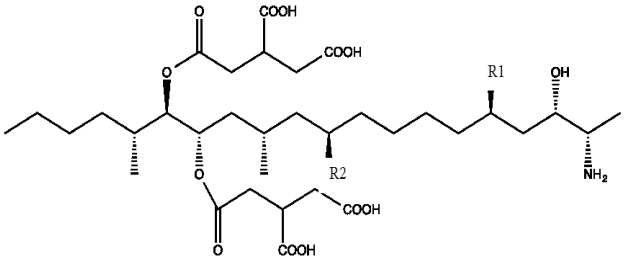

	R_1	R_2
FB_1	OH	OH
FB_2	OH	H
FB_3	H	OH
FB_4	H	H

Figure 1.1 Structures of the major fumonisins

FB_1 is poorly absorbed by animals and humans, and is excreted mainly in the feces unmetabolized or partially hydrolyzed. FB_1 is relatively more bioavailable than FB_2 and FB_3, and the absorbed portion is distributed predominantly to the liver and

kidneys.[17,18] In humans, monitoring FB_1, FB_2, and FB_3 from a maize-based diet revealed that only 0.5% of the FB_1 consumed was excreted in the urine, and FB_2 and FB_3 were not detected. The majority of FB_1 was excreted as the parent compound in the urine, or partially hydrolyzed in the feces.[19]

FB_1 is a potent inhibitor of ceramide synthase (CS) *in vivo,* binding and blocking at the sphinganine and fatty acyl-CoA binding site.[1, 20-25] FB_1-induced inhibition of CS has also been demonstrated *in vitro.*[26] CS inhibition blocks the formation of complex sphingolipids, which have endogenous roles as secondary messengers for cellular regulation,[27] forming binding sites, and maintaining membrane structure[28] (Figure 1.2).

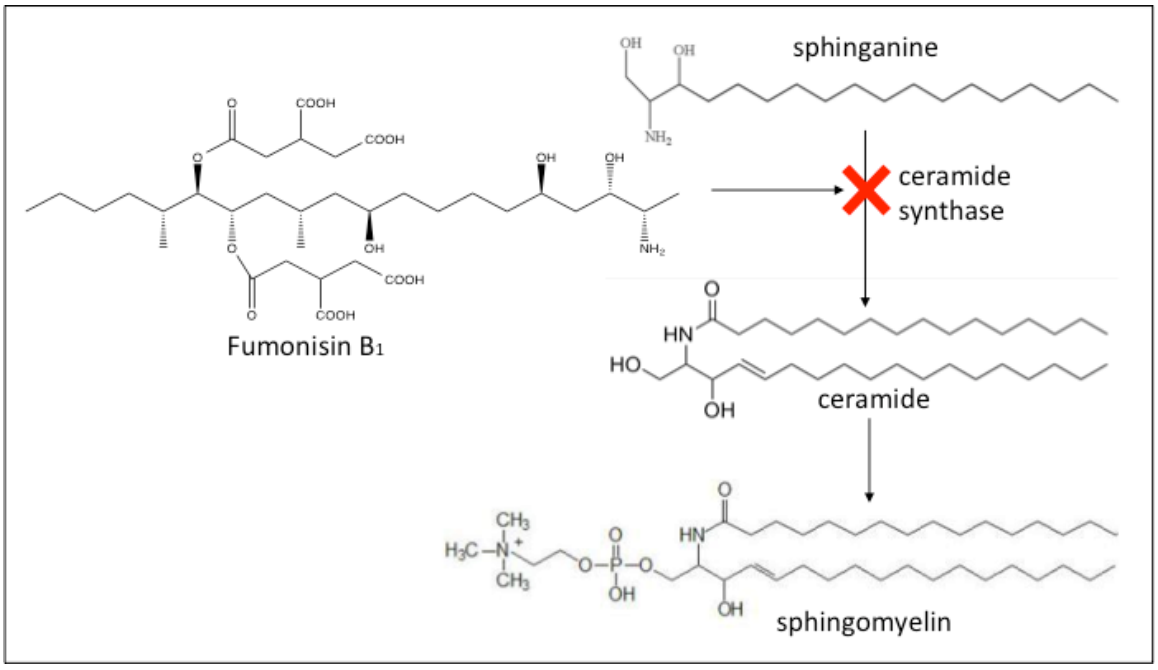

Figure 1.2 A simplified representation of the inhibition of ceramide synthase (CS) by FB_1. CS inhibition will result in a decrease in complex sphingolipid production (ex: sphingomyelin) and a buildup of sphinganine.

The changes in sphingolipid metabolism are a mechanism for FB_1-induced carcinogenesis, effecting cell death and proliferation.[24] Inhibition of CS also results in an increase in free sphinganine, which is toxic to cells[21] and increases the ratio of

sphinganine (Sa) to sphingosine (So) as an *in vivo* biomarker of exposure.[23, 29] FB_1 toxicity is reversible upon removal of exposure.[22]

Other than FB_1, the mycotoxins listed above are stable during food processing. Hydrolyzed FB_1 (HFB_1) or partially HFB_1 is produced during the traditional process of nixtamalization, used to make tortilla flours. In a study with male Sprague Dawley rats it was determined that out of FB_1 and the metabolites, only FB_1 retained toxicity as determined by the Sa:So ratio, indicating that appropriate food processing can help to reduce FB_1 toxicity.[30, 31] N-acyl FB_1 is a metabolite that can be formed *in vivo* localized within the liver, as studied in male rats.[31]

The endpoint to fumonisin toxicity depends on the animal model being studied. The predominant animal toxicities are summarized in the table below, including equine leukoencephalomalacia (ELEM) in horses, porcine pulmonary edema (PPE) in pigs, and carcinogenicity (hepatic, renal) in rodent models (Table 1.2).

Table 1.2 Predominant toxicities associated with FB_1 ingestion in animals (horses, pigs, rats, mice)

Animal	Toxicity from FB_1 ingestion	Description	References
Horses	ELEM	-Neurotoxic disease with liquefactive necrotic lesions -Known since the 1800's, 1989-90 large outbreaks -Induced by dietary exposure, can be fatal -Toxicity at 15-22 mg/kg FB_1	[26, 33-36]
Pigs	PPE	-Acute left-side heart failure resulting in pulmonary edema, can be fatal -Acute toxicity at >16 mg/kg FB_1	[37, 38]
Rats	Carcinogenicity	-Hepatocarcinogenic to male rat -BM (benchmark) LD_{10} = 0.15 mg/kg bw/day	[39]
		-Fisher 344 male rats – renal tubule tumors at 50 and 150 mg/kg FB_1, highly malignant	[40, 41]
		-Fisher 344 male rats, 25 weeks FB_1 at 100 & 250 mg/kg dietary exposure, liver tumors and oval cell proliferation -FB_1-induced changes in phospholipid and fatty acid patterns in a rat liver match well with hepatocyte cancer promotion models	[42, 43]
Mice	Carcinogenicity	-Long-term FB_1 exposure, p53 +/+ and +/- mice, showed non-genotoxic mechanism of carcinogenesis -Hepatic ademonas and cholarginomas at 150 mg/kg FB_1 dietary exposure	[39]
		-B6C3F1 female mice, hepatic tumors at 50 and 80 mg/kg FB_1	[41]

Differences in the tissue, sex, and species differences for FB_1 toxicity can be attributed in part to the effects of sphingolipid biosynthesis in each respective species. Increased Sa correlates strongly with the highest incidences of tumors.[29] The mechanism of FB_1 carcinogenicity has been shown to be non-genotoxic, and there is strong evidence for cancer initiation shown in rodent models and *in vitro*.[39, 41, 44-45]

In humans, consumption of fumonisin-contaminated food has been linked with an increased incidence of a variety of toxic endpoints. FB_1 is classified as a Group 2B

possible human carcinogen,[46] and increased consumption of corn contaminated by FB_1 has been associated with increased risks for esophageal cancer, neural tube and craniofacial defects, and sub-acute effects on the immune system and intestinal health. The table below summarizes human toxicity of FB_1 (Table 1.3).

Table 1.3 Summary of major human toxicity endpoints to FB_1 intoxication

Human toxicity linked to FB_1 exposure	Description	References
Esophageal cancer	-Transkei region (South Africa) had higher incidence of esophageal cancer, linked epidemiologically to FB_1 exposure	[36, 47-48]
Neural tube defects (NTDs)	-Neural tube fails to close in final weeks of gestation -Inhibition of folate transport induced by changes in sphingolipid pathway -1990-91 at the Texas border, NTDs incidence doubled; increased FB_1 exposure was associated with increased odds ratio for NTD occurrence -Mechanism of FB_1-induced NTDs supported by *in vivo* and *in vitro* evidence -In a mouse model, maternal FB_1 exposure (20 mg/kg) resulted in 79% incidence of NTDs, prevented with adequate folate and/or ganglioside glycophospholipid (involved in lipid rafts)	[23, 49-52]
Immune effects and intestinal health	-At sub-acute exposure, FB_1 can increase transepithelial electrical resistance at intestinal barrier; role in host effects to bacteria, parasites, viruses, etc. -*In vitro* evidence in human intestinal and esophageal cell lines has shown FB_1-induced increased proliferation, decreased apoptosis, and increased lipid peroxidation	[53-55]

1.1.3 Ochratoxins

In cereals, *Penicillium verrucosum* is the sole producer of OTA. *P. nordicum* is known to produce OTA on dried salted meats.[56, 57] Many species of *Aspergillus* produce OTA. In the section Circumdati, 13 species are good producers of ochratoxin A: *A. affinis, A. cretensis, A. fresenii, A. muricatus, A. occultus, A. ochraceopetaliformis*, *A.*

ochraceus, A. pseudoelegans, A. pulvericola, A. roseoglobulosus, A. sclerotiorum, A. steynii and *A. westerdijkiae*. Some other species are variable producers of this toxin. Agricultural products damaged by *A. ochraceus*, *A. steynii* and *A. westerdijkiae* are of greatest concern for OTA contamination.[58] The geographic distribution of some of these species remains unclear. OTA contamination of cocoa, coffee, grapes, and wine results from A. *carbonarious* and some strains of *A. niger.* These are an important problem mainly in warm grape growing areas. The other species in section *Nigri* that produces OTA is *A. sclerotioniger* (isolates from coffee).[59]

OTA is a pentaketide with a molecular mass of 403.8 g/mol. The IUPAC name of OTA is *L*-phenylalanine-*N*-[(5-chloro-3,4-dihydro-8-hydroxy-3-methyl-1-oxo-1H-2-benzypyrane-7-yl carbonyl]-(*R*)-isocoumarin. OTA is a highly stable molecule and is fluorescent when excited with blue light.

The mechanism of action of OTA toxicity has several contributing lines of evidence. OTA has been shown to inhibit proteins involved in DNA and RNA synthesis which disrupts mitosis, specifically in the proximal tubules of the kidneys, resulting in cell death.[60] OTA is also implicated in the inhibition of phenylalanine hydroxylase activity.[61]

OTA has a variety of toxic endpoints due to exposure. The most significant toxicity of OTA is nephrotoxicity.[62, 63] OTA is rapidly absorbed and distributed mainly to the kidney, where it is excreted in the urine after enterohepatic cycling (EHC). OTA is also associated with teratogenicity in lab animals,[64] immunosuppressive effects,[62] and neurotoxicity. An IARC report in 1993 classified OTA as a Class 2B possible human carcinogen, although the mechanism of carcinogenicity is still under debate.[65, 66] A

provisional tolerable weekly intake (PTWI) for OTA has been established by JECFA at 100 ng/kg body weight (bw) based on the most sensitive toxic endpoint, nephrotoxicity in pigs.[67]

1.1.4 Challenges with detection and regulation of mycotoxins

1.1.4.1 Analytical detection

Mycotoxin analysis involves many steps, from sampling and sample preparation to analytical techniques and validation. Each phase has an associated margin of error and there are requirements to meet regulatory guidelines.[68] Analytical methods used by regulatory enforcement laboratories that implement legislation must adhere to guidelines to ensure that the methods are reproducible, accurate, and validated through proficiency testing.[69, 70] Common methods for mycotoxin analysis include thin layer chromatography (TLC), high performance liquid chromatography (HPLC), and enzyme-linked immunosorbant assay (ELISA).[69] It is important to differentiate methods intended for screening versus methods intended for confirmatory testing. Optimally, screening methods should be capable of a high throughput and be able to distinguish between a negative (<5% false negatives) and a suspect positive. These methods can either be quantitative (numerical response) or qualitative (binary response); quantitative screening methods are much preferred and recommended.[70] Screening methods, such as ELISA, can have problems with the rate of false positives.[69] This can increase the cost of the screening methods, as all positive samples must be sent for confirmatory testing such as HPLC-MS/MS.[70]

FB_1 can be confirmed with HPLC-MS/MS or HPLC-FD. As FB_1 is not fluorescent, HPLC-FD methods for fumonisin detection use derivitization with o-

phaldialdehyde and 2-mercaptoethanol.[71, 72] Indirect methods for fumonisin determination, mainly as screening methods, are becoming more popular, using aptamers and antibodies integrated into ELISAs, lateral flow devices (LFDs), and biosensors.[72] The most widely used technique for OTA determination is HPLC-FD coupled with immunoaffinity column (IAC) cleanup. IAC cleanup is important for confirmatory detection methods. Although traditionally equipped with antibodies, aptamer-based oligosorbent cleanup columns have been studied and show promise for extracting OTA from complex sample matrices.[73, 74] Other techniques for OTA detection involve immunochemical methods (LFDs, ELISAs), and aptamer-based biosensors (mainly electrochemical).[72] OTA detection is particularly challenging in foods for infants and young children due to the low tolerances by regulatory agencies.[3]

The emphasis on mycotoxin residue analysis involves incorporating QuEChERS (quick easy cheap effective rugged safe) sample preparation, as well as methods for multi-mycotoxin analysis in a single method.[72] The use of synthetic molecular recognition elements (*i.e.* synthetic antibodies, aptamers) is increasing.[75]

1.1.4.2 Regulation and risk management

Mycotoxin control can be at the level of production or exposure. 'In-field' approaches to reducing mycotoxin residues include good agricultural practices, genetic and transgenic approaches, insect and pest control, and biological control. If products have been identified as contaminated, one can treat the products with physical (*i.e.*

sorting) or chemical (*i.e.* adsorbents, binders, pH) treatments.[63, 1] Insect and pest control is especially important for reducing aflatoxin and fumonisin contamination on maize.[3]

The European Commission has established maximum tolerable levels (MTLs) for several mycotoxins, including aflatoxin, OTA, patulin, deoxynivalenol (DON), zearalenone (ZEA), and fumonisins.[68] These regulations are based on health effects as determined from risk assessments and toxicological endpoints in sensitive animal models. However, these MTLs also have a dramatic effect on economics and trade, as they are not globally harmonized. Mycotoxin control integrates health, politics, economy, and technology.[76] Within Canada, maximum limits for natural contaminants in foods, including mycotoxins, are established by Heath Canada's Food Directorate. Mycotoxins including DON, aflatoxin, and patulin have MTLs, and proposals for OTA regulations are ongoing.

Generally speaking, the established regulations over mycotoxin residues are abided by in developed countries. However, in developing countries, where the biggest problems associated with mycotoxin toxicological health effects reside, there is little established control or regulation.[1, 76] There is a divide between 'economics and food security' in developing countries, and 'health and food safety' in developed countries.

Both OTA and FB_1 are classified as Group 2B Possible human carcinogens by the IARC. Regulations for non-genotoxic carcinogens are based on a no adverse effect level (NOEL) from a sensitive animal model with an associated safety factor. The provisional maximum tolerable daily intake (PMTDI) of FB_1 FB_2 and FB_3 alone or in combination has been established as 2 μg/kg bw, based on the NOEL of 0.2 mg/kg bw (in the most sensitive animal model, rat carcinogenesis) and an associated safety factor of 100.[77]

Controversies over the mechanism of carcinogenesis for OTA have implications in regulations, as genotoxic carcinogens do not have a threshold level.[66]

Fumonisins present an interesting dilemma in risk management. The PMTDI was established at 2 μg/kg bw/day.[77] Exposure is based on both the contamination level (regulated by the MTL) and the consumption level of the contaminated product. In many cases in the developing world, the PMTDI is exceeded due to a very high dietary intake of maize.[3, 76, 78] Up to 500 g/day of maize is consumed in many developing countries, which at a FB_1 contamination level of 3 mg/kg results in a daily intake of 25 μg/kg bw/day (based on a 60 kg human) which far exceeds the PMTDI of 2 μg/kg bw/day.[76] In a study in rural Tanzania, 15% of infants (age 6-8 months) were exposed to FB_1 above the PMTDI.[79] Risk can be managed either by: (1) reducing the contamination of maize to 150 μg/kg (regulated by MTLs), or (2) decreasing the average consumption of maize from 43 g/day (max 320 g/day) to 20 g/day. However, enforcing MTLs of 100 – 200 μg/kg would increase crop rejections and result in socioeconomic disruptions.[78] Additionally, reducing the average maize consumption raises the concern of food security.

In the USA alone, mycotoxins result in a combined loss of approximately $1 billion each year through crop losses and health economics.[1] However, as exhibited with the risk management challenges with fumonisins in developing countries, the true challenge in mycotoxin management is at the level of rural and subsistence farmers in Africa. The combination of homogenous food consumption patterns and the absence of conventional surveillance and regulation of mycotoxins intersect. For this reason, there is

an urgent need for rapid, affordable and culturally acceptable interventions for mycotoxin residue analysis.[1, 80]

Challenges with mycotoxins will be responsive to global shifts in climate, as the production of mycotoxins is dependent on optimal temperatures and moisture conditions for fungal growth. Warmer temperatures are likely to bring more mycotoxin contamination to temperate developed regions, and managing these changes in climate and agriculture will be an ongoing challenge.[8, 81]

1.2 Aptamers

1.2.1 General Information

Twenty-five years ago, three independent research groups discovered that nucleic acids could perform functions beyond their traditional genetic role.[82-84] Ellington and Szostak (1990) defined the term aptamer (named for the Greek work 'aptus' meaning 'to fit') describing a short single-stranded oligonucleotide that has affinity and specificity to its target, in their case the target being a small organic dye molecule.[82] Turek and Gold (1990) defined the Systematic Evolution of Ligands by EXponential Enrichment (SELEX), the iterative *in vitro* method for selecting an aptamer that bound to their target, T4 DNA Polymerase.[83] The first research on the catalytic function of short oligonucleotides, DNAzymes, was also published in 1990 by Robertson and Joyce, using selective pressure to generate a Group 1 ribozyme that cleaved ssDNA rather than ssRNA.[84] Unbeknownst to the original research groups that discovered aptamers, nature was, as usual, one step ahead. 'Natural' aptamers have long pre-existed the discovery of their synthetic counterparts, and exist as noncoding RNA and riboswitches that hold key

roles in gene expression regulation through their ability to bind with high affinity and specificity to small molecules.[85]

The discovery of synthetic DNA and RNA aptamers were dependent on advancements in the field of molecular biotechnology. Polymerase chain reaction (PCR) was only discovered four years prior to aptamers[86] and DNA synthesis was inefficient and expensive until a breakthrough in 1983.[87]

The field of aptamers is sometimes referred to as 'functional DNA' to describe the role of short, single-stranded DNA or RNA oligonucleotides that perform a recognition or catalytic function. Wilson and Szostak (1999) described this role of DNA and RNA as the 'phenotypic' role (performing a functional trait) contrary to the 'genotypic' character.[88] The unique three-dimensional structure that a single-stranded aptamer adopts allows for its high affinity and selectivity as a molecular recognition element. Aptamers form thermodynamically stable structures that can include hairpins, junctions, pseudoknots, and G-quadruplexes (a quartet of guanine nucleotides binding through the Hoogsteen and Watson-Crick binding faces to form a planar binding structure).[89] Aptamers interact with targets through non-covalent interactions, including electrostatic and van der Waals forces, and hydrophobic interactions.[90] Most aptamers are between 35 – 100 nucleotides long.[91]

Aptamers are selected through the *in vitro* iterative process of SELEX. SELEX can be separated into three main steps: (1) Binding of the target to the synthetic library (generally ~10^{15} sequences composed of fixed primer binding regions and a random region); (2) Partitioning and elution of binding sequences (approach depends on design of SELEX), and; (3) Amplification using PCR based on fixed primer-binding regions

incorporated into the synthetic library.[90, 92-93] These three basic steps are repeated for a number of rounds, generally with increasing stringency and selective pressure, until the final pool is sequenced and screened for potential high-affinity aptamer candidates for the target.[93-94] The principles of SELEX can be adapted for the selection of aptamers for any desired target (*i.e.* small molecules, toxins, proteins, whole cells, *etc.*).[95] SELEX can be performed in conditions amenable to the downstream use of the aptamer, such as non-physiological conditions of pH, temperature and salinity. Counter selections facilitate aptamer selectivity, as sequences that bind to undesired targets (*i.e.* co-contaminants of a mixture, or structurally-similar derivatives) can be discarded.

There are drawbacks to the labour-intensive process of SELEX. The affinity and success of the aptamers cannot be determined until the end, adding a degree of uncertainty.[85] Computational approaches towards the rational design of SELEX pools as well as optimizing the length or timing of each round have been edifying.[96-97] There is also research towards modification of the original library to either increase the structural diversity, or to incorporate modified bases to increase nuclease resistance.[98-100]

Aptamers have many distinct advantages over their molecular recognition counterparts, antibodies. Monoclonal antibodies have had an over two decade head start over aptamers, although their use is associated with many drawbacks including: (1) *in vivo* selection (uses animals, limited to non-toxic and immunogenic targets selected under physiological conditions); (2) expensive and laborious method of selection; (3) batch-to-batch variation; (4) susceptibility to irreversible denaturation by heat and a limited shelf life.[94, 97, 99] Conversely, aptamers can be selected for virtually any target under a range of conditions due to the *in vitro* selection approach. Aptamers often have an affinity

comparable to that of antibodies, and have a high degree of specificity as highlighted by aptamers that discriminate between very similar targets (*i.e.* L-arginine *vs.* D-arginine,[101] and caffeine *vs.* theophylline (differs by one methyl group).[102] Due to their chemical synthesis, aptamers can also be homogenously modified with reporter sequences for sensing applications.[90, 103]

Synthetic aptamers have had a rapid surge since their inception in 1990, and they have come to rival antibodies in sensing, diagnostics, and therapeutic applications.[85, 89, 95, 99] Therapeutic applications of aptamers *in vivo* require modifications of the aptamer structure to prevent degradation by endogenous nucleases, generally modifications on the phosphate backbone or at the 2' position on the ribose sugar.[85] Aptamers have demonstrated growth in the global market where antibodies hold precedent, with their application in lateral flow devices as one example.[104]

1.2.2 Measuring aptamer structure and affinity

The dissociation constant (K_d) of an aptamer defines its affinity to the target in equilibrium binding conditions. For a more detailed description of K_d, the reader is referred to Section 2.2.1. Determining the K_d of aptamer binding is often a limiting factor in aptamer development and integration, particularly for aptamers binding to small molecules.[89] Although the primary sequence of an aptamer is known, characterizing the aptamer's secondary and tertiary structure can be very informative for modulating the affinity of an aptamer, *i.e.* to modify the affinity to fit within a therapeutic range,[105] truncating regions of the aptamer, or for effective labelling of the sequence for use in sensing applications. RNA Structure is a webserver that predicts the most

thermodynamically stable structure of an aptamer, although it will not predict the formation of G-quadruplex motifs.[106] Experimental approaches to characterize the structure of an aptamer include ^{13}C and ^{15}N labeling of the sequence for NMR analysis[107] and X-ray crystallography.[108] Additionally, Lin *et al* (2011) have used surface plasmon resonance (SPR), circular dichroism (CD) and isothermal titration calorimetry (ITC) to characterize the types of interactions and aptamer structure adopted by two thrombin-binding aptamers.[109] SPR and ITC determine kinetic and thermodynamic parameters of binding, and CD generates conformational data. Aptamers that are well characterized tend to be used extensively in proof-of-concept studies for their applications in sensors, therapeutics, and imaging. For small molecules, these targets include ATP, cocaine, and theophylline; the most widely used protein target for aptamers is thrombin.[89, 109]

1.2.3 Aptamers for mycotoxins

Aptamers that have been selected for small-molecule mycotoxins are summarized in the table below, including their sequence, reported K_d, and general SELEX conditions (Table 1.4). OTA has had aptamer selections performed by three independent research groups,[110-112] FB_1 from two groups,[113-114] and several aflatoxin aptamer selections have been performed.[115-117]

Table 1.4 Aptamers selected for mycotoxins

Mycotoxin	Aptamer	Sequence (5' – 3')	Reported K_d (nM) (method)	SELEX conditions	Ref.
Ochratoxin A	1.12.2	5'GATCGGGTGTGGGTGGCGTAAAGGGAGCATCGGACA-3'	49 ± 3 (equilibrium dialysis)	-14 rounds -OTA bound to agarose resin -N30 random region	[110]
	A08	5'AGCCTCGTCTGTTCTCCCGGCAGTGGGGCGAATCTATGCGTACCGTTCGATATCGGGGGAGACAAGCAGACGT-3'	290 ± 150 (magnetic bead assay)	-15 rounds -OTA bound to magnetic beads (MBs) -N40 random region	[111]
	B08	5'AGCCTCGTCTGTTCTCCCGGCGCATGATCATTCGGTGGGTAAGGRGGRGGRAACGRRGGGGAAGACAAGCAGACG-3'	110 ± 50 (magnetic bead assay)		
	H12	5'GGGAGGACGAAGCGGAACCGGGTGTGGGTGCCTTGATCCAGGGAGTCTCAGAAGACACGCCCCGACA-3'	96 (magnetic bead assay)	-14 rounds -OTA bound to MBs -N30 random region	[112]
	H8	5'GGGAGGACGAAGCGGAACTGGGTGTGGGGTGATCAAGGGAGTAGACTACAGAAGACACGCCCGACA-3'	130 (magnetic bead assay)		
Fumonisin B_1	$FB_1$39	5'ATACCAGCTTATTCAATTAATCGCATTACCTTATACCAGCTTATTCAATTACGTCTGCACATACCAGCTTATTCAATTAGATAGTAAGTGCAATCT-3'	100 ± 30 (magnetic bead assay)	-18 rounds -FB_1 bound to MBs -N60 random region	[113]
	F10	5'AGCAGCACAGAGGTCAGATGCGATCTGGATATTATTTTTGATACCCCTTTGGGGAGACATCCTATGCGTGCTACCGTGAA-3'	62 ± 5 (magnetic bead assay)	-13 rounds -FB_1 bound to MBs -N40 random region	[114]
Zearalenone	$8Z_{31}$	5'AGCAGCACAGAGGTCAGATGTCATCTATCTATGGTACATTACTATCTGTAATGTGATATGCCTATGCGTGCTACCGTGAA-3'	41 (magnetic bead assay)	-14 rounds -ZEA bound to MBs -N40 random region	[118]
T-2 toxin	Seq. 16	5'CAGCTCAGAAGCTTGATCCTGTATATCAAGCATCGCGTGTTTACACATGCGAGAGGTGAAGACTC- GAAGTCGTGCATCTG-3'	20.8 ± 3.1 (CD)	-10 rounds -Free T-2, GO quench non-binding sequences -N40 random region	[119]
Aflatoxin B_1	AFAB3	5'ATCCGTCACACCTGCTCTATTCCTCTGTTGAAGAACCACTTCCGGAAATAAGAGTGGTGTTGGCTCCCGTAT-3'	96.6 ± 8.6 (magnetic bead assay)	-6 rounds -AFB_1 bound to MBs -N36 random region	[116]
	No. 17	5'AGCAGCACAGAGGTCAGATGCTGACACCCTGGACCTTGGGATTCCGGAAGTTTTCCGGTACCTATGCGTGCTACCGTGAA-3'	9.83 ± 0.99 (magnetic bead assay)	-10 rounds -AFB_1 bound to MBs -N40 random region	[115]
Aflatoxin M_1	AFAS3	5'ATCCGTCACACCTGCTCTGACGCTGGGGTCGACCCGGAGAAATGCATTCCCCTGTGGTGTTGGCTCCCGTAT-3'	35.6 ± 2.9 (magnetic bead assay)	-10 rounds -AFM_1 bound to MBs -N36 random region	[116]
Aflatoxin B_2	No. 1	5'AGCAGCACAGAGGTCAGATGGTGCTATCATGCGCTCAATGGGAGACTTTAGCTGCCCCCACCTATGCGTGCTACCGTGAA-3'	11.39 ±1.27 (magnetic bead assay)	-10 rounds -AFB_2 bound to MBs -N40 random region	[117]

1.3 Aptasensors

1.3.1 Components of an aptasensor

An aptasensor converts an aptamer-mediated molecular recognition event into a sensor through signal production.[120-122] Aptamer recognition of a target is either through 'outside' binding with a large protein target, allowing for the possibility of multi-site interactions, or 'embedded' binding with a small molecule target, usually occurring in a 1:1 ratio.[120, 122]

Signal reporting can be based on a change in physical properties upon target binding. For example, a change in mass is converted to a signal through surface plasmon resonance (SPR),[123] quartz crystal microbalance (QCM),[124] surface acoustic wave (SAW) sensors,[91] and microcantilevers.[125] Alternatively, a change in conductance is exploited in electrochemical impedance spectroscopy (EIS) sensors.[126] Molecular reporters can be coupled to the aptamer-target binding event for signal generation. Examples of molecular reporters include molecular beacons,[127-128] fluorescence resonance energy transfer (FRET),[129-130] redox-active reporters such as methylene blue,[131] and inorganic nanoparticles such as gold nanoparticles.[132] Additionally, various amplification techniques can be used to achieve ultrasensitive detection through either amplification of the signal or recycling the target.[133] The advantage of using DNA as a molecular recognition element is that aptamers come with built in mechanisms for amplification (PCR, rolling circle amplification (RCA)),[134-136] or digestion with nucleases.[130] Additionally, ssDNA also has many unique adsorptive properties with inorganic

nanoparticles and carbon-based nanomaterials which can be used for signal generation, amplification, and fluorescence donors and acceptors.[133, 137]

Many aptasensors take advantage of aptamers that undergo a structure-switching event upon target binding. Nutiu *et al* (2004) demonstrated 'structure-switching aptamers' through a molecular beacon-like approach.[138] The aptamer is labelled with a fluorophore, and a complementary probe is labelled with a quencher. The dsDNA complex is quenched, and upon addition of target, the complementary probe will be displaced, resulting in an increase in the fluorescent signal. Other approaches can modify the structure switching to result in a fluorescence 'off' signal, or to modify only complementary probes instead of the aptamer.[128, 137-139] Either way, the folding and conformational change upon target binding can be exploited to generate a signal.

1.3.2 Colourimetric sensors

Antibody-based enzyme-linked immunosorbent assays (ELISAs) use reporter enzymes to generate a colourimetric response proportional to the target concentration. Similarly, aptamer-based enzyme-linked aptamer assays (ELAAs) or enzyme-linked oligosorbent assays (ELONAs) use enzymes such as horseradish peroxidase (HRP) to generate a signal upon the aptamer binding to its target. For example, aptamer-recognition mediated ELAAs / ELONAs have been developed for OTA,[112] cocaine[140] and thrombin.[141] Competitive assay formats for ELAAs and ELONAs are more sensitive.[112] When applicable, a sandwich assay can be formed if there are two aptamers for the same target, which has been done for thrombin[141] and cocaine.[140] A chemiluminescence (CL)

based aptasensor for ATP, thrombin, and peptide detection uses ABEI-Au colloids (N-(aminobutyl)-N-(ethylsoluminol)) as a signal reporter.[142]

Gold nanoparticles (AuNPs) form a colloidal suspension with unique colourimetric properties based on their SPR absorbance. When dispersed, AuNPs form a red solution (Absorbance 520 nm), and when aggregated, the absorbance shifts to 650 nm and they appear blue-purple in colour.[143] AuNPs can be used in aptasensors by coupling the aggregation state to aptamer-target binding. The first use of an AuNP-aptamer sensor detected two small molecules (cocaine and adenosine) based on target-induced dispersion of aptamer-linked AuNPs.[144-145] Thrombin, with two aptamers facilitating a sandwich-like binding design, can be used to initiate target-induced aggregation of AuNPs.[146-147] A different approach to AuNP based aptasensors uses ssDNA aptamers to stabilize AuNPs against aggregation with electrostatic repulsion from the negatively charged DNA backbone.[137, 148] When the target binds to the aptamer and displaces it from the AuNP surface, the suspension is susceptible to salt-induced aggregation and a subsequent rapid colour change to detect targets such as OTA[132] and cocaine.[149]

AuNP colourimetric sensing can also be applied to a lateral flow device (LFD) for rapid, on-site, semi-quantitative detection. In a LFD, the aptamer-AuNPs are separated along a nitrocellulose membrane; test and control zones are used to confirm the presence or absence of the target in a sample. A common design for aptamer-AuNP based LFDs uses probe DNA on the membrane test and control zones to immobilize AuNPs for a colourimetric response to the target concentration. This design has been used to detect

OTA[150] and AFB_1[151] offering rapid results (< 30 min) and a relatively long shelf life without loss of performance (30 days).

1.3.3 Fluorometric sensors

Fluorescence has a lot of promise for aptasensors, particularly for multiplex sensors with high sensitivity.[91] Fluorometric detection is generally based on fluorescence resonance energy transfer (FRET) between a fluorophore (donor) and a quencher (acceptor). FRET transfers the non-radiative energy from a donor to acceptor through dipole-dipole interactions over a range of ~ 20 nm.[152-154] Aptasensors can use FRET to develop a 'turn on' or 'turn off' fluorescent sensor in response to target binding. Fluorophores are generally organic fluorophores,[127, 130] quantum dots (QDs),[155-157] or upconversion nanoparticles (UCNPs),[153] and quenchers are often metallic nanoparticles (AuNPs),[155, 158] or carbon-based nanomaterials (carbon nanotubes, graphene).[129, 159-160] Table 1.5 summarizes a selection of aptasensors developed for detecting OTA and FB_1. For further information on the nanomaterials used in FRET sensing, the reader is directed to Section 3.1.

1.3.4 Electrochemical sensors

Electrochemical aptasensors represent many of the most sensitive techniques for measuring target concentrations based on aptamer recognition. Both electrochemical amperometry and voltammetry have a high working range and high sensitivity.[161] The high sensitivity can be attributed to signal amplification through enzyme-catalyzed target recycling, using a ssDNA endonuclease to release the target after aptamer binding to

increase the apparent target concentration.[134, 162] Electrochemical impedance spectroscopy (EIS) has also been used as a signal for small molecule aptamer binding; the aptamer is linked to AuNPs on a glassy carbon electrode, and target binding increases the electric resistance in a concentration-dependent manner.[126] Table 1.5 summarizes a selection of aptasensors developed for detecting OTA and FB_1 using a variety of techniques.

Table 1.5 Selection of aptasensors developed for FB_1 and OTA. LOD (limit of detection), LDR (linear dynamic range)

Aptasensor design	Target (aptamer)[Ref]	LOD (LDR)	Reference
SPR (mass-sensitive)	OTA (1.12.2) [110]	0.094 – 10 ng/ml	[123]
Microcantilever array biosensor	FB_1 ($FB_1$39)[113]	33 ng/ml (0.1 – 40 μg/ml)	[125]
Evanescent wave biosensor	OTA (1.12.2) [110]	3 nM (6 nM – 500 nM)	[163]
Colourimetric – ELAA with enzyme-signal enhancement	OTA (H8)[112]	1 ng/ml direct competitive	[112]
Colourimetric (AuNP solution, NaCl induced aggregation)	OTA (1.12.2) [110]	20 nM (20 – 625 nM)	[132]
Colorimetric – LFD	OTA (1.12.2) [110]	(0 – 2.5 ng/ml) semi-quantitative	[164]
Fluorescence polarization (FP)	OTA (1.12.2) [110]	5 nM	[110]
Fluorometric – LFD	OTA (1.12.2) [110]	1.9 ng/ml semi-quantitative	[165]
Fluorescence – FRET (UCNPs, GO)	OTA (1.12.2) [110]	(0.05-100 ng/ml)	[129]
	FB_1 ($FB_1$39) [113]	(0.1 – 500 ng/ml)	
Fluorescence – FRET (GO) with catalytic target recycling	OTA (1.12.2) [110]	20 nM	[130]
Fluorescence (label-free PicoGreen)	OTA (1.12.2) [110]	1 ng/ml (1 ng/ml – 100 μg/ml)	[166]
Fluorescence (label-free SG)	OTA (A08min)[111]	(9-100 nM)	[111]
Fluorescence (aptamer-linked QDs-MB suspension)	OTA (1.12.2) [110]	5.4 pg/ml (15-100 ng/ml)	[157]
Fluorescence – structure switching	OTA (1.12.2)[110]	0.8 ng/ml (1-100 ng/ml) corn matrix	[128]
Fluorescence – FRET (UCNPs, AuNPs)	FB_1 ($FB_1$39)[113]	(0.01 – 100 ng/ml)	[160]
Fluorescent (FAM-labelled probe release upon binding)	OTA (1.12.2) [110]	0.25 pg/ml (0.01 – 1 ng/ml)	[127]
	FB_1 ($FB_1$39) [113]	0.16 pg/ml (0.001 – 1 ng/ml)	
Electrochemical (voltammetric signal)	FB_1 ($FB_1$39) [113]	(0.1 – 500 ng/ml)	[134]
Electrochemical (ECL) using target recycling	OTA (1.12.2) [110]	0.64 pg/ml	[162]
Electrochemical (Methylene Blue redox)	OTA (1.12.2) [110]	30 pg/ml (0.1 – 20 ng/ml)	[131]
Electrochemical (EIS)	FB_1 (F10)[114]	2 pM (0.1 nM – 100 μM)	[126]

1.4 Thesis objectives

Aptamer selection (SELEX) has been performed previously for the agriculturally important small molecule mycotoxins FB_1 and OTA. The existing FB_1 and OTA aptamers will be characterized using a novel DNase I digestion assay to determine their in-solution binding affinity and to derive structural information. From this, minimer sequences for *$FB_1$39* will be designed and tested to characterize regions of the aptamer involved in binding. A magnetic bead binding assay will be used to confirm the binding affinity of *$FB_1$39* minimer sequences. Several fluorescent nano-aptasensor applications will be tested to exploit the aptamer binding event to generate a signal proportional to the mycotoxin concentration. Aptasensors for both OTA and FB_1 will be studied with the aim of developing a sensitive, selective, and robust sensor for mycotoxins using aptamer-mediated molecular recognition.

2.0 Aptamer optimization

2.1 Statement of Contributions

The DNase I assay for OTA aptamers was performed by Nadine Frost and McKenzie Smith. 5'-fluorescein modified aptamers for OTA were synthesized by McKenzie Smith and Kayla Hill. Nadine Frost performed all other experiments and syntheses. DNase I assay analysis of OTA and FB_1 aptamers was published in the following manuscripts:

McKeague M., De Girolamo A., Valenzano S., Pascale M., Ruscito A., Velu R., Frost N.R., Hill K., Smith M., McConnell E.M., DeRosa M.C. (2015) Comprehensive analytical comparison of strategies used for small molecule aptamer evaluation, *Analytical Chemistry,* DOI: 10.1021/acs.analchem.5b02102

Frost N.R., McKeague M., Falcioni D., DeRosa M.C. (2015) An in solution assay for interrogation of affinity and rational minimer design for small molecule-binding aptamers, *Analyst,* DOI: 10.1039/c5am01075f

2.2 Introduction

2.2.1 Binding affinity (K_d) determination

Generally, the quality of an aptamer is evaluated through its binding affinity, depicted by its dissociation constant, K_d. For an aptamer-target interaction, the K_d is an equilibrium binding association governed by the proportion of aptamer and target bound

in a complex relative to the unbound aptamer and target. This can be depicted as in equation [2.1].

$$[2.1]\quad K_d = \frac{[aptamer][target]}{[aptamer+target\ complex]}$$

The K_d can also be affected by the kinetics of aptamer binding, notably the 'on' and 'off' rates of aptamer binding, denoted by k_{on} and k_{off} respectively. In this regard, K_d can be expressed as in equation [2.2].

$$[2.2]\quad K_d = \frac{[aptamer][target]}{[aptamer+target\ complex]} = \frac{k_{off}}{k_{on}}$$

There are a multitude of existing techniques for measuring the apparent K_d of aptamer-target interactions. Each of these relies on either varying the concentration of the aptamer or target, while maintaining a constant concentration of the other. Many of these, such as SPR, atomic force microscopy, HPLC, and equilibrium dialysis, are separation- or mass-based techniques that rely on the target-aptamer binding event to result in a change in mass or mobility of the complex.[89, 167] One of the challenges of determining the K_d of aptamers for small molecules is that a small molecule binding event is not accompanied by a large change in mass. Many techniques that are well suited to small molecule aptamer binding rely on tethering either the aptamer or target to a solid support (*i.e.* magnetic bead chromatography), or the inherent fluorescence of the target molecule (*i.e.* fluorescence polarization).[89, 142] Steric hindrance introduced by tethering the aptamer or target to a solid support will result in the reported K_d not being an accurate representation of the K_d of binding in solution. Downstream sensor applications generally require aptamers to bind to a target in solution, not covalently bound to a bead or resin prior to sensing. A limited number of techniques are available that yield structural and/or

thermodynamic information to aptamer interactions with small molecules, such as CD and ITC.[168-169]

There is a need for rapid screening methods for determining the affinity of in-solution binding between aptamers and small molecule targets. This will help alleviate the bottleneck for aptamer development of many important small molecule aptamers important for aptamer-based technology such as diagnostics and biosensor development.[89]

2.2.2 Aptamer structure and minimer determination

Characterizing DNA structure is vital to understanding and predicting interactions between an aptamer and other molecules.[170] The structure of an aptamer is based on duplex, triplex, or quadruplex formation between complementary nucleotides within the primary sequence. There are several approaches to predict the structure of an aptamer. Computational programs, such as RNA Structure, predict the secondary structure of DNA or RNA sequences based on thermodynamic parameters and the probability of base pair interaction to form the most likely secondary structure.[106] This provides a good starting point for structure analysis. However, it must be noted that it does not take into account interactions with a target molecule, and some parameters that may impact folding (such as salinity and pH) are not controlled for.

A full-length aptamer from SELEX generally contains three regions: (1) the region (generally with a high degree of secondary structure) that contacts the target directly (10-25 nt); (2) nucleotides with important roles in supporting the regions contacting target directly (25-40 nt); and (3) non-essential nucleotides with no role in binding.[171] It is important to truncate the non-essential regions of the full-length

sequence, forming what is referred to as a minimer, or a minimal binding aptamer. Three prominent advantages of using a minimer over an aptamer include; (1) the shorter minimer sequence is cheaper to synthesize, and cost is less of a barrier for aptamer integration into downstream sensor applications; (2) the minimer may contribute to a higher affinity than the full length sequence;[110, 172] (3) the minimized aptamer may result in a more sensitive nanosensing device due to reduced steric hindrance.[171]

Designing a minimer can be quite complex and laborious and can be approached with many strategies to identify the region(s) of the aptamer critical to binding. The simplest approach to shortening the aptamer sequence is to truncate the primer binding regions (PBRs), artifacts from the SELEX process that may or may not be important in binding, and evaluate the shortened sequence for binding.[111] A more laborious but informative variation of this approach is to synthesize a suite of short complementary oligonucleotides (labelled to facilitate tracking) and evaluate which probes are displaced upon target binding, indicating that the region is a site where target binding is favourable over probe binding.[171] Mutations can also be introduced within the sequence to evaluate changes in binding affinity (increased or decreased) in regions within the aptamer to determine what motifs are important for binding.[172] From a computational approach, minimer regions have been derived by identifying consensus sequences or conserved regions through a SELEX selection that are important for binding.[173] Computational modeling has also made progress in predicting sequences that have the highest

probability of interacting with a target to build a 'minimal' aptamer for a given target.[174-175]

Although there are many techniques for identifying a minimer, they often involve very laborious techniques (*i.e.* screening point mutations within the sequence), require advanced programs (*i.e.* computational approaches), or require a high degree of structural understanding of the aptamer-target interaction complex, which is more amenable to protein targets than small molecule targets. There is a need for more generalizable, cost-effective, rapid techniques to derive information on both the structural effects and affinity of different regions of an aptamer to identify and screen putative minimer sequences.

2.2.3 DNase I

DNase I footprinting is a classical molecular biology technique that was developed to characterize the binding of regulatory proteins to DNA. DNase I is an endonuclease that cleaves DNA to produce 5'-phosphorlyated di-, tri-, and oligonucleotide segments.[176] Footprinting assays based on the digestion of genomic DNA by DNase I have been used to map protein binding sites on ^{32}P-labeled DNA and examine structural changes in the DNA upon protein binding.[176] DNA is labelled at one terminus for a protection assay. The phosphodiester backbone is protected from DNase I cleavage by binding of regulatory proteins, resulting in regions with no fragments. This results in a 'footprint' of the binding site(s) when DNase I digested fragments are separated by gel electrophoresis.[177-179] This technique generates structural and thermodynamic information relevant to the site(s) of protein interaction. A binding isotherm is generated by concentration-dependent protection, allowing for binding affinity to be quantified.[177] Many variations of DNase I footprinting have been used to

improve resolution or obtain sequence specific information for a variety of important protein-DNA interactions.[180-183] While DNase I footprinting has been used to discern the binding sites of aptamers for large targets such as proteins and bacteria,[181-183] it is unexplored in its capacity to map the secondary structure of aptamers, and to characterize the subtle changes in secondary structure that result upon aptamer-target binding. The secondary structure of an aptamer facilitates its selective binding to a target. However, binding of a small molecule target to an aptamer may not necessarily result in a large change in conformation. Therefore, contrary to protein-DNA interactions, small molecule target binding would not be expected to mask or protect large portions of an aptamer.[184] As a result, aptamer binding sites arising from small molecules are more difficult to map and less understood.

A related approach to examine aptamer structure was reported by Burgstaller *et al* (1995). They used chemical probes (DMS, kethoxal, and CMCT) with reactivity at various nucleotides within the sequence. Binding of the small molecule target inhibited structure probe binding and generated a "footprint" at binding sites in the ^{32}P-labelled cDNA. This method was useful for identifying binding sites in aptamers, however one drawback is that the chemical probes show bias in their reaction to each nitrogenous base.[185] Therefore, this method may not be generally applicable to certain nucleotide-rich aptamers. It would be advantageous to use a simplified alternative to this approach for the facile comparison and screening of aptamers. DNase I digests double stranded DNA with

a significantly higher efficiency (~1000x greater) than single stranded DNA. A DNase I digestion profile of an aptamer is directly related to its duplex structure.[176]

2.3 Chapter Objectives

The existing FB_1 and OTA aptamers will be analyzed using a DNase I digestion assay to elucidate in-solution binding affinity and local structural information. *$FB_1$39* will be further characterized and putative minimer sequences, designed with the assistance of the DNase I assay, will be screened for affinity to FB_1 in solution (DNase I assay).

2.4 Materials and Methods

2.4.1 Buffers

Table 2.1 Buffers used in Chapter 2

Buffer	Composition	pH
FB_1 binding buffer	100 mM NaCl, 20 nM Tris, 2 mM $MgCl_2$, 5 mM KCl, 1 mM $CaCl_2$	7.6
DNase I reaction buffer	10mM Tris-HCl, 2.5 mM $MgCl_2$, 0.5 mM $CaCl_2$	7.0
Phosphate buffered saline (PBS)	137 mM NaCl, 2.7 mM KCl, 10 mM Na_2HPO_4, 1.8 mM KH_2PO_4	7.4

2.4.2 DNA Synthesis, purification, and quantification

All aptamers were synthesized on a BioAutomation Mermade 6 oligonucleotide synthesizer using standard phosphoramidite chemistry. 1000 Å controlled pore glass (CPG) columns were used (BioAutomation), and aptamers were modified with 5'-fluorescein phosphoramidite (Glen Research). After synthesis, the sequences were cleaved from the beads by incubation with 1 ml ammonium hydroxide at 55°C for 3 hours followed by 21 hours at room temperature. After centrifugation to pellet out the beads, the supernatant was transferred to a clean tube. The beads were washed with 1 ml

deionized water, centrifuged, and the supernatants were combined and dried overnight on a Savant AE2010 SpeedVac. Aptamers were purified by 12% denaturing polyacrylamide gel electrophoresis (PAGE). Gel solution (31.5 g urea, 23.5 ml acrylamide (acrylamide/bis-acrylamide 40% solution), 15 ml 1x TBE buffer, 14 ml deionized water for 2 gels) was heated with stirring to 37°C. The solution was filtered through Whatman No. 1 filter paper, and cooled to room temperature. 450 µl 10% ammonium persulfate and 35 µl TEMED (N,N,N',N'-tetramethylethylenediamine) were added, and the solution was poured between two glass plates with a plastic comb, and polymerized for approximately 30 minutes. After polymerization, the gels were pre-run for 15 minutes at 300 V using a SE 600 Chroma Standard Dual gel electrophoresis unit. DNA samples were dissolved in 350 µl deionized water and 350 µl formamide, heated at 55°C for 5 minutes, and loaded into the gel to run for 100 minutes at 300 V. Gels were visualized with epiUV (excitation 254 nm) and fluorescence (fluorescein filter) with an AlphaImager Multi Image Light Cabinet (Alpha Innotech). The fluorescent band (5'-fluorescein labelled aptamer) was cut out of the gel and incubated in 20 ml deionized water at 37°C overnight in a New Brunswick Scientific Innova 40 incubation shaker. The solution was filtered through 0.22 µm cellulose acetate syringe filters to remove gel fragments, and dried on a Labconco freezone lyophilizer. The aptamers were then reconstituted in a minimal volume of deionized water, and desalted with Desalting Amicon-Ultra 0.5 ml 3 kDa centrifuge units. DNA was quantified at 260 nm using a Varian Cary 300 Bio UV-Vis spectrophotometer.

Table 2.2 DNA aptamers synthesized, *F* indicates 5'-fluorescein modification

DNA aptamer	Sequence (5'-3')	Length (nt)
$FB_1$39	*F*ATACCAGCTTATTCAATTAATCGCATTACCTTATACCAGCTTATTCAATTACGTCTGCACAT ACCAGCTTATTCAATTAGATAGTAAGTGCAATCT	96
FB1_39t3	*F*ATACCAGCTTATTCAATTAATCGCATTACCTTATACCAGCTTATTCAATTACGTCTGCACAT ACCAGCTTATTCAATT	78
FB1_39t5	*F*AATCGCATTACCTTATACCAGCTTATTCAATTACGTCTGCACATACCAGCTTATTCAATTAG ATAGTAAGTGCAATCT	78
FB1_39t3-5	*F*AATCGCATTACCTTATACCAGCTTATTCAATTACGTCTGCACATACCAGCTTATTCAATT	60
FB1_39m3	*F*TTACGTCTGCACATACCAGCTTATTCAATTAGATAGTAAGTGCAATCT	48
FB1_39m5	*F*ATACCAGCTTATTCAATTAATCGCATTACCTTATACCA	38
FB1_39cm	*F*CCTTATACCAGCTTATTCAATTACGTCTGCACATACCAGCTTATTCAATT	50
$FB_1$32	*F*ATACCAGCTTATTCAATTAATGTACGATGTGTGGGCAACATGAGTATGTCGTGTGATATC TAGATGAGGTAGCGGTGGAGATAGTAAGTGCAATCT	96
FB1_32t3	*F*ATACCAGCTTATTCAATTAATGTACGATGTGTGGGCAACATGAGTATGTCGTGTGATATC TAGATGAGGTAGCGGTGG	78
FB1_32t5	*F*AATGTACGATGTGTGGGCAACATGAGTATGTCGTGTGATATCTAGATGAGGTAGCGGTG GAGATAGTAAGTGCAATCT	78
FB1_32t3-5	*F*AATGTACGATGTGTGGGCAACATGAGTATGTCGTGTGATATCTAGATGAGGTAGCGGTG G	60
$FB_1$31	*F*ATACCAGCTTATTCAATTCGGGGACGTGTATACCAGCTTATTCAATTCACAGTTATGTCCT ATACCAGCTTATTCAATTAGATAGTAAGTGCAATCT	96
$FB_1$23	*F*ATACCAGCTTATTCAATTGCGGATGCGTAAATGACGATAAACATAGATGGGGTATATCGC GATGCGACAGGGTGTAGATAGTAAGTGCAATCT	96
$FB_1$14	*F*ATACCAGCTTATTCAATTCTATACGGAGTGGATATCGATCTGTAACGTGAGTGAGATAAT GTGATGCATAGTCGTGGAGATAGTAAGTGCAATCT	96
$FB_1$16	*F*ATACCAGCTTATTCAATTCATCCAGTAACAAACACATAAGTAACGGCGATATGTCAAAGC GGTATCGGCTACAGATGAGATAGTAAGTGCAATCT	96
F10	*F*AGCAGCACAGAGGTCAGATGCGATCTGGATATTATTTTTGATACCCCTTTGGGGAGACAT CCTATGCGTGCTACCGTGAA	80
2-way junt'n	*F*AAAAAAAACCCCCCCCCCAAAAAAAAAAGGGGGGGGGAAAAAAAAAAGGGGGAAAAA CCCCC	62
3-way junt'n	*F*AAAAAGGGGGAAAAACCCCCCCCCCCAAAAAAAAAAGGGGGTTTTTTTTTAAAAATTTTT	60
long HP bulge	*F*AAAACCCCAAGGGGAAAAGGGGAACCCCAAAACCCCAAGGGGAAAAGGGGAACCCCA AAA	60
A08	*F*AGCCTCGTCTGTTCTCCCGGCAGTGTGGGCGAATCTATGCGTACCGTTCGATATCGTGGG GAAGACAAGCAGACGT	80
A08m	*F*GGCAGTGTGGGCGAATCTATGCGTACCGTTCGATATCGTG	40
B08	*F*AGCCTCGTCTGTTCTCCCGGCGCATGATCATT CGGTGGGTAAGGTGGTGGTAACGTTGG GGAAGACAAGCAGACGT	80
H12	*F*GGGAGGACGAAGCGGAACCGGGTGTGG GTGCCTTGATCCAGGGAGTCTCAGAAGACACGCCCGACA	66
H8	*F*GGGAGGACGAAGCGGAACTGGGTGTGG GGTGATCAAGGGAGTAGACTACAGAAGACACGCCCGACA	66
1.12.2	*F*GATCGGGTGTGGGTGGCGTAAAGGGAGCA TCGGACA	36

2.4.3 Variable-temperature UV-Vis spectroscopy

Variable-temperature UV-Vis spectroscopy melting studies (T_m determination) were performed with a Varian Cary 300 Bio UV-Vis Spectrophotometer equipped with a 6x6 Peltier-Thermostatted Multicell Holder. For each sequence, 3 ml of 5'-fluorescein labelled aptamer was prepared at 2 μM in FB_1 binding buffer. Absorbance was monitored at 260 nm over three temperature ramps (Ramp 1 80°C - 20°C; Ramp 2 20°C - 80°C; Ramp 3 80°C - 20°C). The ramp rate was set at either 0.5°C/min (slow), and 5°C/min (fast), with a five minute hold between each temperature change. Melting temperatures were determined by fitting the change in absorbance at 260 nm relative to temperature using Standard Curves Analysis on SigmaPlot.

2.4.4 DNase I assay

For clarity, the methods outline the procedure performing the DNase I assay on the FB_1 aptamers. The protocol was followed for DNase I assay analysis of the OTA aptamers as well. OTA was purchased from Sigma Aldrich.

Prior to each DNase I digestion assay, 10 μl of 50 μM 5'-fluorescein modified aptamer and 10 μl FB_1 (varying concentrations) were incubated for 30 min on a vortex shaker at room temperature. For control tests, the same concentration range was used but with an off-target molecule (ie: FB_2, OTA, warfarin). FB_1 was obtained from Dr. David Miller (Chemistry Department, Carleton University). The conditions are summarized in Table 2.3 below.

Table 2.3 DNase I assay conditions

Sample	[FB_1] (nM)	FB_1 volume (µl) at various concentrations	Volume DNA (50 µM)	DNase I volume (µl)	DNase I Reaction Buffer volume (µl)
1	0	0	10	0	92
2	0	0	10	1	90
3	0.1	10	10	1	80
4	1	10	10	1	80
5	10	10	10	1	80
6	100	10	10	1	80
7	1 000	10	10	1	80
8	10 000	10	10	1	80

DNase I (New England BioLabs) was added, briefly vortexed to ensure complete mixing, and incubated at 37°C for precisely 1 minute in a heat block. DNase I digestion was stopped with the addition of 1 µl of 0.5 M EDTA at 90°C, vortexed to mix, and heat inactivated at 90°C for 10 minutes. The samples were mixed 1:1 with formamide and heated at 55°C for 5 minutes prior to separation for 3 hours at 300 V on a 19% denaturing PAGE gel in a SE 600 Chroma Standard Dual gel electrophoresis unit. Gels were visualized with the fluorescent setting (fluorescein filter) in an AlphaImager Multi Image Light Cabinet (Alpha Innotech).

Fluorescent digestion bands were quantified using the SpotDenso program on AlphaImager. Each band produced from the digestion was calculated as a ratio relative to the entire sample to avoid any errors stemming from loading volume discrepancies. The density of each band (A, B, C, etc.) relative to FB_1 concentration (log of 0.1 nM – 10 µM)

was plotted with GraphPad Prism (version 5.00) using non-linear regression one site specific binding [2.3].

$$[2.3] \quad Y = \frac{(B_{max})(X)}{(K_d + X)}$$

To facilitate comparison between replicates from different gels, data was standardized to the % of change in band intensity using the following equation [2.4].

$$[2.4] \quad \%change\ band\ intensity = \left[\frac{[min_{trial} - x]}{min_{trial} - max_{trial}]}\right] x\ 100$$

2.4.5 Magnetic Bead conjugation with FB_1

M-270 Amine Dynabeads® (Life Technologies) are superparamagnetic and allow for efficient separation of beads from solution when placed in a DynaMag-2 magnet. Beads are suspended in PBS buffer at 30 mg/ml and washed three times with buffer, separating on the magnet each time. The beads were re-suspended in 5% glutaraldehyde (Sigma Aldrich) in PBS buffer, and incubated for 2 hours at room temperature on a vortex shaker. Control beads were incubated without glutaraldehyde. The beads were again washed three times with PBS buffer, and suspended in 20 μM FB_1 in buffer, and incubated at room temperature on a vortex shaker overnight. After five buffer washes to remove unbound FB_1, unbound NH_2 groups on the bead surface were capped with a 20 mg/ml solution of Sulfo-NHS Acetate (Thermo Scientific) in buffer, incubated for two hours at room temperature on a vortex shaker. The beads were again washed three times with buffer, and stored upright at 4°C.

2.4.6 Magnetic bead binding assay

5'-fluorescein modified aptamers were pre-heated at 90°C for 10 min and room temperature for > 30 minutes prior to the binding assay. FB_1-conjugated beads prepared

as above were washed three times in FB_1 binding buffer prior to the assay. For each assay, six concentrations of aptamer were tested ($1x10^{-6}$, $5x10^{-7}$, $2x10^{-7}$, $1x10^{-7}$, $5x10^{-8}$, and $2x10^{-8}$ M) in 100 µl total volume of FB_1-conjugated beads as prepared above in binding buffer. The beads and aptamers were incubated for 60 min at room temperature on a vortex shaker. Beads were placed on the DynaMag-2 magnet, and washed four times with 100 µl of FB_1 binding buffer at room temperature to remove non-binding aptamers. Binding sequences were then eluted with three 100 µl FB_1 binding buffer elutions by incubating at 90°C for 10 min to disrupt binding aptamer. All fractions were quantified on a Fluorescence Spectrophotometer (Horiba Jobin Yvon, USA) with SpectrAcq controller. Fluorescein-modified aptamer was excited at 494 nm and an emission spectrum of 500 – 600 nm was collected. The amount of total aptamer in each wash was quantified by comparing the fluorescence intensity of the bound aptamer fractions at 520 nm to standards of known aptamer concentrations. For each sample ($1x10^{-6}$, $5x10^{-7}$, $2x10^{-7}$, $1x10^{-7}$, $5x10^{-8}$, and $2x10^{-8}$ M) the total amount of aptamer bound was quantified. K_d binding isotherms were generated using GraphPad Prism (version 5.00) non-linear regression one-site specific binding analysis.

2.5 Results and Discussion

2.5.1 Preliminary structural analysis and minimer design

2.5.1.1 FB_1 39 and minimers

FB_139 is 96 nucleotides (nt) in length, containing two 18-nt primer binding regions (PBRs) and a 60-nt random region from the SELEX pool design. The full-length sequence was separated into regions and minimers were synthesized representing a range

of lengths and regions within the full length structure. The *FB1 39* minimers are: *FB1_39t3* (removing the 3' PBR, 78 nt), *FB1_39t5* (removing the 5' PBR, 78 nt), *FB1_39t3-5* (removing the 3' and 5' PBRs, 60 nt), *FB1_39m3* (3' stem loop motif, 48 nt), *FB1_39m5* (5' region, 38 nt), and *FB1_39cm* (central minimer, 50 nt). The minimers are depicted below in Figure 2.1.

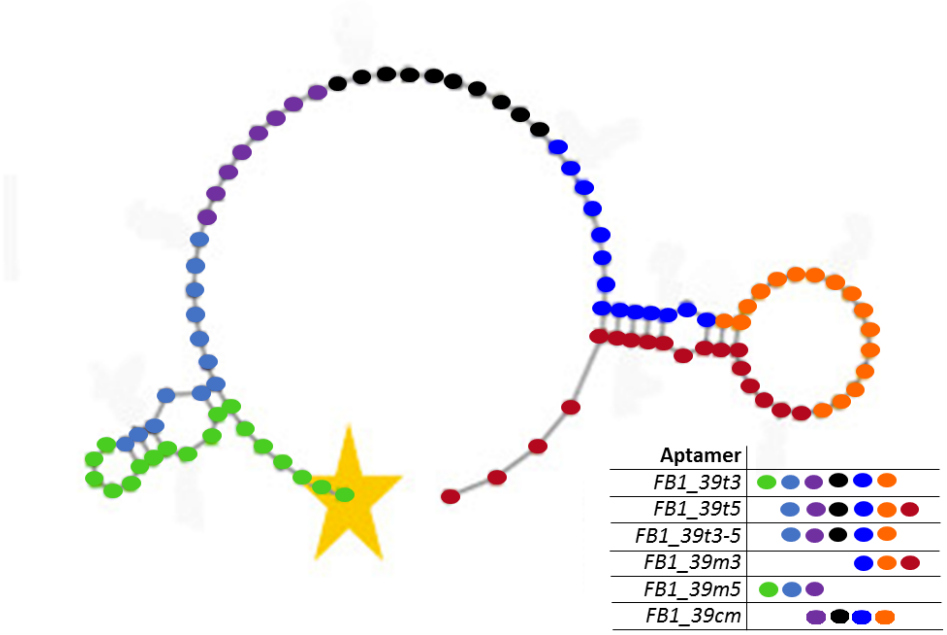

Figure 2.1 *FB1 39* minimer regions

Preliminary structural analysis of *FB1 39* and minimers was performed to characterize the aptamers. Variable temperature UV-Vis spectroscopy is an experimental technique used to determine the melting temperature (T_m) of an aptamer. A higher melting temperature is indicative of a greater stability in structure. T_m is determined by measuring the absorbance of the sequence at 260 nm over a range of temperatures. When

DNA duplex regions are denatured by heat, they exhibit hyperchromicity and the absorbance at 260 nm is increased.

For *FB1 39* and minimers, the sequences with the highest degree of predicted secondary structure from RNA Structure were *FB1 39*, *FB1_39t5,* and *FB1_39m3*. These sequences corresponded with the highest T_ms from the thermal melting temperature studies, with T_ms of 41.0°C, 42.9°C, and 40.9°C respectively. The minimers with lower degrees of predicted secondary structure (*FB1_39t3*, *FB1_39t3-5*, *FB1_39m5* and *FB1_39cm*) corresponded with the lower T_ms from the thermal melting temperature studies, at 13.3°C, 19.1°C, 27.7°C, and 19.0°C respectively (Table 2.4).

Table 2.4 RNA Structure folds and T_m data for *FB1 39* and minimers

FB1 aptamer	RNA structure fold	Melting studies			
		Ramp 1 (80°C - 20°C)	Ramp 2 (20°C - 80°C)	Ramp 3 (80°C - 20°C)	Average Tm (°C)
FB1_39	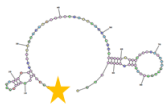	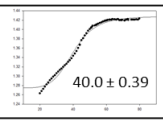 40.0 ± 0.39	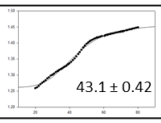 43.1 ± 0.42	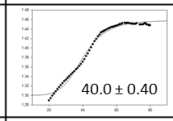 40.0 ± 0.40	41.0 ± 0.4
FB1_39t3	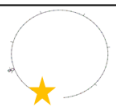	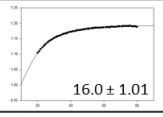 16.0 ± 1.01	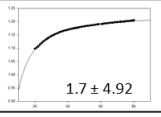 1.7 ± 4.92	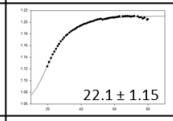 22.1 ± 1.15	13.3 ± 2.4
FB1_39t5	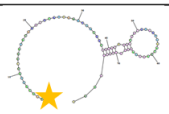	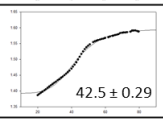 42.5 ± 0.29	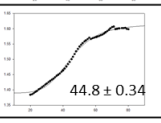 44.8 ± 0.34	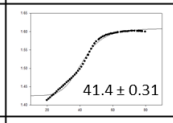 41.4 ± 0.31	42.9 ± 0.1
FB1_39t3-5	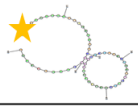	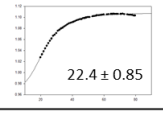 22.4 ± 0.85	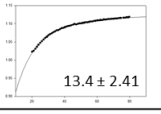 13.4 ± 2.41	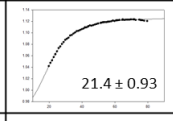 21.4 ± 0.93	19.1 ± 1.1
FB1_39m3	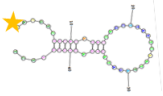	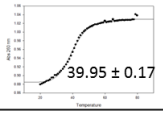 39.95 ± 0.17	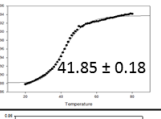 41.85 ± 0.18	N.D.	40.9 ± 0.2
FB1_39m5	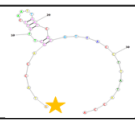	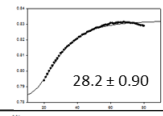 28.2 ± 0.90	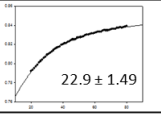 22.9 ± 1.49	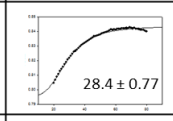 28.4 ± 0.77	27.7 ± 4.6
FB1_39cm	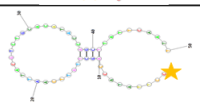	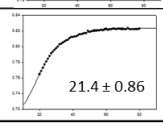 21.4 ± 0.86	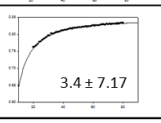 3.4 ± 7.17	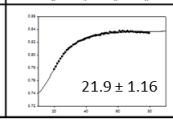 21.9 ± 1.16	19.0 ± 6.6

2.5.1.2 *FB1 32* and minimers

FB1 32 is 96 nt in length, containing two 18-nt primer binding regions (PBRs) and a 60-nt random region from the SELEX pool design. The full-length sequence was separated into regions and minimers were synthesized. The *FB1 32* minimers are: *FB1_32t3* (removing the 3' PBR, 78 nt), *FB1_32t5* (removing the 5' PBR, 78 nt), and

FB1_32t3-5 (removing the 3' and 5' PBRs, 60 nt). The minimers are depicted below in Figure 2.2.

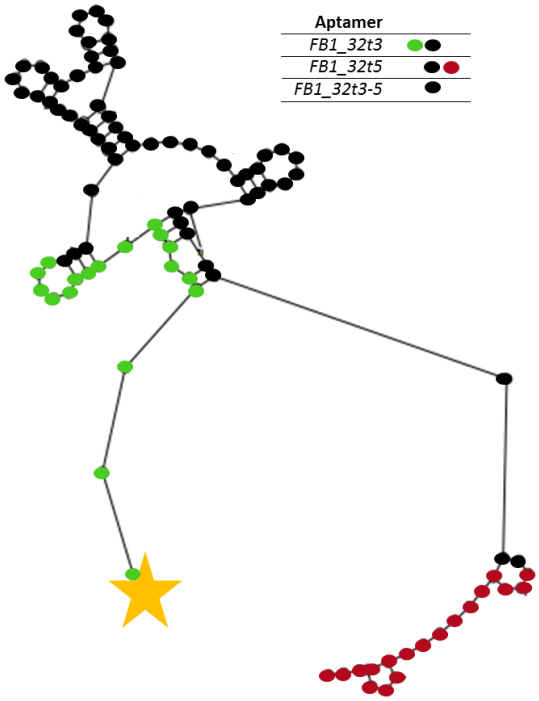

Figure 2.2 *FB$_1$ 32* minimer regions.

For *FB$_1$32* and minimers, all sequences had a similar degree of secondary structure and T_m, indicating that the PBRs were not highly involved in forming the secondary structure within the sequence (Figure 2.5).

Table 2.5 RNA Structure folds and T_m data for *$FB_1$32* and minimers

FB_1 aptamer	RNA structure fold	Melting studies			
		Ramp 1 (80°C - 20°C)	Ramp 2 (20°C - 80°C)	Ramp 3 (80°C - 20°C)	Average Tm (°C)
FB1_32	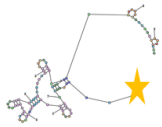	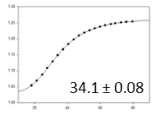 34.1 ± 0.08	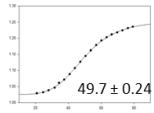 49.7 ± 0.24	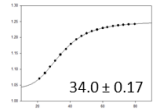 34.0 ± 0.17	40.2 ± 3.0
FB1_32t3	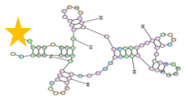	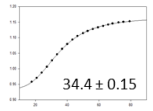 34.4 ± 0.15	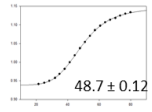 48.7 ± 0.12	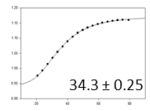 34.3 ± 0.25	39.8 ± 2.8
FB1_32t5	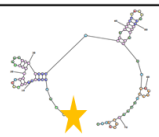	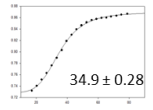 34.9 ± 0.28	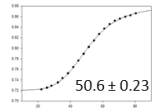 50.6 ± 0.23	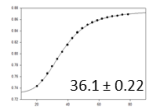 36.1 ± 0.22	40.2 ± 2.0
FB1_32t3-5	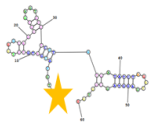	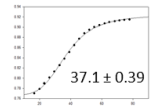 37.1 ± 0.39	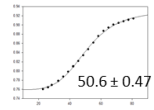 50.6 ± 0.47	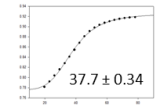 37.7 ± 0.34	41.0 ± 1.7

2.5.1.3 $FB_1$14, $FB_1$16, $FB_1$23, $FB_1$31 & F10

$FB_1$14, $FB_1$16, *$FB_1$23*, and *F10* all had similar T_ms indicating a similar degree of secondary structure within their sequences (37.5°C, 40.4°C, 39.2°C, and 38.4°C respectively). *$FB_1$31* had a slightly lower T_m (27.6°C). The RNA Structure folds of each of these sequences had a wide range of secondary structure motifs, from multiple small hairpins (*$FB_1$14*) to a long hairpin bulge-like structure (*$FB_1$16*) (Table 2.6).

Table 2.6 RNA Structure folds and T_m data for *$FB_1$14*, *$FB_1$16*, *$FB_1$31*, *$FB_1$23*, and *F10*

FB1 aptamer	RNA structure fold	Melting studies			
		Ramp 1 (80°C - 20°C)	Ramp 2 (20°C - 80°C)	Ramp 3 (80°C - 20°C)	Average Tm (°C)
FB1 14	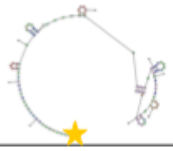	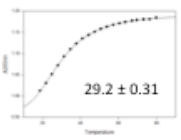 29.2 ± 0.31	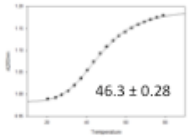 46.3 ± 0.28	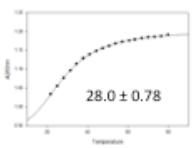 28.0 ± 0.78	37.5 ± 3.7
FB1 16	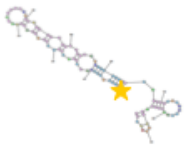	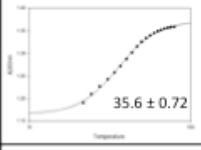 35.6 ± 0.72	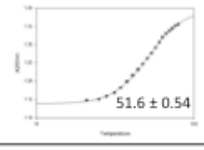 51.6 ± 0.54	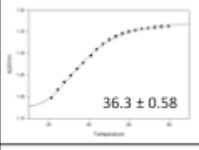 36.3 ± 0.58	40.4 ± 4.0
FB1 31		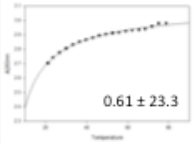 0.61 ± 23.3	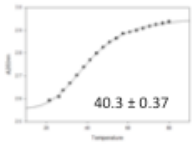 40.3 ± 0.37	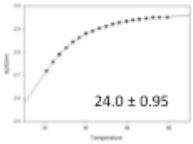 24.0 ± 0.95	27.6 ± 18.7
FB1 23		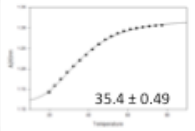 35.4 ± 0.49	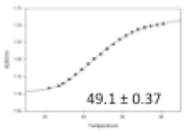 49.1 ± 0.37	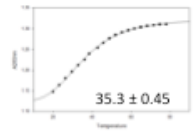 35.3 ± 0.45	39.2 ± 2.4
F10	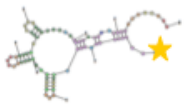	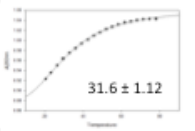 31.6 ± 1.12	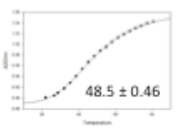 48.5 ± 0.46	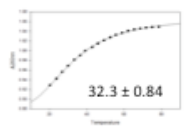 32.3 ± 0.84	38.4 ± 3.9

2.5.2 DNase I assay for determining in-solution structure and affinity of aptamers

2.5.2.1 Assay design

The DNase I digestion assay was designed to study the binding affinity of aptamers binding to small molecule targets in solution. The assay design is shown below (Figure 2.3). An aptamer is subjected to DNase I, which retains preferential endonuclease activity for regions of duplex DNA within an aptamer structure. The DNase I digest of a fluorescently labelled aptamer is separated by size on a denaturing PAGE gel. In the presence of a range of target concentrations, one can characterize the changes in digestion fragment band intensity (lanes B, C) in the presence of a range of target concentrations.

From this, an in-solution affinity (K_d) can be calculated for local regions of aptamer binding. One can compare the apparent local K_d of binding at various regions within the aptamer with this method. For example, if target binding results in stabilization of duplex structure in one region, the digestion fragment produced when DNase I digests at that site will increase in intensity based on target concentration. Conversely, if target binding inhibits DNase I from digesting at one site, similar to a DNase I protection footprinting assay, that digestion fragment will decrease in intensity with target concentration. Based on this, it is possible to derive multiple apparent K_ds for a single aptamer-target interaction in solution; this information can be used to optimize minimer design by selecting local regions of the aptamer with the highest apparent K_d.

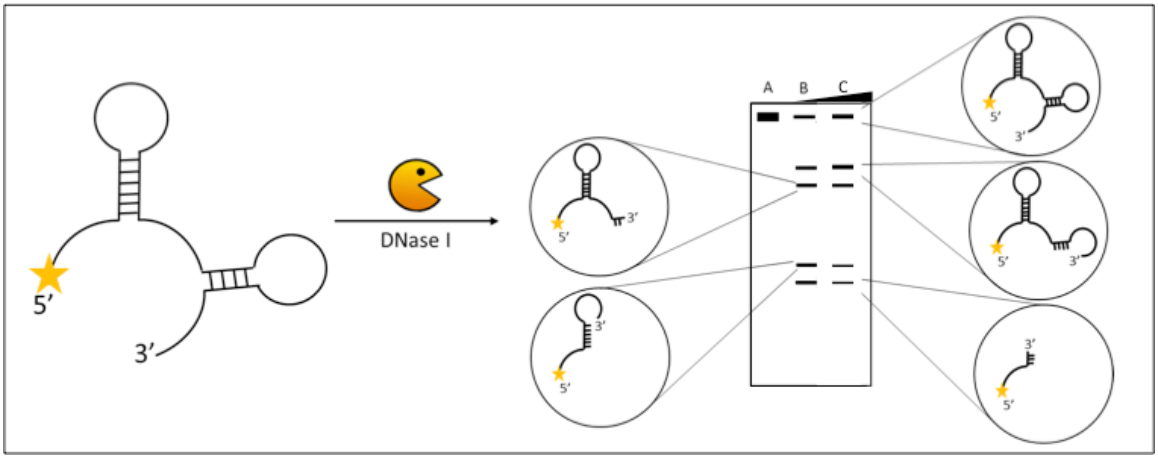

Figure 2.3 Schematic illustrating the DNase I assay. DNA aptamer with a unique secondary structure tagged with 5'-fluorescein, represented by a yellow star. Digestion by DNase I produces fragments (fluorescently tagged at the 5' end) that are separated by size using denaturing PAGE. Only fragments retaining the label are visualized on the gel. Undigested full-length DNA with no DNase I treatment is shown in lane A, fragmented DNA after DNase I digestion in lane B, and band intensity change due to the subtle effects of target binding is shown in lane C.

One drawback of this assay is that there is a relatively high degree of error associated with the affinity measurements. This is due to the fact that the variations in band intensity are subtle with changing target concentration. Regardless, this assay allows for a clear distinction of binding vs. non-binding. More importantly, it facilitates rapid screening of sequences to determine retention of binding affinity in solution.

2.5.2.2 Proof of concept study

To instill confidence in the structural information that can be derived from the DNase I assay, a proof-of-concept study was designed to examine the digestion patterns produced by DNase I treatment on sequences with rationally designed secondary structure. Three sequences were designed and synthesized with a 5'-fluorescein tag: a 2-way junction, 3-way junction, and a long hairpin bulge (Section 2.4.2). The prominent digestion fragments from the 5' terminus (fluorescently tagged) from DNase I digestion can be separated and visualized by PAGE gel. The hairpin regions in the rationally designed structures can be assigned to prominent digestion fragments after DNase I digestion (Table 2.7). The lengths of these fragments have been confirmed by comparison to a fluorescently tagged DNA ladder (Figure 2.8). Note that DNase I activity is slightly less efficient in runs of consecutive A's or T's and G-C rich regions due to the narrowing of the minor groove and decreased flexibility.[176]

Table 2.7 DNase I digestion fragment patterns of three rationally designed sequences. F = 5'-fluorescein modification (denoted by a yellow star in the RNA Structure). A green box outlines the full-length aptamer sequence (undigested) in the DNase I PAGE gel. Numbers are used to align the regions of digestion with the predicted secondary structures.

Structure	DNA sequence (5′ – 3′)	RNA Structure	DNase I digestion on denaturing PAGE
2-way junction	FAAAAAAAACCCCCCCCCAAAA AAAAAAGGGGGGGGGAAAAAA AAAAGGGGGAAAAACCCCC	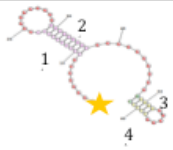	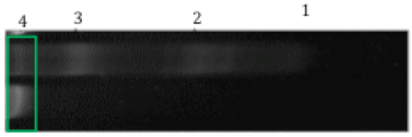
3-way junction	FAAAAAGGGGGAAAAACCCCC CCCCCCAAAAAAAAAAGGG GGTTTTTTTTTAAAAATTTTT	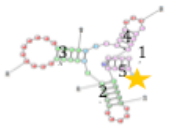	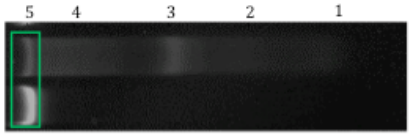
Long bulge hairpin	FAAAACCCCAAGGGGAAAAG GGGAACCCCAAAACCCCAAGGG GAAAAGGGGAACCCCAAAA	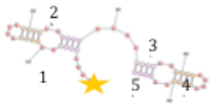	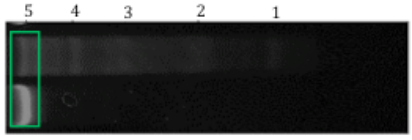

2.5.2.3 Fumonisin aptamers

2.5.2.3.1 *FB1*39 and minimers

2.5.2.3.1.1 DNase I digestion fragment analyses

Each *FB1*39 aptamer and minimer was digested by DNase I and run on a PAGE gel with a fluorescently-labelled DNA ladder to calculate the approximate lengths of each digestion fragment. Through this, the approximate sites of DNase I digestion within each aptamer could be determined (Figure 2.4).

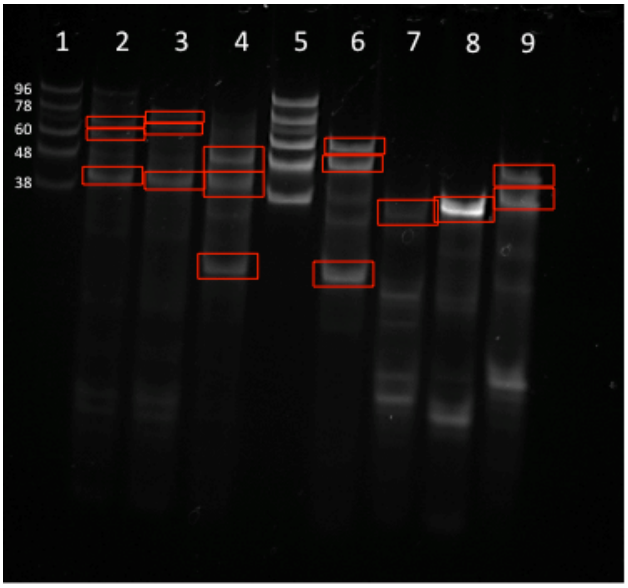

1 – 5′-fluorescein labelled DNA ladder
2 – *FB$_1$ 39* DNase digest – 71 (B); 65 (C); 44 (E)
3 – *FB1_39t3* DNase digest – 76 (B); 69 (C); 44 (E)
4 – *FB1_39t5* DNase digest – 52 (D); 42 (E); 21 (G)
5 – 5′-fluorescein labelled DNA ladder (5x conc.)
6 – *FB1_39t3-5* DNase digest – 57 (C); 49 (D); 20 (G)
7 – *FB1_39m3* DNase digest – 34 (E)
8 – *FB1_39m5* DNase digest – 35 (E)
9 – *FB1_39cm* DNase digest – 45 (D); 37 (E)

Figure 2.4 PAGE gel with the DNase I digests of *FB$_1$39* and minimers compared to a fluorescently labelled DNA ladder to calculate approximate lengths of digestion fragments. For each lane, the digestion fragment length is indicated in the legend with the corresponding band from the DNase I PAGE gel analysis for each aptamer. Fragment lengths were calculated with the Molecular Weight function in AlphaImager, AlphaInnotech.

From this gel (Figure 2.4) the approximate length of "Band E" across each of the minimers is determined to be between 34 – 44 nt. The minimer designed to correspond to "Band E", *FB1_39m5*, is 38 nt in length. Bands B and C are fragments produced by digestion within the 3' stem loop structure. *FB1_39t3-5*, *FB1_39t5* and *FB1_39cm* share a common prominent digestion fragment, "Band D", approximately 50 nt in length from the truncated 5' terminus. The digestion site to produce "Band D" within these minimers corresponds to the same sequence region as "Band B" and "Band C" are digested in the non-5'-truncated sequences within the 3' stem loop hairpin. The region for this shift in size in the PAGE gel is that *FB1_39t3-5*, *FB1_39t5* and *FB1_39cm* all have the 5' PBR

truncated and the same DNase cut will produce a digestion fragment shifted down by 18 nt (the size of the PBR).

Many of these prominent digestion bands (E, D, C) are produced consistently in regions without a high degree of predicted secondary structure based on the RNA Structure analysis. DNase I digestion occurring at these regions is likely due to structure that is not predicted by 2D secondary structure predictions. It is also possible that a motif within the aptamer structure at this location has a higher propensity for DNase I cleavage based on cleavage bias.[176]

2.5.2.3.1.2 DNase I assay results

After 5'-fluorescein labelled aptamers are subjected to DNase I digestion with a range of FB_1 concentrations, the samples are separated by size on a PAGE gel. Each fluorescent band represents a fragment produced from DNase I digestion that is tagged at the 5' terminus.

The digestion bands for *$FB_1$39* have been assigned alphabetically (A – L) and the corresponding bands within the minimer gels are maintained for clarity. A minimum of 6 gel replicates for each sequence have been assembled to determine an average K_d for each prominent band based on the change in total band intensity due to target concentration. In Figure 2.5, panel A indicates the prominent digestion fragments (A-C; E; J-K) from *$FB_1$39* and a representative depiction of the fragment based on estimated size from gel migration (Figure 2.4). Panel B shows the average K_d of each prominent band within the *$FB_1$39* digestion profile. The reported K_ds ± error are presented in Table 2.8.

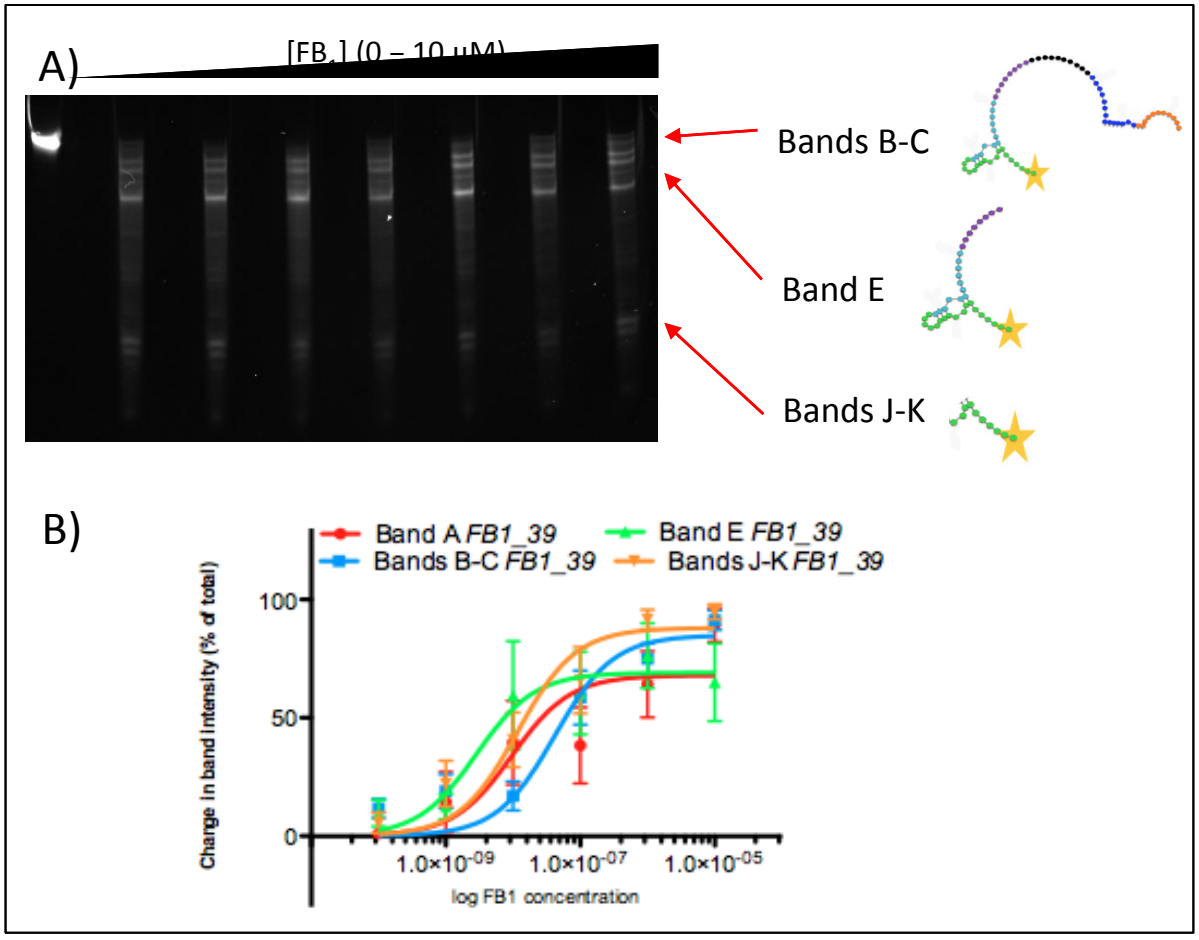

Figure 2.5 A) *FB1_39* DNase I digestion PAGE gel. B) K_ds of each prominent group of digestion fragment bands.

Within *FB1_39*, the most prominent digestion fragment, Band E, also corresponded to the K_d with the highest affinity of binding (2.8 ± 2.4 nM). The majority of the bands produced by digestion corresponded to digestion within the 3' region of the aptamer, where the majority of the secondary structure was predicted based on RNA Structure and experimental T_ms (Table 2.4).

The *FB1_39* minimers are presented below in Figure 2.6. Each panel contains the DNase I digestion PAGE gel of *FB1_39t3* and resulting K_ds for each prominent group of

digestion bands. Panel A: *FB1_39t3*; Panel B: *FB1_39t5*; Panel C: *FB1_39t3-5*; Panel D: *FB1_39m3*; Panel E: *FB1_39m5*; Panel F: *FB1_39cm*.

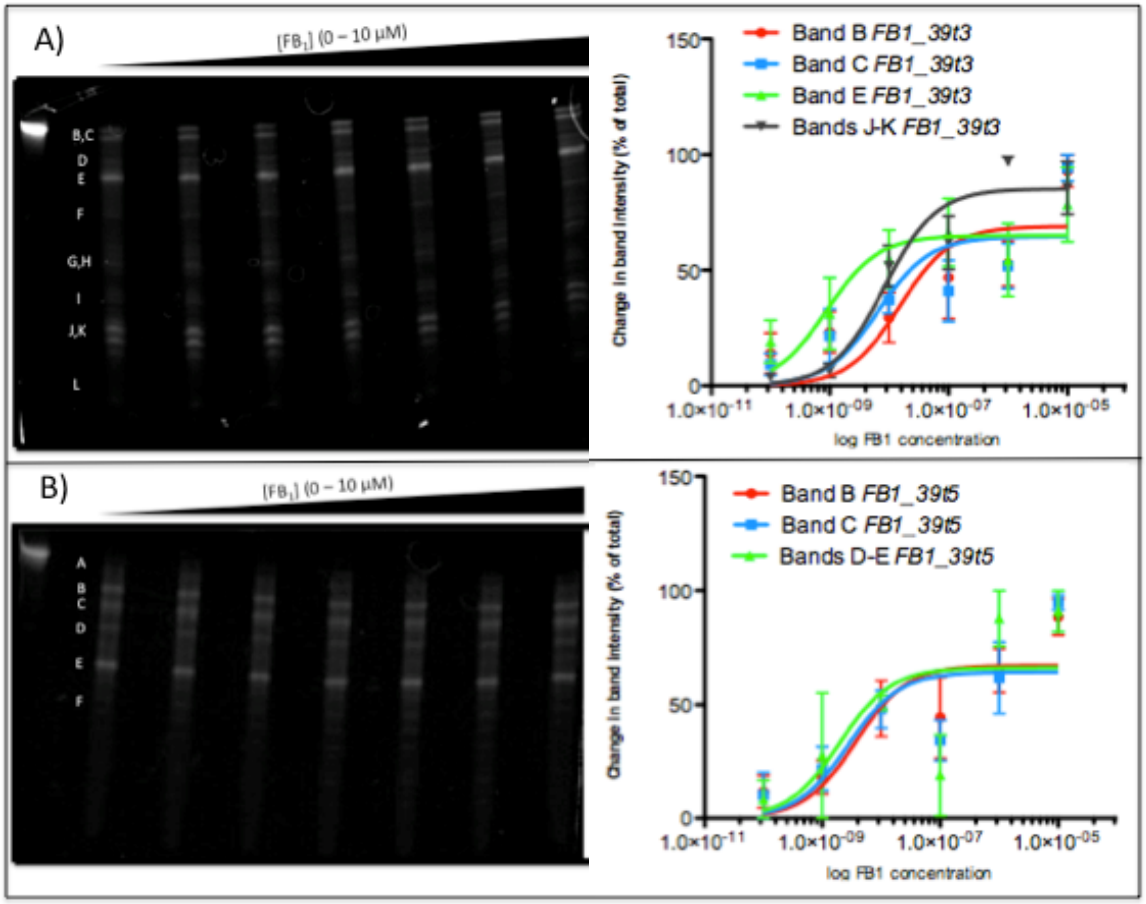
A)
[FB1] (0 – 10 µM)
B,C
D
E
F
G,H
I
J,K
L
Band B FB1_39t3
Band C FB1_39t3
Band E FB1_39t3
Bands J-K FB1_39t3
Change in band intensity (% of total)
150
100
50
0
1.0×10-11
1.0×10-09
1.0×10-07
1.0×10-05
log FB1 concentration
B)
[FB1] (0 – 10 µM)
A
B
C
D
E
F
Band B FB1_39t5
Band C FB1_39t5
Bands D-E FB1_39t5
Change in band intensity (% of total)
150
100
50
0
1.0×10-11
1.0×10-09
1.0×10-07
1.0×10-05
log FB1 concentration

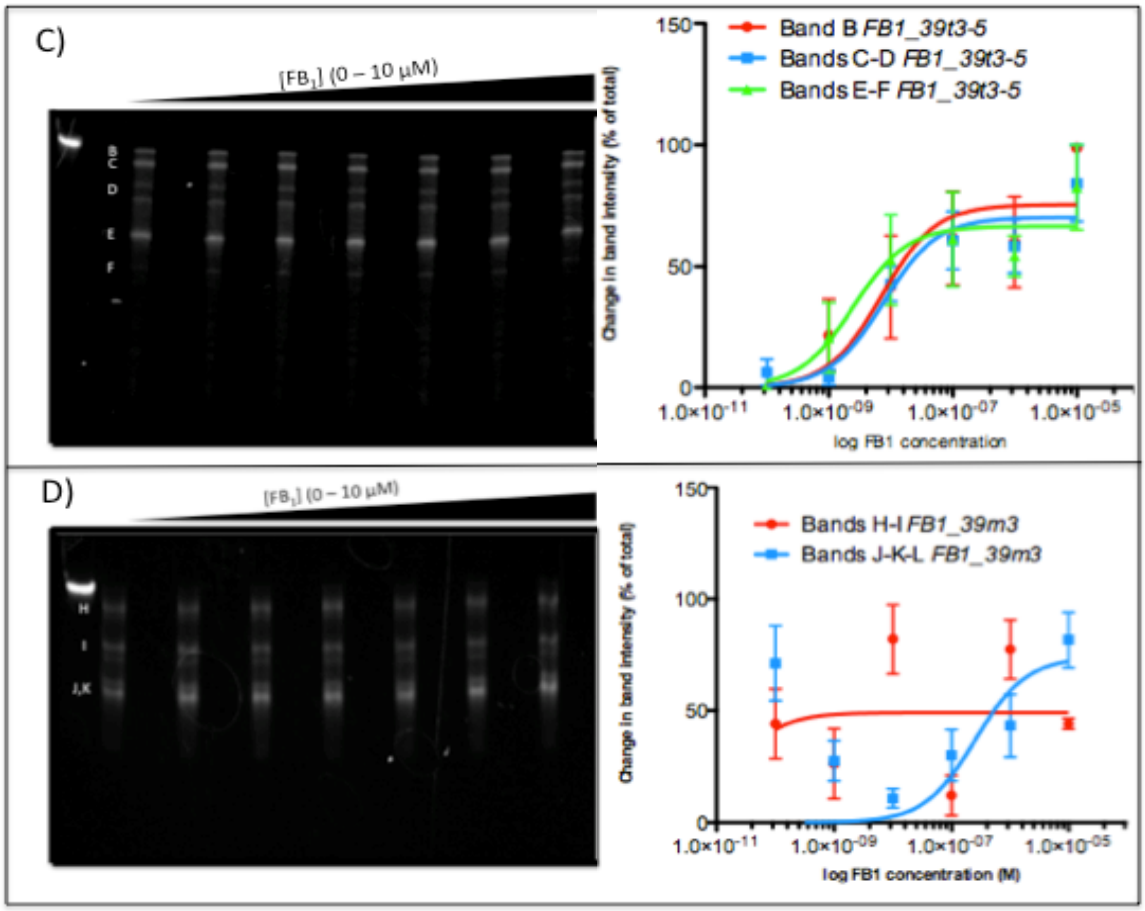
C)
[FB1] (0 – 10 µM)
B
C
D
E
F
Change in band intensity (% of total)
150
100
50
0
Band B FB1_39t3-5
Bands C-D FB1_39t3-5
Bands E-F FB1_39t3-5
1.0×10-11
1.0×10-09
1.0×10-07
1.0×10-05
log FB1 concentration
D)
[FB1] (0 – 10 µM)
H
I
J,K
Change in band intensity (% of total)
150
100
50
0
Bands H-I FB1_39m3
Bands J-K-L FB1_39m3
1.0×10-11
1.0×10-09
1.0×10-07
1.0×10-05
log FB1 concentration (M)

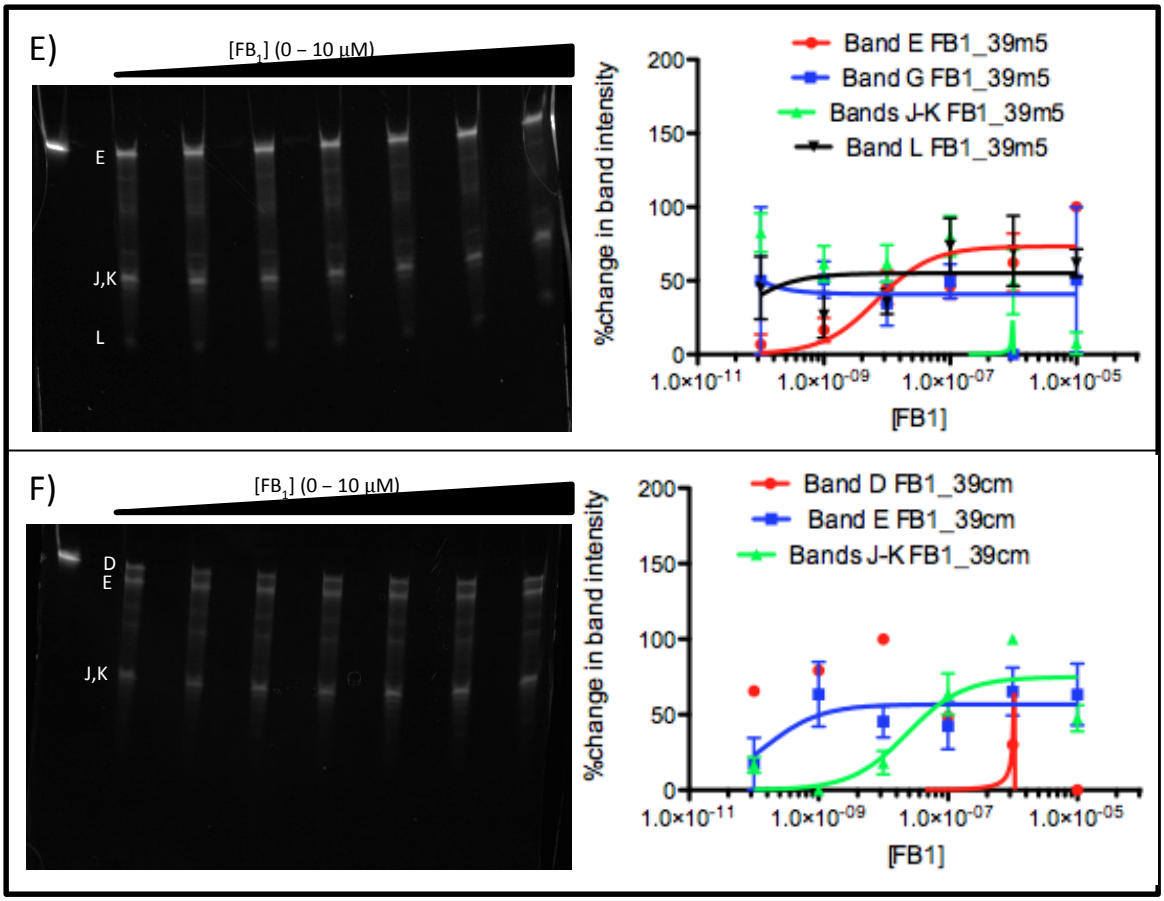

Figure 2.6 DNase I digestion PAGE gels and K_d results for *FB1_39* minimers. A) *FB1_39t3*, B) *FB1_39t5*, C) *FB1_39t3-5*, D) *FB1_39m3*, E) *FB1_39m5*, F) *FB1_39cm*

Table 2.8 Summary table of average K_d ± error for each aptamer (*$FB_1$39* and minimers) for each region of the PAGE gel, separated into Top / Middle / Bottom, representing the regions of fragments produced as separated by PAGE. N.B. = no binding, indicating band intensity did not consistently change with target concentration at this digestion band

Aptamer	Avg. K_d ± error (nM)					
	Top		Middle	Bottom		
FB1 39	9.6 ± 7.7	41.8 ± 16.3	2.8 ± 2.4	11.6 ± 5.0		
FB1_39t3	15.1 ± 11.5		6.5 ± 4.6	0.9 ± 0.8		
FB1_39t5	3.7 ± 2.8		2.8 ± 2.7	2.0 ± 2.7		
FB1_39t3-5	7.1 ± 5.9		7.6 ± 4.4	2.5 ± 2.2		
FB1_39m3	N.B.		N.B.	N.B.		
FB1_39m5	6.9 ± 4.6		N.B.	N.B.	N.B.	
FB1_39cm	0.2 ± 0.2		N.B.	23.3 ± 16.8		

From Table 2.8, it can be noted that the "Top" region of digestion bands produces the most consistent K_d's. The shorter minimers (*FB1_39m3*, *FB1_39m5*, and *FB1_39cm*) have the least consistent binding; *FB1_39m3* retains no affinity to FB_1, and *FB1_39m5* only retains affinity in the "Top" digestion band (full minimer). The full length *FB_1 39* and longer minimers (*FB1_39t3*, *FB1_39t5*, and *FB1_39t3-5*) retain the most consistent binding affinity over all regions of the aptamer. One digestion fragment, Band E, is conserved within all of the minimer sequences except *FB1_39m3*, which did not display any affinity. "Band E" displayed the greatest change in intensity with concentration of target, and is the most intense band within the PAGE gels. This indicates that there is a high propensity of DNase I cleavage at the site producing this fragment and that its structure is modified in some way by target binding. The average K_d of Band E in each sequence is summarized below (Figure 2.7).

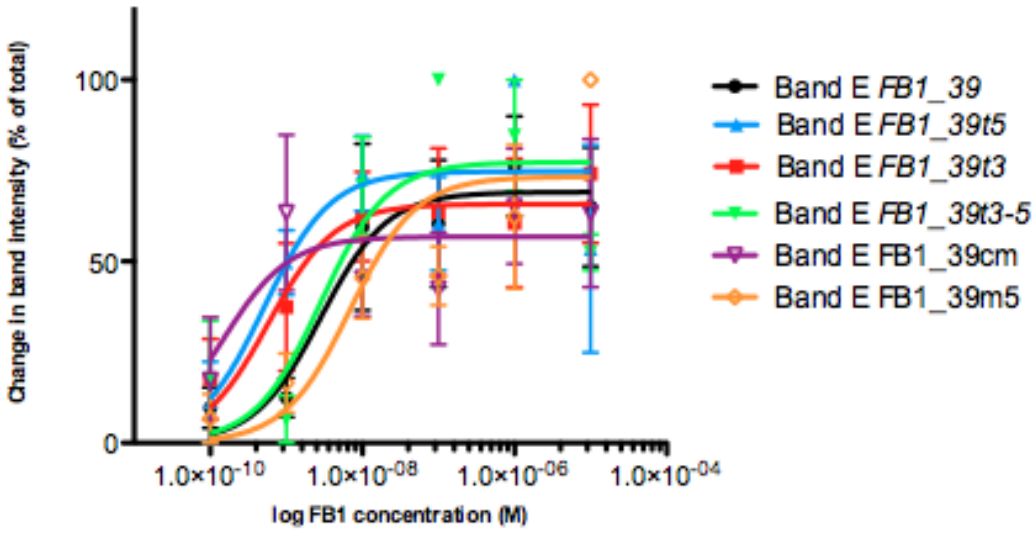

Aptamer	Avg. K_d ± error Band E (nM)
FB1 39	2.9 ± 2.4
FB1_39t3	0.6 ± 0.5
FB1_39t5	0.5 ± 0.4
FB1_39t3-5	2.8 ± 2.7
FB1_39m3	N.B.
FB1_39m5	6.9 ± 4.6
FB1_39cm	0.2 ± 0.2

Figure 2.7 Average K_d ± error for "Band E" from *FB1 39* and all minimers. N.B. indicates no binding was observed (not present)

The minimer *FB1_39m5* corresponds to digestion fragment (from the 5' terminus) of Band E, and is 38 nt in length. *FB1_39cm* is a central minimer designed to surround the site of digestion that produces Band E, and is 50 nt in length. *FB1_39cm* was also designed to include the probe region in the 3' stem loop motif that has been suggested to

be involved in FB_1 binding in probe-displacement sensor designs[127, 160] (Figure 2.1). All minimers except for *FB1_39m3* displayed low nM affinity for FB_1 at this region.

2.5.2.3.2 $FB_1$14, $FB_1$23, $FB_1$31, $FB_1$32 & F10

2.5.2.3.2.1 DNase I digestion fragment analyses

The FB_1 aptamer sequences were digested by DNase I and separated by PAGE gel to estimate fragment lengths (Figure 2.8).

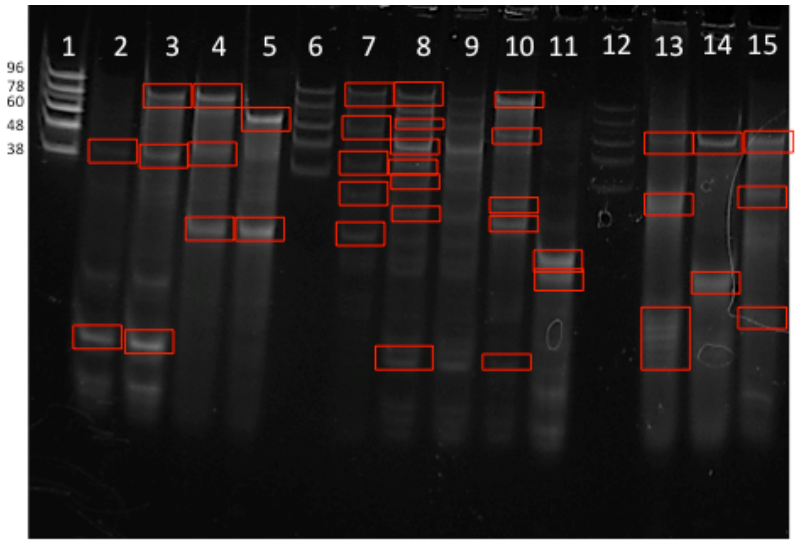

1 – 5′-fluorescein labelled DNA ladder (5x conc.)
2 – *FB_1 32* DNase digest – 49 (B); 16 (F)
3 – *FB1_32t3* DNase digest – 79 (A); 48 (B); 9 (F)
4 – *FB1_32t5* DNase digest – 78 (A); 48 (B); 25 (C)
5 – *FB1_32t3-5* DNase digest – 65 (A); 24 (C)
6 – 5′-fluorescein labelled DNA ladder
7 – *FB_1 14* DNase digest – 81 (B); 58 (C); 43 (D); 33 (E); 23 (H)
8 – *FB_1 16* DNase digest – 79 (B); 62,70 (C); 50 (D); 43 (E); 37,29 (F); 19,17 (G,H); 8 (I)
9 – *FB_1 16* DNase digest (repeat)
10 – *FB_1 31* DNase digest – 76 (A); 56 (B); 30 (C); 26 (D); 7 (G)
11 – *F10* DNase digest – 19 (C); 16 (D)
12 – 5′-fluorescein labelled DNA ladder
13 – *2-way junction* DNase digest – 53 (4); 29 (3); 10 (2)
14 – *3-way junction* DNase digest – 52 (5); 15 (3)
15 – *long hairpin bulge* DNase digest – 53 (5); 33 (3); 11 (2)

Figure 2.8 PAGE gel with the DNase I digests of *$FB_1$14, $FB_1$23, $FB_1$16, $FB_1$31, $FB_1$32* and minimers, *F10,* and rationally designed secondary structure sequences. Lane 1 is a fluorescently labelled DNA ladder to calculate approximate lengths of digestion fragments. For each lane, the digestion fragment length is indicated in the legend with the corresponding band from the DNase I PAGE gel analysis for each aptamer. Fragment lengths were calculated with the Molecular Weight function in AlphaImager, AlphaInnotech.

Similarly, the 5' PBR-truncated minimers for *$FB_1$32* (*FB1_32t5* and *FB1_32t3-5*, Lanes 4 and 5) display an apparent new digestion fragment of approximately 25 nt, which corresponds to a digestion site in the sequence that produces the 48 nt fragment in the non-5'-truncated sequence. *$FB_1$32* has a high degree of predicted secondary structure, particularly in its central region. From Table 2.6, the T_ms and RNA Structure folds were very similar between the full-length structure and minimers.

$FB_1$14, *$FB_1$16*, and *$FB_1$31* have very regular increments of predicted secondary structure (Figure 2.8), and accordingly their digestion profiles after DNase I treatment produce a regular banding pattern (Lanes 7, 8 and 10). *F10* has two prominent bands, "Band C" and "Band D" that correspond to DNase I cleavage within a region of high predicted secondary structure (Figure 2.9 Panel F).

2.5.2.3.2.2 DNase I assay results

The FB_1 aptamers (*$FB_1$14*, *$FB_1$23*, *$FB_1$31*, *$FB_1$32*, and *F10*) were analyzed by the DNase I assay. The digestion bands for each aptamer have been assigned alphabetically. A minimum of four gel replicates for each sequence have been assembled to determine an average K_d for each prominent band based on the change in total band intensity due to target concentration. The FB_1 aptamers are presented below in Figure 2.9. Each panel contains the DNase I digestion PAGE gel of the aptamer and resulting K_ds for each prominent group of digestion bands. Panel A: *$FB_1$14*; Panel B: *$FB_1$16*; Panel C: *$FB_1$23*; Panel D: *$FB_1$31*; Panel E: *$FB_1$32*; Panel F: *F10*.

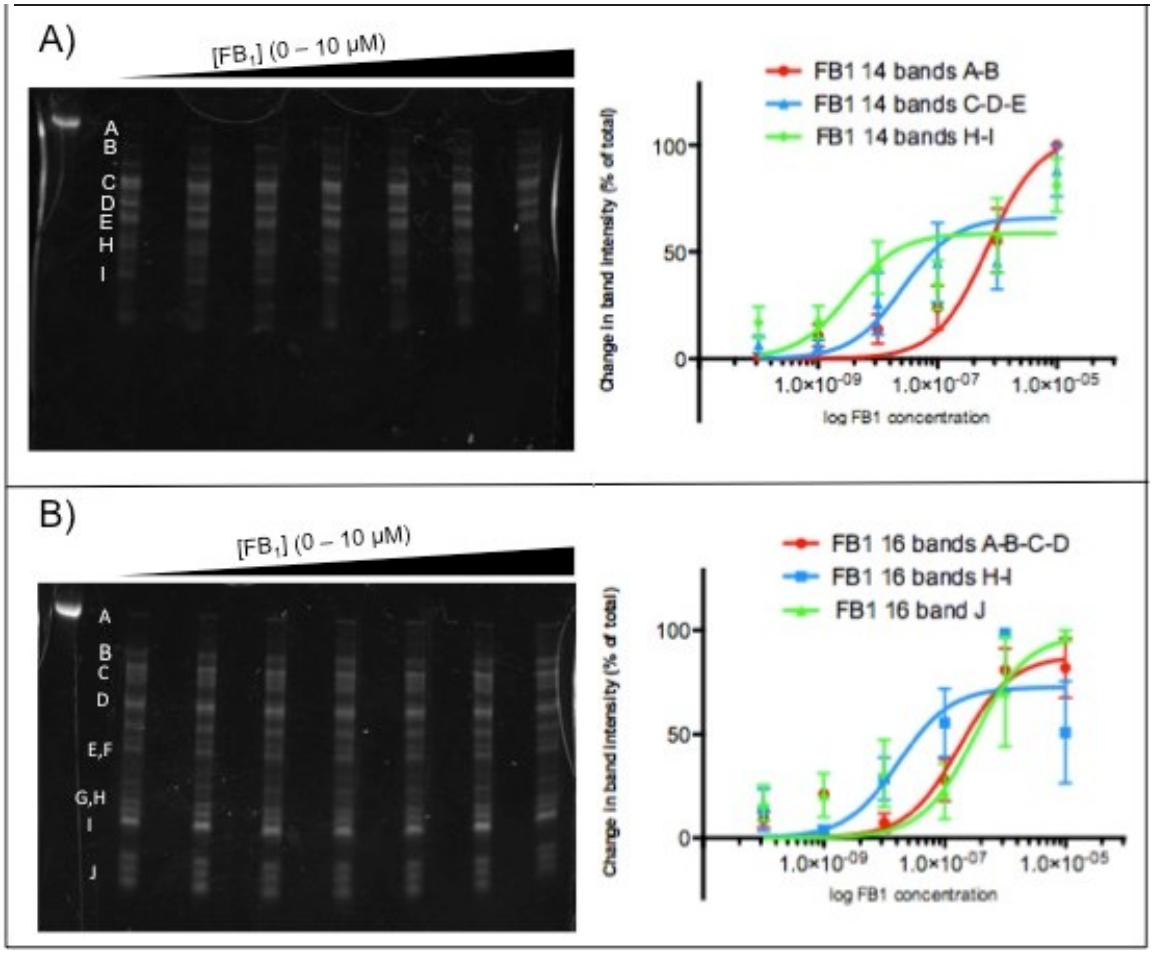
A)
[FB1] (0 – 10 μM)
A
B
C
D
E
H
I
FB1 14 bands A-B
FB1 14 bands C-D-E
FB1 14 bands H-I
Change in band intensity (% of total)
100
50
0
1.0×10-09
1.0×10-07
1.0×10-05
log FB1 concentration
B)
[FB1] (0 – 10 μM)
A
B
C
D
E,F
G,H
I
J
FB1 16 bands A-B-C-D
FB1 16 bands H-I
FB1 16 band J
Change in band intensity (% of total)
100
50
0
1.0×10-09
1.0×10-07
1.0×10-05
log FB1 concentration

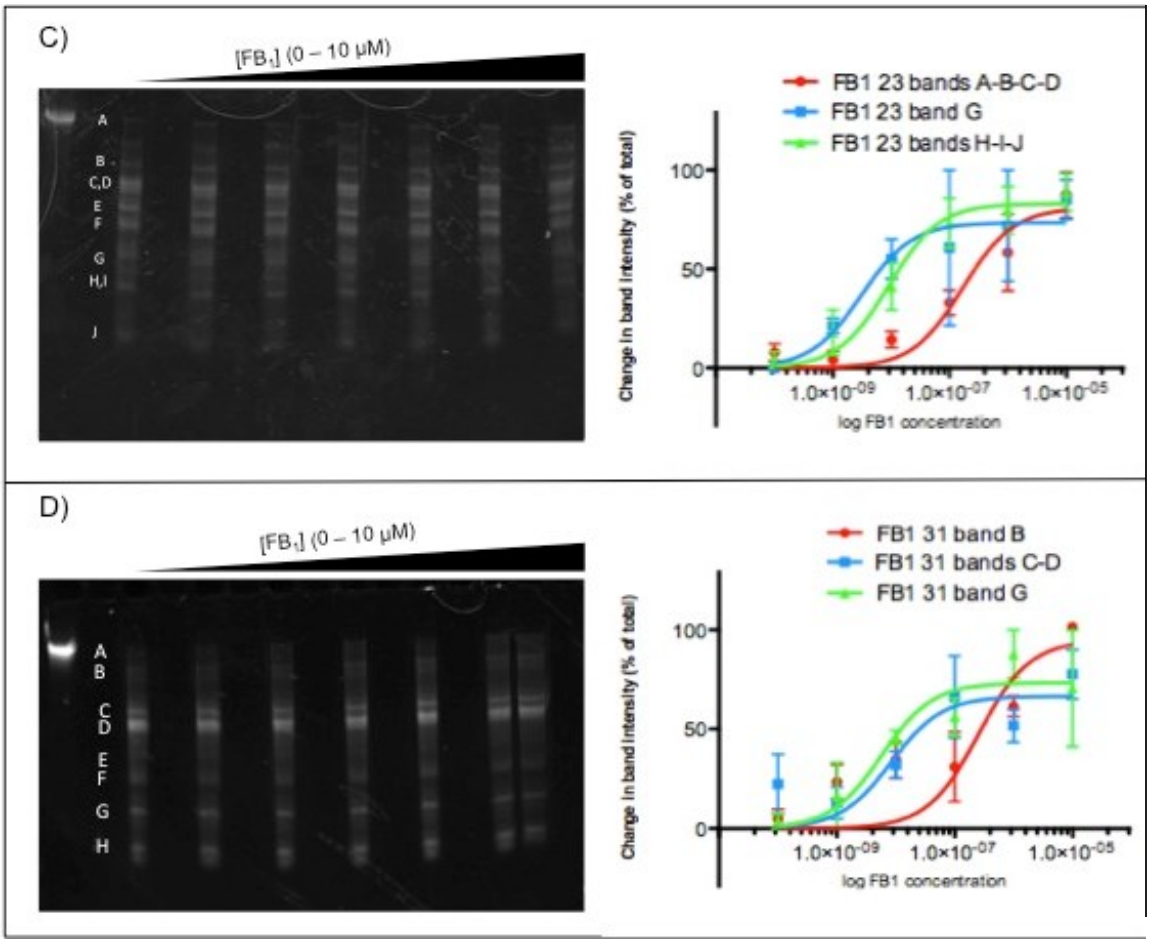
C)
[FB1] (0 – 10 µM)
A
B
C,D
E
F
G
H,I
J
FB1 23 bands A-B-C-D
FB1 23 band G
FB1 23 bands H-I-J
Change in band intensity (% of total)
100
50
0
1.0×10-09
1.0×10-07
1.0×10-05
log FB1 concentration
D)
[FB1] (0 – 10 µM)
A
B
C
D
E
F
G
H
FB1 31 band B
FB1 31 bands C-D
FB1 31 band G
Change in band intensity (% of total)
100
50
0
1.0×10-09
1.0×10-07
1.0×10-05
log FB1 concentration

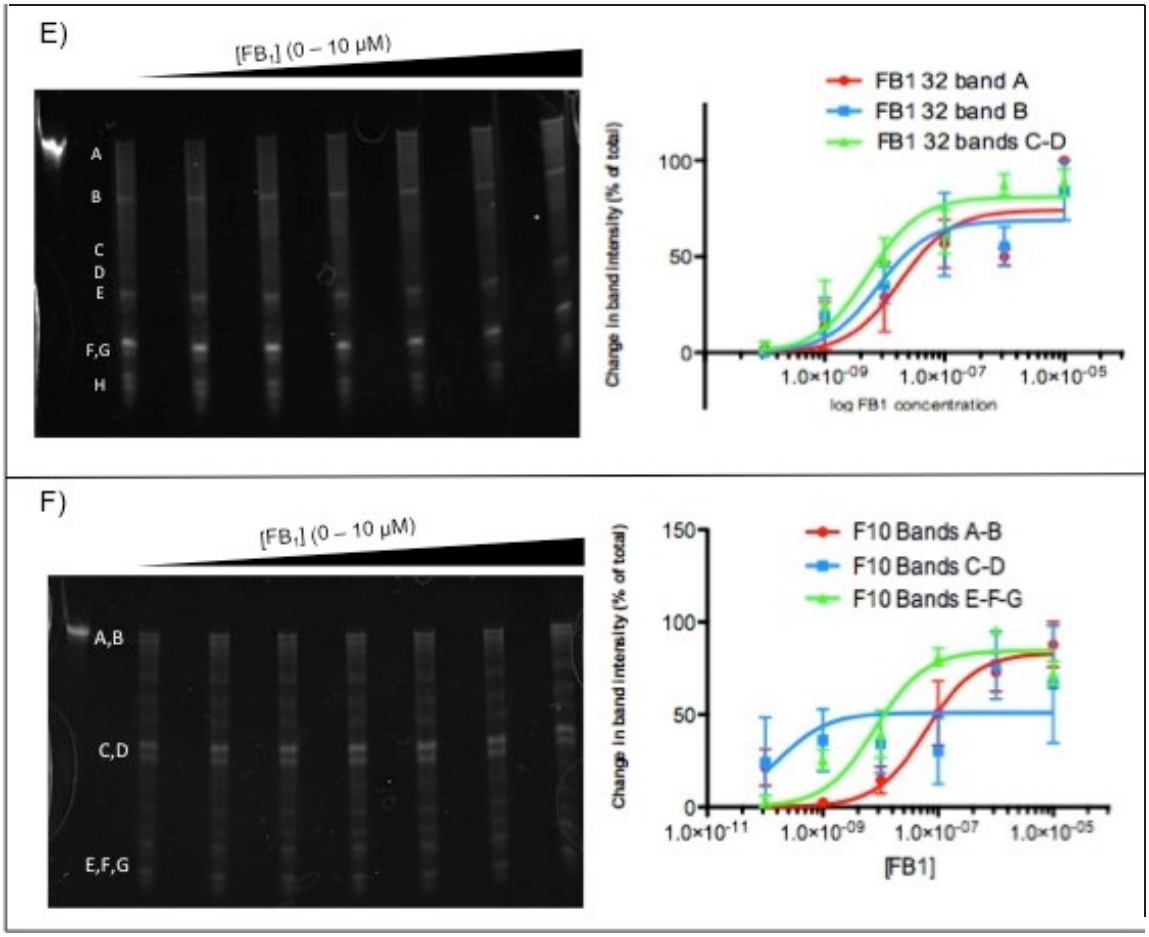

Figure 2.9 DNase I digestion PAGE gels and K_d results for remaining FB_1 aptamers. A) *$FB_1$14*, B) *$FB_1$16*, C) *$FB_1$23*, D) *$FB_1$31*, E) *$FB_1$32*, F) *F10*

Table 2.9 Summary table of average K_d ± error for each aptamer for each region of the PAGE gel, separated into Top / Middle / Bottom, representing the regions of fragments produced as separated by PAGE. N.B. = no binding, indicating band intensity did not consistently change with target concentration at this digestion band

Aptamer	Avg. K_d ± error (nM)		
	Top	Middle	Bottom
FB_1 14	698.6 ± 297.3	25.9 ± 22.3	3.2 ± 3.0
FB_1 16	174.1 ± 14.9	17.2 ± 14.9	311.5 ± 257.7
FB_1 23	170.0 ± 94.8	3.1 ± 3.0	89.9 ± 4.4
FB_1 31	254.4 ± 161.2	8.4 ± 6.7	5.7 ± 4.4
FB_1 32	18.3 ± 13.5	7.8 ± 5.9	5.4 ± 2.6
F10	61.7 ± 35.8	0.2 ± 0.3	7.9 ± 2.9

Table 2.9 summarizes the average K_d and associated error for the regions of each aptamer (top, middle, bottom). *$FB_1$14* had the most prominent bands in the middle and bottom of the PAGE gel, corresponding the lowest K_d, or highest affinity. Similarly for *$FB_1$16*, the most prominent bands in the PAGE gel (H, I) corresponded with the highest affinity (17.2 ± 14.9 nM). *$FB_1$23* and *$FB_1$31* had the highest affinity of interaction with FB_1 in the middle and bottom regions of the PAGE gel. Of these FB_1 aptamers, *$FB_1$32* had the highest affinity of change based on target concentration, with all regions of the aptamer associated with low nM affinity. *F10* also retained low nM affinity to target over all digestion regions, but with less consistency between digestion bands.

It is interesting to note that for many of the FB_1 aptamers examined, the PAGE gels of DNase I digestion indicated that a very small fraction of full-length aptamer was remaining. For most sequences, with increasing target concentration, the intensity of the full-length aptamer increased (particularly for *$FB_1$32*, Figure 2.9 panel E). This suggests

that as more target binds to the aptamer, the aptamer is less accessible to DNase I digestion suggesting a subtle protection against DNase I by target binding.

2.5.2.3.3 Summary K_ds for FB_1 aptamers

Figure 2.10 below summarizes the average K_ds for all bands of each FB_1 aptamer by DNase I assay. When averaged out between all bands, the aptamers clustered into two ranges: low nM affinity (*$FB_1$39*, *$FB_1$31*, *$FB_1$32*, *F10*) and mid-nM affinity (*$FB_1$14*, *$FB_1$16*, and *$FB_1$23*).

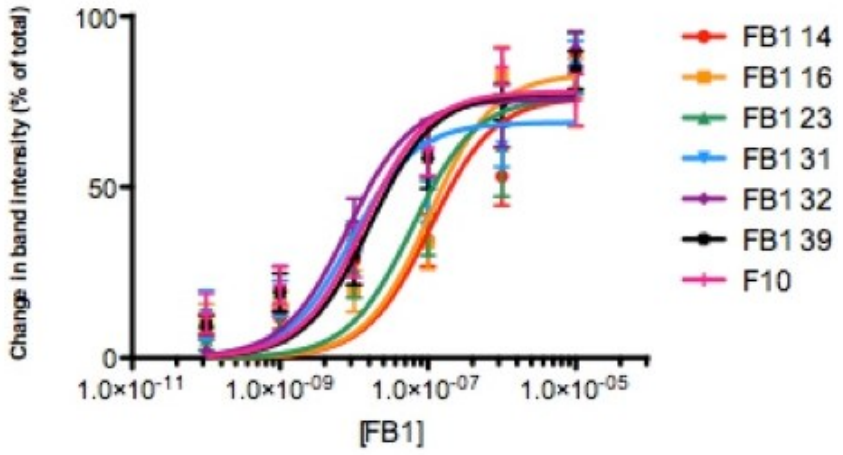

Aptamer	Avg. K_d ± error (nM)
$FB_1$39	16.3 ± 5.9
$FB_1$14	107.8 ± 44.0
$FB_1$16	104.3 ± 40.7
$FB_1$23	61.4 ± 33.6
$FB_1$31	9.2 ± 4.3
$FB_1$32	8.3 ± 2.9
F10	13.5 ± 5.1

Figure 2.10 Summary of overall average K_ds ± error for each FB_1 aptamer studied

Further work would be merited to examine the relationship between aptamer structure and affinity for this group of FB_1 aptamers. The affinities of the aptamers are

split into two clusters, mid- and low-nM K_d. There is no obvious distinction between the mid- and low-nM binders with regards to their predicted secondary structures or experimental melting temperatures.

2.5.2.3.4 Controls (OTA, FB_2)

$FB_1$39 was analyzed by the DNase I assay with two non-FB_1 targets as controls (Figure 2.11). FB_2 is structurally very similar to FB_1 and differs by the absence of a single hydroxyl residue at the carbon 11 position (Figure 1.1). OTA was chosen as a small molecule mycotoxin control. FB_2 and OTA were not used as counter-selections during the SELEX of *$FB_1$39*.[113]

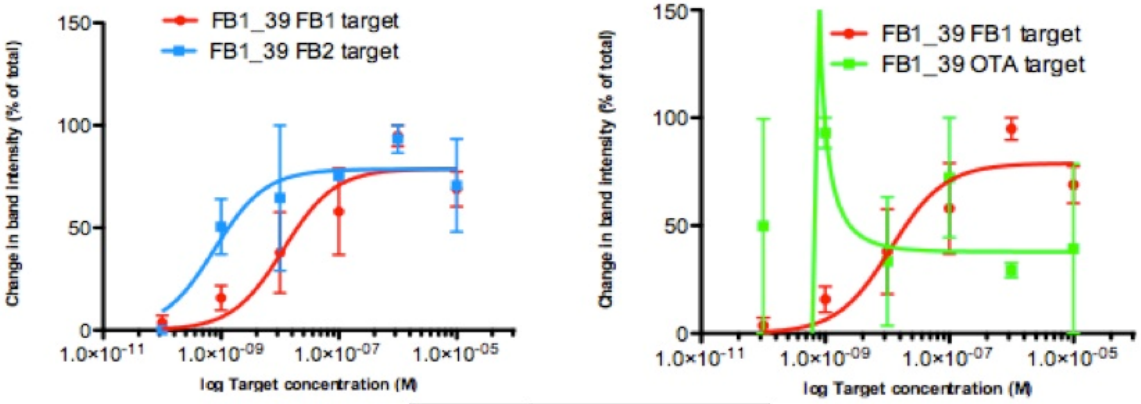

Target	Avg. K_d ± error (nM) Band E FB_1 39
FB_1	2.8 ± 2.4
FB_2	0.8 ± 0.7
OTA	N.B.

Figure 2.11 DNase I assay control targets FB_2 and OTA indicating the K_d of "Band E" for comparison to binding to FB_1

$FB_1$39 displayed no affinity to OTA and retained a low nM binding affinity to the structurally similar FB_2 under the conditions of the DNase I assay. Given the close

structural similarity between FB_2 and FB_1, it is not surprising to see high affinity binding of *$FB_1$39* to FB_2 in solution.

2.5.2.4 Ochratoxin aptamers

OTA aptamers (*A08*, *B08*, *1.12*, *1.12.2*, *H8*, and *H12*) were analyzed by the DNase I assay. A minimum of two gel replicates for each sequence have been assembled to determine an average K_d for each aptamer. The average K_d has been represented by the K_d of a prominent fragment band that displayed consistent change in total band intensity due to target concentration. The OTA aptamers are presented below in Figure 2.12. The predicted secondary structure for each aptamer is shown as determined by RNA Structure. It must be noted that RNA Structure does not predict the G-quadruplex motif, which is known to be important in binding of *1.12.2* to OTA.[110] DNase I activity is also known to be slightly less efficient in G-rich regions.[176] Each panel also contains the DNase I digestion PAGE gel of the aptamer, with a red box highlighting the digestion band selected for K_d analysis.

1.12

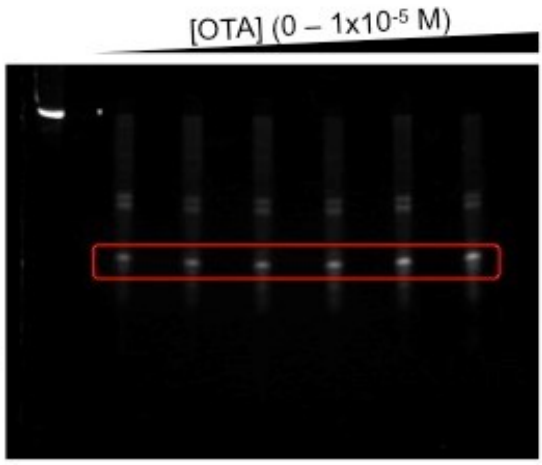

A08

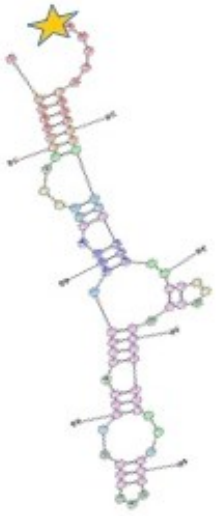

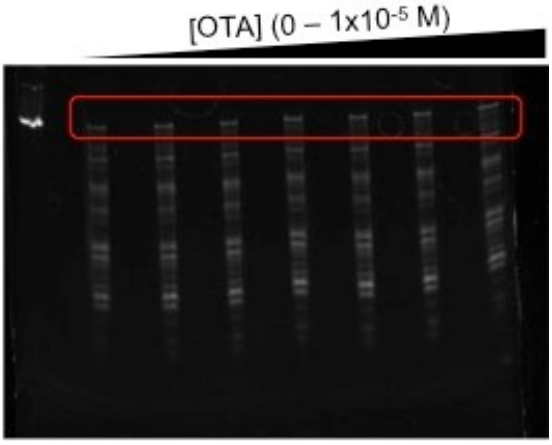

1.12.2

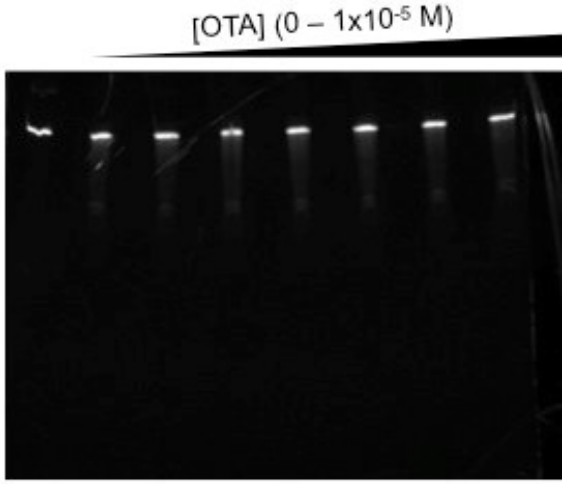

B08

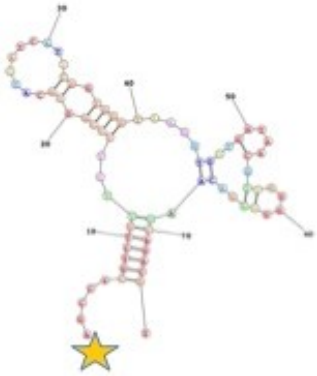

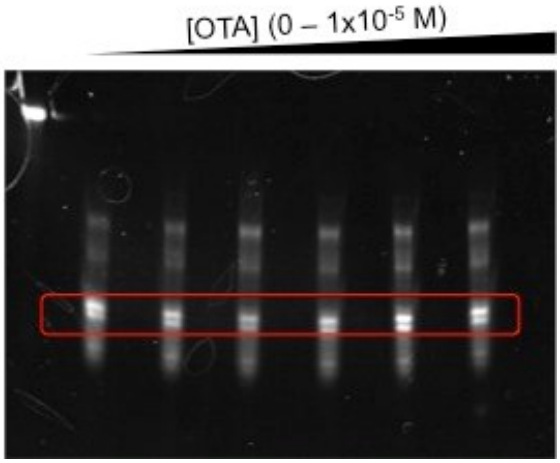

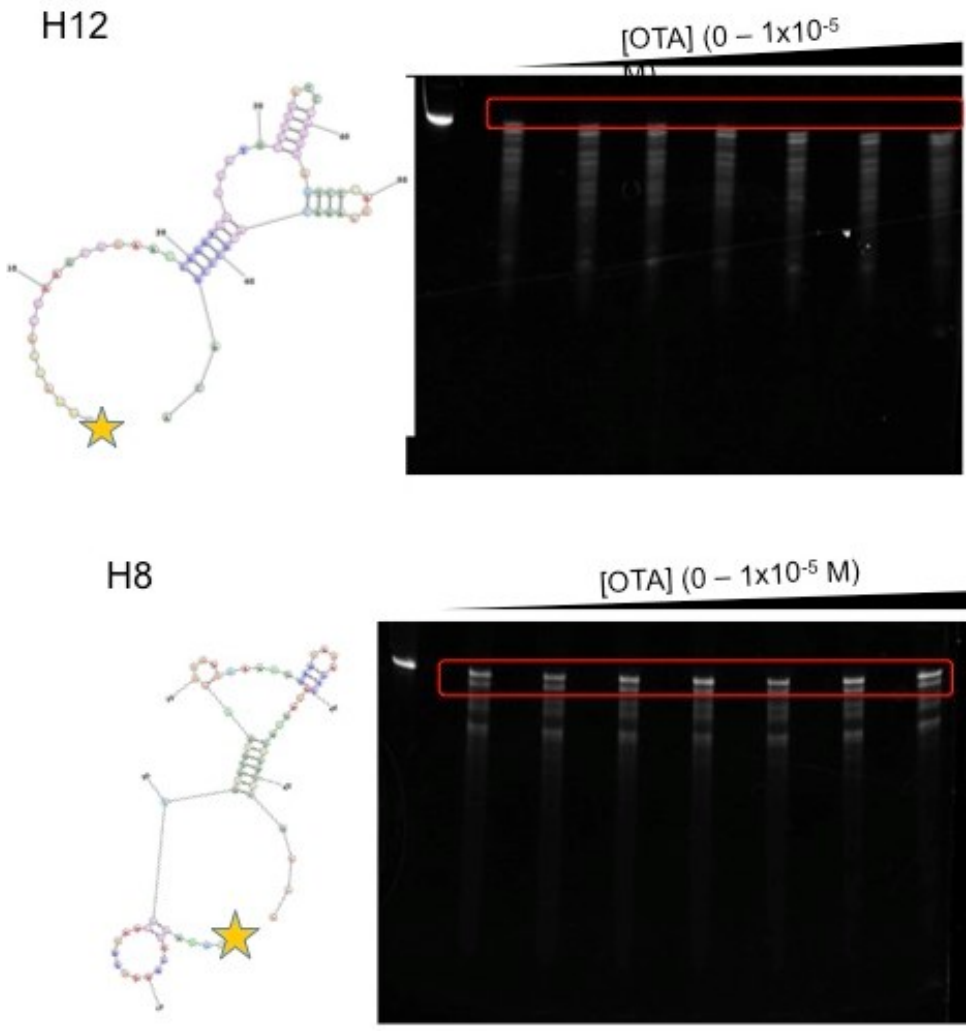

Figure 2.12 OTA aptamer analysis by DNase I assay

All of the OTA aptamers studied displayed binding to OTA in solution when measured by this assay with the exception of *1.12.2*. It must be noted that a drawback of this assay is that it is not compatible with previously minimized aptamers. Essentially no cleavage results from the digestion of *1.12.2* with DNase, thus monitoring a change in band pattern is not possible. This is likely due to the fact that the previously minimized sequence (36 nt) is not accessible to DNase I digestion. Both *A08* and *B08* have a high

degree of predicted secondary structure and accordingly display a large number of digestion fragments after DNase I treatment.

The resulting in-solution K_ds from the DNase I assay for each OTA aptamer are summarized in Figure 2.13.

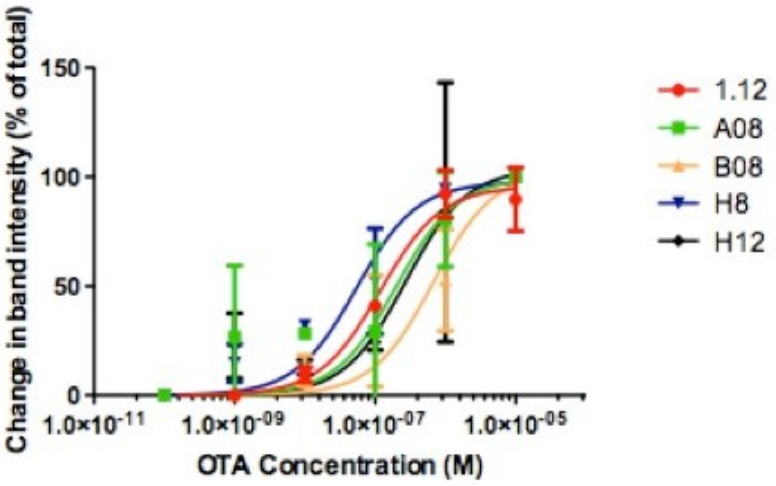

Aptamer	Avg. K_d ± error (nM)
1.12	118 ± 30
A08	200 ± 157
B08	670 ± 331
H8	53.8 ± 23.3
H12	270 ± 201

Figure 2.13 K_ds for the OTA aptamers from the DNase I assay, fit by GraphPad Prism version 5.00 non-linear regression one-site specific binding.

H8 displays the highest in-solution binding affinity (53.8 nM), *H12*, *1.12* and *A08* are in the mid-nM range, and *B08* is in the high nM range. The OTA aptamers have been further characterized by multiple other K_d determining methods suitable for small molecules.[186] Due to the inherent fluorescence of OTA, more methods are available as the target molecule can be easily tracked in an in-solution system. The K_ds determined by DNase I assay track well with the range of magnitude of K_ds from other methods

(equilibrium dialysis, ultra-filtration, fluorescence polarization, affinity chromatography, SPR, and SYBR Green I) within error and understanding that the method of determining K_d will affect the resulting K_d due to changes in many factors, such as tethering either the target or aptamer, or buffer conditions.

2.5.3 Magnetic bead binding assay

2.5.3.1 Assay design

Magnetic bead affinity chromatography is often used as a screening method of putative aptamers after SELEX, particularly in cases where the SELEX is performed with target bound to magnetic beads. The scheme of the technique used to evaluate binding affinity of FB_1 aptamers to a bound FB_1 target is shown below (Figure 2.14).

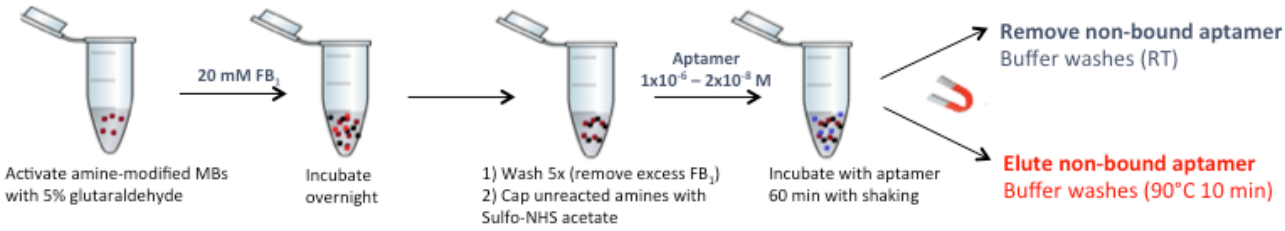

Figure 2.14 Assay design of magnetic bead assay for determining affinity of aptamers to bound target

The affinities of the OTA aptamers studied by the DNase I assay have been previously tested with the magnetic bead binding assay, and were therefore not tested again. The K_ds of the OTA aptamers from the magnetic bead binding assay were: *A08* (286 ± 159 nM), *B08* (125 ± 44 nM), *H12* (40 ± 14 nM), *H8* (14 ± 7 nM), and *1.12.2* (374 ± 255 nM).[186]

2.5.3.2 Binding of *FB1 39* and minimers

Figure 2.15 below shows the binding affinity of *FB1 39* and four minimers to FB_1 covalently conjugated to magnetic beads.

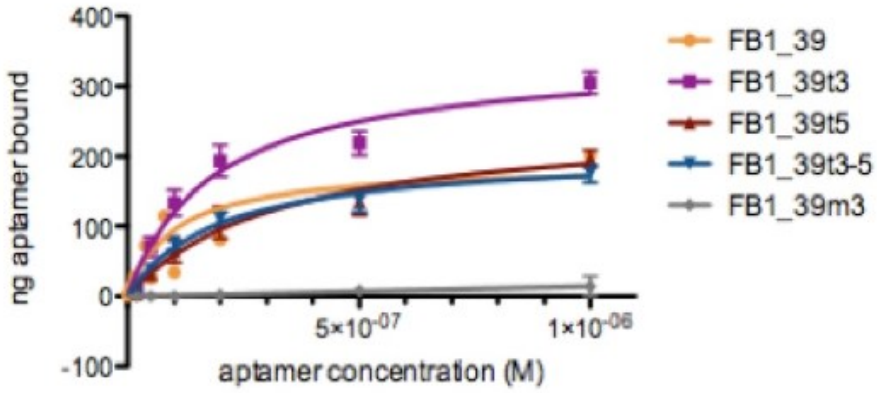

Aptamer	K_d ± error (nM)
FB1_39	99 ± 31
FB1_39t3	184 ± 43
FB1_39t5	328 ± 106
FB1_39t3-5	195 ± 45
FB1_39m3	N.B.

Figure 2.15 Magnetic bead binding affinity of *FB1 39*, *FB1_39t3*, *FB1_39t5, FB1_39t3-5*, and *FB1_39m3*. The reported K_d is the average of three independent replicates.

All aptamers were tested on control beads (free amine groups capped with Sulfo-NHS Acetate, no FB_1 present) and negligible levels of non-specific binding were observed. The full-length *FB1 39* aptamer bound with the highest affinity to bound FB_1, with a K_d of 99 ± 31 nM. This result is very similar to the K_d of *FB1 39* (100 ± 30 nM) reported by McKeague *et al* (2010) using a similar FB_1-bound magnetic bead assay.[113] Obtaining essentially an identical K_d value for the full-length aptamer ensues confidence to compare the performance of the developed minimers to bound FB_1 (Figure 2.15). Of

the tested minimers, *FB1_39t3* and *FB1_39t3-5* had the best affinities (184 ± 43 and 195 ± 45 nM respectively), and *FB1_39t5* reported a slightly lower affinity (328 ± 106 nM). It can be noted that of all the sequences tested, *FB1_39t3* had the highest total bound aptamer to the FB_1-bound magnetic beads. *FB1_39m3* had negligible binding to the FB_1-bound magnetic beads, and no observed affinity. This minimer also displayed no affinity to FB_1 in the DNase I assay (Figure 2.7). Through comparing both assays to determine binding to both in-solution and bound target, it can be concluded that this minimer has no affinity for FB_1 under the tested conditions. This indicates that, although the 3'-stem loop motif may be an important contributor to aptamer binding, it can not bind to FB_1 independently of regions further 5' downstream of this minimer.

2.5.3.3 Control aptamer (*A08*)

To confirm the binding of the tested aptamers to FB_1-bound magnetic beads, a control aptamer (*A08*, with affinity for OTA) was tested under identical conditions (Figure 2.16). Some non-specific binding was observed, but no strong affinity was noted.

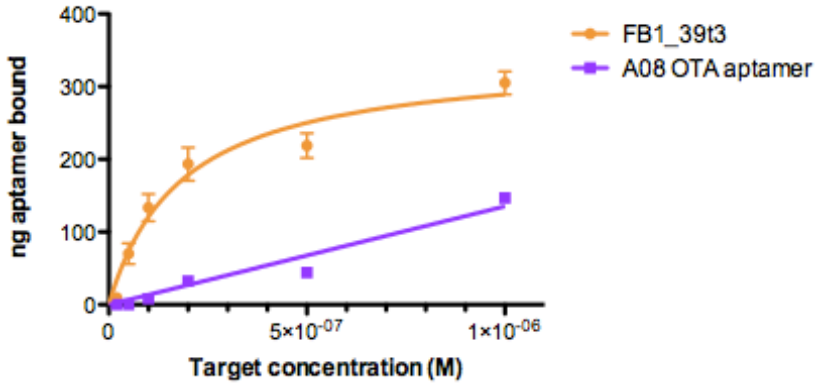

Figure 2.16 *A08* control aptamer (with affinity for OTA)[111] showing a background level of non-specific binding to FB_1-bound magnetic beads. *FB1_39t3* is shown in comparison.

The magnetic bead binding assay is useful for rapid affinity testing of aptamers, and is often used as an initial screening method for putative aptamer sequences after SELEX if the selection was performed with bead-bound target. However, this assay is susceptible to non-specific binding of aptamer to beads, and is limited to measuring the affinity of the aptamer to the target covalently bound to a solid support. The increase in steric hindrance can affect the apparent affinity. Additionally, this assay is not applicable to screening affinity of aptamers for many downstream sensor applications that require aptamer recognition in solution to a free target rather than to a bound target.

2.6 Conclusions

A novel application of a DNase I digestion assay is described, which facilitates study of the structure and affinity of aptamers binding to small molecule targets. FB_1 and

OTA are important small molecule mycotoxins, and aptamers for these two compounds were used as model aptamers for the DNase I assay.

Six putative *$FB_1$39* minimers were screened with the DNase I assay to cover the range of the aptamer structure and determine what regions were imperative to retain binding affinity to FB_1 in solution. Five of these minimers displayed low nM affinity to FB_1 in solution, ranging from 78 nt to 38 nt in length. These affinities were compared to the results from the well-established magnetic bead assay. *FB1_39t3* and *FB1_39t3-5* (78 and 60 nt respectively) displayed comparable high affinity binding to FB_1 both bound and in solution to the full-length sequence, and would be excellent candidates to integrate into downstream sensor applications.

Six OTA aptamers were screening with the DNase I assay to facilitate a comparison of this technique to other well-established and novel K_d methods that have been performed on these aptamers. This assay was shown to not be effective for determining the K_d of previously minimized sequences containing a G-quadruplex (*1.12.2*).

Importantly, this assay is one of the few methods that permits the measurement of aptamer–small molecule binding in solution that does not rely on inherent fluorescence properties of the target. This makes the method generally applicable to all small molecule aptamers and furthermore, provides a more realistic understanding of the aptamer-target interaction for downstream sensor applications that would also require free target in solution.

3.0 Nanoaptasensors for mycotoxins

3.1 Introduction

3.1.1 Quantum dots

Quantum dots (QDs) are fluorescent semiconductor nanocrystals with unique properties that render them useful as probes for imaging and sensing, in addition to many other diverse applications. QDs are predominantly composed of CdSe or CdTe nanocrystals, and can be coated with high-band gap semiconductor materials such as ZnS to achieve enhanced quantum yields.[153] QDs are defined by the fact that their diameters are less than the Bohr exciton radius and their energy levels are quantized, resulting in a very narrow electron band with a long lifetime during photon emission.[187] The unique size- and shape-tunable optical and electronic properties of QDs can be controlled during their synthesis.[187] QDs have tunable emission wavelengths that facilitate multi-colour QD emissions upon excitation at a single wavelength, making them excellent FRET donors, especially in multiplex assays.[137, 153, 187-189] QDs have shown superior photostability relative to organic fluorophores.[153, 187] One challenge for integrating QDs into sensors is the need for a hydrophilic coating to maintain the colloidal stability of the nanocrystals during use.[153] QDs have been shown to undergo fluorescence quenching through aggregation[190] or through surface disruption by surfactant molecules.[191]

3.1.2 Gold nanoparticles (AuNPs)

AuNPs are formed by the reduction of chlorauric acid ($HAuCl_4$) to form a colloidal suspension with unique optical properties. AuNPs have strong localized surface plasmon resonance (SPR) absorption when incident wavelengths of light cause free electron oscillation in their conduction bands. The SPR absorption of AuNPs is distance

dependent; dispersed AuNPs absorb at ~ 520 nm and aggregated AuNPs absorb at ~ 650 nm.[137, 188] In sensors, AuNPs are often exploited for their colourimetric response upon aggregation (visual red to purple transition). AuNPs can also be used as fluorescence quenchers through FRET, acting as fluorescence acceptors.[137] Gold nanorods (AuNRs) can also be used in this manner, with the added benefit of having two SPR absorptions, latitudinal and longitudinal.[192]

3.1.3 Carbon-based quenchers

Carbon nanotubes (CNTs) were discovered by Iijima *et al* (1991) by transforming sheets of graphitic carbon into cylindrical tubes using an arc-discharge evaporation method.[193] Single-walled CNTs (SWCNTs) can be either semiconducting or metallic depending on their orientation (*i.e.* zig zag, armchair). The chemically stable nanotubes have a high length to diameter ratio.[194] SWCNTs can be used as fluorescence quenchers (FRET acceptors) in nanosensors.

Unmodified (pristine) SWCNTs have high cohesive forces that bundle them together limiting their solubility and dispersion in aqueous conditions. Dispersion of SWCNTs is achieved by physical means (*i.e.* sonication in the presence of surfactant), or physiochemical covalent modifications (*i.e.* oxidation by treatment with HNO_3). Oxidized SWCNTs add functional groups (*i.e.* COOH, COH) to the carbon matrix, converting the modified bonds from sp^2 to sp^3.[195] The dispersion of SWCNTs can be monitored and quantified by imaging (TEM, SEM) or spectroscopic techniques. Optical

absorptions and emissions in NIR range are most informative for monitoring dispersion.[196]

Graphene oxide (GO) is an oxidized graphite monolayer that contains dispersed nanosheets soluble in aqueous conditions. GO is a highly efficient quencher for use as a fluorescence acceptor in FRET sensors.[153] Due to its wide range of absorption over the fluorescence (*i.e.* QDs) and luminescence (*i.e.* UCNPs) spectra, GO is well suited to multiple sensors.[153]

ssDNA will adsorb to the surface of SWCNTs and GO through $\pi - \pi$ stacking, bringing fluorophores into close proximity to facilitate quenching.[137] ssDNA adsorbs to GO and SWCNTs with a much higher efficiency than dsDNA through interactions with the exposed nitrogenous bases; desorption is facilitated by adding either an aptamer complement or target.[197-198]

3.1.4 SYBR Green I

SYBR Green I (SG) is an asymmetrical cyanine dye that interacts with dsDNA to emit fluorescence at 520 nm (excitation 497 nm). The structure of SG is shown in Figure 3.1 below.

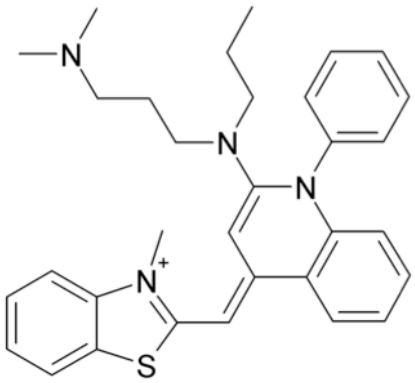

Figure 3.1 SYBR Green I chemical structure: N',N'-dimethyl-N-[4-[(E)-(3-methyl-1,3-benzothiazol-2-ylidene)methyl]-1-phenylquinolin-1-ium-2-yl]-N-propylpropane-1,3-diamine

SG is used in label-free fluorescence sensors, exploiting the increase in fluorescence emission at 520 nm upon intercalation into dsDNA. Generally, this approach results in a fluorescence 'turn off' sensor, where the addition of a target reduces SG fluorescence by displacing a complementary probe from the aptamer to reduce the dsDNA character. This approach has been used for aptamer-mediated sensing of small molecule (ATP) and protein (thrombin) targets.[199-200] A similar approach by McKeague *et al* (2014) exploited the change in dsDNA character of the aptamer upon target binding to produce a fluorescence 'turn-off' sensor for OTA without the use of a complementary probe.[111] Other dsDNA-intercalating dyes that have been used in similar approaches, including Pico Green, used the same principles of SG intercalation to detect OTA.[166] Additional nucleic acid chromophores can measure aptamer-target interactions including ethidium bromide (EtBr), thiazole orange, YOYO, and Hoeschst.[200]

3.1.5 Paper-based sensing platforms

The use of paper and paper-like products as an analytical platform is promising as an inexpensive, portable, and accessible alternative to solution-based sensing.[201] The

main areas of paper-based sensing include lateral flow devices (LFDs), dipstick tests, and microfluidic paper-based analytical devices (μPADs). Colourimetric detection is predominant in paper-based sensors.[202]

LFDs, as discussed in Section 1.1.4.1, have been used to detect a range of target molecules using aptamer-based molecular recognition, including adenosine,[144] cocaine,[144] thrombin,[203] mercury,[204] glucose,[205] and OTA.[205] These are predominantly based on the colourimetric detection of aptamer-bound AuNPs, immobilized on test and control regions of the membrane, with aptamer probes conjugated to the nitrocellulose surface.[203-205] Zhu *et al* (2014) designed the strip test with a 'tree' design to facilitate comparison of standards to the test sample in the same strip, and reduce inter-test variability.[205]

Paper-based platforms for sensing have been performed on simple printer paper,[206-207] filter paper,[208] or even fabric.[146, 209] Zhao *et al* (2008) applied the classic AuNP-aptamer test (measuring dispersion and target concentration based on colour change) to a paper substrate to test for DNase I and adenosine targets.[208] Similarly, Lee *et al* (2013) detected thrombin through an aptamer sandwich assay with aggregation of aptamer-linked AuNPs upon addition of thrombin.[146] Other designs have used fluorescence (UCNPs, QDs) instead of colourimetric responses to increase the sensitivity of the paper-based assay.[206-207]

For both LFD and paper-based platforms, it has been reported that the paper-based assay displayed higher sensitivity (lower LOD) than the analogous solution-based test.[144, 146] This is likely due to the integrated binding, separation, and detection all occurring on a single platform with reduced background interference. Other advantages

of paper-based tests are the very small volumes required to operate a test, rapid results, and robust sensor design. Advances with cameras, scanners, and strip readers are improving the quantitative nature of these assays, offering more promise to tests of this nature for use in-field and for point-of-care detection.[206, 210]

3.2 Chapter Objectives

This chapter will investigate various models for incorporating the *FB$_1$39* minimers (*FB1_39t3* and *FB1_39t3-5*) from Chapter 2 and an established OTA aptamer (*A08*) into novel nano-aptasensors. Approaches include: (1) linkage-inversion assembled nano-aptasensors (LIANAs) utilizing QDs and AuNPs in a FRET pair for sensing FB_1 and OTA in solution and on a paper test; (2) fluorescent 'turn-on' sensors with aptamer-coupled fluorophores (fluorescein, QDs) quenched by carbon-based quenchers for FB_1 detection; (3) label-free fluorescence detection of FB_1 based on intercalation of SYBR Green I generating a 'turn off' fluorescent sensor, and; (4) testing the selectivity and performance of *FB$_1$39*, *FB1_39t3*, *FB1_39t3-5* and *A08* aptamers in contaminated grape samples.

3.3 Statement of Contributions

5'-5' reverse phosphoramidite DNA linkers were purchased from the University Core DNA Services, University of Calgary, Calgary AB. Experiments for the fluorescence sensor paper test (LIANA) for OTA were conducted by Ranganathan Velu and Nadine Frost (Section 3.5.1). Sample preparation for aptamer selectivity and performance in a sample matrix (Section 3.5.5) was performed by Annamaria Ruscito and Nadine Frost; sample analysis was conducted by Justin Renaud at the Southern Crop Protection and Food Research Centre Agriculture and Agri-Food Canada in London, ON.

All other experiments were performed by Nadine Frost. LIANA paper-based OTA sensor was published in the following manuscript:

Velu R., Frost N., DeRosa M.C. (2015) Linkage inversion assembled nano-aptasensors (LIANAs) for turn-on fluorescence detection, *ChemComm,* DOI: 10.1039/c5cc06013c

3.4 Materials and Methods

3.4.1 Buffers

Table 3.1 Buffers used throughout Chapter 3

Buffer	Composition	pH
FB_1 binding buffer	100 mM NaCl, 20 nM Tris, 2 mM $MgCl_2$, 5 mM KCl, 1 mM $CaCl_2$	7.6
A08 binding buffer	10 mM Na_2HPO_4, 2 mM KH_2PO_4, 2.7 mM KCl, 137 mM NaCl	7.4
PBS buffer	137 mM NaCl, 2.7 mM KCl, 10 mM Na_2HPO_4, 1.8 mM KH_2PO_4	7.4
MES buffer	10 mM MES	5.0
Na_2PO_4 buffer	10 mM Na_2PO_4	7.0
Borate buffer	50 mM Borate	9.0
Citrate buffer	425 mM Citrate	3.0
HEPES buffer	0.5 M HEPES	7.5
TBE buffer	89 mM Tris, 89 mM Boric acid, 2 mM EDTA	7.0

3.4.2 LIANA for OTA (Paper Test)

3.4.2.1 Aptamers

5’NH_2- and 5’-SH-modified *A08* aptamer was purchased from Integrated DNA Technologies. 5’-5’ reverse phosphoramidite linker DNA was purchased from University Core DNA Services, University of Calgary, Calgary, Alberta.

A08min sequence:

5’-NH_2-GGCAGTGTGGGCGAATCTATGCGTACCGTTCGATATCGTG-3’

5’-5’ linker sequence: 3’-AGCAC-(5’-5’)-CACGA-3’

3.4.2.2 Synthesis of gold nanorods (AuNRs)

The AuNRs used in this study were synthesized by a surfactant-stabilized, seedless one-step technique.[192] $HAuCl_4$ (20 mM), $AgNO_3$ (0.1 mM), and ascorbic acid (0.1 M) were mixed in 10 ml of 0.1 M aqueous cetyl trimethylammonium bromide (CTAB) solution. 40 ml of 1.6 mM $NaBH_4$ was used as the reducing agent to generate AuNRs. AuNRs were purified by centrifugation at 14 000 g for 30 min to remove the excess metal ions and CTAB molecules in the supernatant solution for terminating the self-assembly growth. The AuNRs (aspect ratio = 3.5) had plasmon absorption peaks around 520 and 650 nm.

3.4.2.3 Functionalization of AuNRs with SH-aptamer

3 µl of 230 pM AuNRs were mixed with 1.2 µl of 0.1 µM thiol-modified aptamer and incubated on a vortex shaker at room temperature for two hours. In this step, thiol groups of the modified aptamer are conjugated onto the terminal edges of AuNRs. AuNRs were then washed and the resulting conjugates were collected by centrifugation at 14 000 g for 30 min and resuspended in A08 binding buffer.

3.4.2.4 Functionalization of carboxyl-QDs with NH_2-aptamer

5'-NH_2-*A08* aptamer was conjugated to the carboxyl CdSe/ZnS 525 core/shell QDs using 1-ethyl-3-(3-dimethylaminopropyl) carbodiimide (EDC) and N-hydroxysulfo-succinimide (Sulfo-NHS) as cross-linking reagents. QDs (920 pM, 5 µl) were mixed with 0.5 µL of EDC (25eq to carboxyl QDs) and 1.45 µl of Sulfo-NHS (50eq to carboxyl QDs) in phosphate buffered saline (PBS, pH 7.4) total volume 450 µl. After shaking for 30 min, amine-modified aptamer (0.1 µM, 1.2 µl) was added and placed on a shaker at room

temperature for an additional two hours. The resulting samples were centrifuged at 14 000 g for 20 minutes.

2.4.2.5 Preparation of OTA-spiked complex extract

Two grams of each sample (wheat, barley, corn, oats and malted barley) from Trilogy Analytical was mixed with 50 ml of deionized water and incubated (with shaking) for 10 minutes at room temperature. The mixture was centrifuged for 10 minutes and the supernatant was filtered through Whatman 1 filter paper and a syringe filter (PES 0.45 µm, 30 mm diameter). The clear solution was spiked with OTA to concentrations from $1x10^{-9}$ to $1x10^{-4}$ M.

3.4.2.6 Preparation of LIANA2

Aptamer-functionalized AuNRs (230 pM, 3 µl) were mixed with aptamer-functionalized QDs (2.5 µl at 0.460 nM of each CdSe/ZnS and CdTe QDs) and incubated for 60 minutes. 5'-5' reverse phosphoramidite linker DNA was added to 0.2 µM to assemble LIANA2.

3.4.2.7 Paper test

Three rows of sample zones (~8 mm diameter circles) were prepared on unmodified Whatman 41 filter paper. The top row was a control lane of OTA samples. LIANA2 sample (1 µl in A08 buffer) was applied onto the bottom two rows of sample zones and left to dry for two minutes. 1 µl of 10^{-4} – 10^{-9} M OTA solutions in complex extract were spotted on to the top and bottom rows of sample zones. The middle row of sample zones was spotted

with 1 µL of the matrix alone (no OTA). The paper test was then illuminated with a hand-held UV light (254 nm) and visualized with a Nikon camera (model: D7000).

3.4.3 LIANA for FB_1 (solution tests)

3.4.3.1 DNA synthesis

Aptamer synthesis was performed following the same methods outlined in Chapter 2 (Section 2.4.1) with the following modifications. Aptamers were modified with either 5'-NH_2 (5'-Amino modifier C6, Glen Research) or 5'-SH (Thiol modifier C6-S-S, Glen Research). Correct masses were confirmed by LC-MS.

Table 3.2 Sequences of modified aptamers for FB_1 LIANA design

DNA aptamer	Sequence (5'-3')	Length (nt)
FB_1 39 5'NH_2	*NH_2-$(CH_2)_6$ -* ATACCAGCTTATTCAATTAATCGCATTACCTTATACCAGCTTATTCAATTACG TCTGCACATACCAGCTTATTCAATTAGATAGTAAGTGCAATCT	96
FB1_39t3 5'NH_2	*NH_2-$(CH_2)6$-* ATACCAGCTTATTCAATTAATCGCATTACCTTATACCAGCTTATTCAATTACG TCTGCACATACCAGCTTATTCAATT	78
FB1_39t3-5 5'NH_2	*NH_2-$(CH_2)_6$-* AATCGCATTACCTTATACCAGCTTATTCAATTACGTCTGCACATACCAGCTTA TTCAATT	60
FB_1 39 5'-SH	*SH-$(CH_2)_6$ -* ATACCAGCTTATTCAATTAATCGCATTACCTTATACCAGCTTATTCAATTACG TCTGCACATACCAGCTTATTCAATTAGATAGTAAGTGCAATCT	96
FB1_39t3 5'-SH	*SH-$(CH_2)_6$-* ATACCAGCTTATTCAATTAATCGCATTACCTTATACCAGCTTATTCAATTACG TCTGCACATACCAGCTTATTCAATT	78
FB1_39t3-5 5'-SH	*SH-$(CH_2)_6$-* AATCGCATTACCTTATACCAGCTTATTCAATTACGTCTGCACATACCAGCTTA TTCAATT	60

5’-5’ reverse phosphoramidite linker DNA was ordered from University Core DNA Services, University of Calgary, Calgary AB. Synthesis was performed on a 0.2 µmol scale.

Table 3.3 5’-5’ DNA linkers for FB_1 LIANA

DNA linker	Sequence (5’-3’)	Length (nt)
F8	ACGTTAGA(5'-5')AGATTGCA	16
F5	TTAGA(5'-5')AGATT	10
M8	TAAGTTAA(5'-5')AATTGAAT	16
M5	GTTAA(5'-5')AATTG	10

3.4.3.2 AuNP synthesis and quantification

98 ml deionized water and 2 ml 50 mM $HAuCl_4$ (Sigma Aldrich) was heated to a boil with stirring in a 250 ml Erlenmeyer flask. 10 ml of 38.8 mM sodium citrate (Sigma Aldrich) was added and the colour of the solution was monitored from clear to pale yellow to purple to wine red. Once the colour was stabilized as wine red, the flask was removed from heat, cooled with stirring, and quantified by UV-Vis spectroscopy on a CARY 300 spectrophotometer (Varian) with an extinction coefficient of 2.7×10^8 and a λ_{max} of 520 nm.

3.4.3.3 AuNP functionalization with SH-modified aptamer

SS-DNA to SH-DNA reduction with TCEP (tris-(2-carboxyethyl) phosphine) was achieved by dissolving 1×10^{-10} mol of SS-modified DNA in 100 µl 10 µM TCEP and incubating on a shaker at room temperature for 60 minutes. Excess TCEP was removed by desalting DNA through Desalting Amicon Ultra 0.5 ml 3 kDa centrifuge units and washing with 0.5 ml Milli-Q water twice. Conjugation of SH-DNA to AuNPs was achieved by suspending 1×10^{-10} moles of SH-DNA, as prepared above, in 100 µl AuNPs

(11.32 μM). 2.4 μl of 425 mM citrate buffer (pH 3) was added, vortexed to mix, and shaken for 3 min at room temperature. 20 μl of 0.5 M HEPES buffer (pH 7.5) was added, vortexed to mix, and shaken for 10 min at room temperature. The SH-modified AuNPs were centrifuged at 13 000 g for 10 min and the pellet was washed twice with 100 μl Milli-Q water, and finally resuspended in 100 μl FB_1 binding buffer. The aptamer-modified AuNPs were stored at 4°C. To confirm conjugation, SH-aptamer was quantified on a CARY UV-Vis spectrophotometer (λ_{max} 260 nm) before and after conjugation to AuNPs.

3.4.3.4 Functionalization of carboxyl-QDs with NH_2-aptamer

CdTe/ZnS and CdTe carboxy-quantum dots (QDs) were purchased from Molecular Probes Life Technologies. 5 μl of the 8 μM QD solution was diluted to 40 μl in FB_1 binding buffer. 60 μl 200 nM EDC and 30 μl 200 nM Sulfo-NHS (prepared fresh) were added and the solution was incubated on a vortex shaker at room temperature for 15 min (dark). $1x10^{-9}$ mol 5'-NH_2 modified aptamer was added, and the solution was incubated on a vortex shaker at room temperature for an additional 60 min (dark). 0.6 μl ethanolamine was added to quench unreacted NH_2 groups, and incubated on the shaker for an additional 2 hours (dark). The aptamer-QD conjugates were collected by centrifugation (30 min, 14 000 g), washed twice with Milli-Q water, and resuspended in FB_1 binding buffer. Samples were sonicated at room temperature for 5 min to disperse aggregates, and stored at 4°C in the dark. Variations on this procedure included the following modifications. Alternate buffers were employed in this procedure to attempt to avoid salt-induced aggregation of the QDs (attributed to charge-masking effects). The following buffers were used in trials as alternatives to FB_1 binding buffer:

a) FB_1 binding buffer with 50 mM NaCl, pH 7.6

b) FB_1 binding buffer with 10 mM NaCl, pH 7.6

c) 10 mM MES, pH 7.6

d) 10 mM Na_2HPO_4, pH 7.6

e) 50 mM Borate, pH 9

3.4.3.5 Agarose gel of carboxyl-QD conjugation

In a 500 ml Erlenmeyer flask, 2.5 g agarose, 36 ml 5xTBE buffer, and 144 ml Milli-Q H_20 were heated in a microwave for 3 min. The solution was cooled to ~60°C and 10 µl of 10 mg/ml EtBr solution was added before casting into the gel apparatus and allowing it to set for ~ 30 min. 1xTBE was used as a running buffer. Samples were mixed with 1 µl DNA gel loading dye (Life Technologies) and run for 2 hours at 185 V.

3.4.3.6 Fluorescence measurements

Fluorescence spectra were recorded on a fluorescence spectrophotometer (Horiba Jobin Yvon, USA) with a SpectrAcq controller with an excitation wavelength of 400 nm and an emission spectra of 480 – 650 nm (CdTe/ZnS QDs).

3.4.4 Single walled carbon nanotube (SWCNT) studies

3.4.4.1 DNA synthesis

Aptamers used were previously synthesized (5'-fluorescein labelled) and purified (Table 2.2).

3.4.4.2 SWCNT preparation

SWCNTs were purchased from Sigma Aldrich. Unmodified SWCNTs were dissolved in MilliQ H_2O at ~ 1 mg/ml and sonicated extensively. The majority of the SWCNTs pellet out when the solution was left un-agitated for several hours; the pale

yellow supernatant was used as the unmodified SWCNT stock for trial experiments without further quantification.

3.4.4.3 Fluorescence measurements

Fluorescence measurements of 5'-fluorescein DNA was performed on a Fluorescence spectrophotometer (Horiba Jobin Yvon, USA) coupled with a SpectrAcq controller with an excitation wavelength of 494 nm and an emission range from 500 – 600 nm. Efforts were made to maintain consistency of buffer salinity and pH within experiments and dilutions to avoid the effects of buffer variability on the fluorescein tag. For each experiment, a sample volume of 100 µl was used, and unless otherwise noted experiments were performed in FB_1 binding buffer. 1 – 2 µl *FB139* (5'-fluorescein modified) at $1x10^{-5}$ M was added to the solution of FB_1 in buffer (or buffer control), and incubated at room temperature for 20 min. The fluorescence spectrum was recorded before and after addition of SWCNTs; after addition of SWCNTs the solution was mixed by pipette 10 times and measured directly.

3.4.4.4 Acid-modification of SWCNTs

3.4.4.4.1 Procedure

5.2 mg of SWCNTs were dissolved in 15 ml of 3.18 M HNO_3 (diluting 5 ml of conc. HNO_3 with 20 ml H_2O) and placed in a 25 ml round bottom flask equipped with a stir bar, hot plate, and condenser. The solution was heated to reflux for 27 hours and left for 3 days at room temperature. The grainy black solution was transferred to a 50 ml falcon tube and sonicated at room temperature for 60 min, before being transferred back to the reflux apparatus and heated to reflux for an additional 24 hours. After cooling, the

solution was again transferred to a 50 ml falcon tube and sonicated for 60 min at room temperature, resulting in a black solution that, upon settling, separated into a yellow supernatant and black aggregated pellet. The supernatant was passed through Spin X centrifuge filter tubes with a 0.22 μm cellulose acetate membrane (Corning) for 3 min at 2000 g. The flow-through was then passed through a 200 nm Millipore filter (1000 g, 3min) and the retained acid-modified SWCNTs on the filter were subsequently washed five times (500 μl MilliQ H_2O, 1000g 3 min) until the flow-through wash had a pH > 6.0 as measured by pH paper. The acid-modified SWCNTs on the filter paper were dried in a dessicator overnight. The dried product was weighed and dissolved in MilliQ H_2O to a concentration of 0.1 mg/ml and sonicated for 90 min at room temperature. The resulting solution after settling had a small black pellet and a transparent grey-yellow supernatant.

3.4.4.4.2 Characterization (TEM, UV-Vis)

For UV-Vis characterization of the acid-modified SWCNTs, the spectra was collected on a CARY 300 UV-Vis spectrophotometer from 800 – 200 nm. For HR-TEM, 10 μl of the dispersed acid-modified SWCNTs were dried completely on a carbon coated copper grid. HR-TEM images were captured on a FEI Tecani F20 FETEM (Chemistry Department, Carleton Univeristy).

3.4.5 Graphene oxide studies

3.4.5.1 DNA synthesis

5'-NH_2-modified *FB139*, *FB1_39t3* and *FB1_39t3-5* was prepared as described previously (Table 3.2).

3.4.5.2 CdSe/ZnS QDs conjugation with 5'NH_2 aptamers

5 µl of 8 µM carboxyl CdSe/ZnS (Green) quantum dots (QDs) (Life Technologies) were activated with 4 µl of 10 mg/ml Sulfo-NHS (Life Technologies) and 2 µl of 10 mg/ml EDC (Sigma Aldrich) for 30 min in 10 mM MES buffer (100 µl total volume) at room temperature. The QDs were centrifuged at 13 000 g for 30 min and the pellet was resuspended in 10 mM Na_2PO_4 buffer with 1 nmol 5'-NH_2 modified aptamer. After incubation on a vortex shaker for 2 hours to allow for coupling, the aptamer-QDs were centrifuged for 30 min at 13 000 g and the pellet was resuspended in 100 µl 10 mM Na_2PO_4 buffer and stored at 4°C.

3.4.5.3 CdTe QDs conjugation with 5'NH_2 aptamers

5 µl of 8 µM carboxyl CdTe (Red) quantum dots (QDs) (Life Technologies) were activated with 2 µl of 50 mg/ml Sulfo-NHS (Life Technologies) and 2 µl of 50 mg/ml EDC (Sigma Aldrich) for 30 min in 10 mM MES buffer (100 µl total volume) at room temperature. The QDs were centrifuged at 13 000 g for 30 min and the pellet was resuspended in 10 mM Na_2PO_4 buffer with 1 nmol 5'-NH_2 modified aptamer. After incubation on a vortex shaker overnight to allow for coupling, the aptamer-QDs were centrifuged for 30 min at 13 000 g and the pellet was resuspended in 100 µl 10 mM Na_2PO_4 buffer and stored at 4°C.

3.4.5.4 UV-Vis spectroscopy

UV-Vis spectroscopy (CARY 300 Bio UV-Spectrophotometer) was performed to calculate the aptamer coupling efficiency to the QDs. Absorption was monitored at 260

nm and the concentration of aptamer was calculated with the respective extinction coefficients.

3.4.5.5 Fluorescence measurements

Fluorescence measurements were performed with a Fluorolog Horiba Jobin Yvon (USA) coupled with a SpectrAqc controller. QDs were excited with a wavelength of 400 nm. Green-QDs were monitored with an emission range of 480-650 nm and Red-QDs were monitored with an emission range of 550 – 750 nm. 3 µl aptamer-QD conjugate as prepared above was dissolved in 97 µl buffer. The initial fluorescence was recorded. Graphene oxide (2 mg/ml solution, Sigma Aldrich) was added incrementally and incubation times were noted. To avoid variation between samples of aptamer-QDs, a single sample of aptamer-QD ~50% quenched by graphene oxide was split into two samples; a control (H_2O) and FB_1 addition to monitor fluorescence recovery upon target binding after an incubation period of 90 min.

3.4.6 Label-free SYBR Green I sensors for FB_1

3.4.6.1 DNA synthesis

5'-NH_2 modified *$FB_1$39* was synthesized and prepared as described above (Table 3.2). *cFB1_39t3* was synthesized in the same method as 5'-NH_2 *$FB_1$39*, but with no 5' modification. All DNA was confirmed by LC-MS prior to use.

3.4.6.2 Variable-temperature UV-Vis melting temperature determination

Variable-temperature UV-Vis spectroscopy melting studies (T_m determination) were performed with a Varian Cary 300 Bio UV-Vis Spectrophotometry equipped with a 6x6 Peltier-Thermostatted Multicell Holder. For each sequence, 3 ml of aptamer (*$FB_1$39*

+ *cFB1_39t3*) was prepared at 2 µM in FB_1 selection buffer (Table 3.1). Absorbance was monitored at 260 nm over three temperature ramps (Ramp 1 80°C - 20°C; Ramp 2 20°C - 80°C; Ramp 3 80°C - 20°C). The ramp rate was set at either 0.5°C/min (slow), and 5°C/min (fast), with a five minute hold between each temperature change. Melting temperatures were determined by fitting the change in absorbance at 260 nm relative to temperature using Standard Curves Analysis on SigmaPlot.

3.4.6.3 SYBR Green I fluorescence assay

Fluorescence measurements were performed with a Fluorolog Horiba Jobin Yvon (USA) coupled with a SpectrAqc controller. Each sample had a total volume of 125 µl comprised of: 120 µl FB_1 in FB_1 binding buffer (concentration range from 0 – $1x10^{-5}$ M), 4 µl aptamer (5'-NH_2 *$FB_1$39* alone, or 5'-NH_2 *$FB_1$39* + *cFB1_39t3*), and 1 µl 10x SYBR Green (SG) (SYBR Green I, 10 000x stock, Life Technologies). The mixture was incubated for 30 min at room temperature on a vortex shaker prior to fluorescence measurement. The excitation wavelength was 497 nm and emission range from 500 – 650 nm with the SG peak ~ 520 nm.

3.4.7 Aptamer selectivity and performance in a grape matrix

3.4.7.1 Conjugation of NH_2-modified aptamers to magnetic beads

M-270 Amine Dynabeads® (Life Technologies) were suspended in PBS buffer (Table 3.1) and washed three times, separating on the magnet each time. The beads were re-suspended in 5% glutaraldehyde (Sigma Aldrich) in PBS buffer, and incubated for 2 hours at room temperature on a vortex shaker. Control beads were incubated without glutaraldehyde. The beads were again washed three times with PBS buffer and

resuspended in 1 ml NH_2-modified aptamer (10 μM) and incubated overnight at room temperature on a vortex shaker. For fumonisin extraction, three aptamer sequences were conjugated on separate aliquots of beads, *FB_139*, *FB1_39t3* and *FB1_39t3-5*. For ochratoxin extraction, one aptamer sequence, *A08*, was conjugated onto beads. All DNA synthesis was as described in Section 3.4.3.1. After conjugation, the beads were washed 3 times in PBS buffer (1 ml) and capped with 20 mg/ml Sulfo-NHS Acetate (Life Technologies, prepared fresh) incubated with shaking for 2 hours at room temperature to block unreacted amine groups. Control beads (no aptamer) were just capped with Sulfo-NHS Acetate. The beads were washed 3 times (1 ml) with PBS buffer and stored at 4°C.

3.4.7.2 Fumonisin and ochratoxin extraction from contaminated grapes

Grapes obtained from the local produce market in Ontario, Canada were selected as a natural substrate for *Aspergillus welwitschiae* and *Aspergillus carbonarius* producing fumonisins and ochratoxin respectively. 6.03 g (*A. welwitschiae*) and 6.14 g (*A. carbonarius*) were diluted into 15 ml of acetonitrile:H_2O:acetic acid 80:18:2 in a 50 ml falcon tube and sonicated at 30°C for 60 min to extract fumonisins and ochratoxins respectively. Samples were then filtered through a 0.45 μm PES syringe filter to remove large particulates, and diluted in buffer (Table 3.1, FB_1 binding buffer, A08 binding buffer) to obtain 1x 5x and 10x dilutions. Direct grape must samples were obtained by diluting the original grape must in buffer and filtering through a 0.45 μm PES syringe filter. Dilutions included 90:10 and 50:50 buffer:grape must mixtures from the fully concentrated grape must and a 10x dilute grape must solution.

3.4.7.3 Aptamer binding studies from direct and extracted grape must

Grape must 'extract' and 'direct' samples were dried down in a Savant AE2010 SpeedVac overnight in 100 µl aliquots at the correct dilution factor and reconstituted with 100 µl aptamer-modified magnetic beads (prepared as above, suspended in appropriate buffer). Samples were incubated on a vortex shaker for 60 min to allow for aptamer-target binding. Three aliquots of 100 µl buffer were used to wash off non-binding components of the grape matrix, separating the magnetic beads with a DynaMag-2 magnet each time. Compounds that bound to the aptamer were eluted off by heat denaturation, with three 100 µl aliquots of buffer incubated at 90°C for 10 min. Fractions of bound components were retained for analysis by LC-HRMS^2 to determine aptamer selectivity and performance in the matrix.

3.4.7.4 LC-HRMS^2 analysis of bound fractions

Each sample volume was adjusted to 500 µl with MeOH to allow for the bound fractions (300 µl) to be compared to the "Before" fractions (100 µl) representing the total initial matrix that was incubated with the aptamer. HRMS analysis was performed on a Thermo Scientific Q-Exactive Quadrupole Orbitrap Mass Spectrometer, coupled to an Agilent 1290 HPLC system. Five µl of each sample was injected onto a Zorbax Eclipse Plus RRHD C18 column (2.1 x 50 mm, 1.8 µm; Agilent) maintained at 35˚C. Samples were separated using a flow rate of 0.3 mL/min with a mobile phase of water with 0.1% formic acid (A), and acetonitrile with 0.1% formic acid (B). Mobile phase B was held at 0% for 30 seconds, before increasing to 100% over three minutes. B was then held at 100% for 1 minute before returning to 0% over 30 seconds. The following conditions were used for HESI(+): capillary temperature, 400˚C; sheath gas, 17 units; auxiliary gas,

8 units; probe heater temperature, 450 ˚C; S-Lens RF level, 45; capillary voltage, 3.9 kV. OTA was analyzed in full MS was acquired in positive mode using the following settings: scan range, *m/z* 75 – 1125; resolution, 70,000; AGC, 1e6; max IT, 250 ms. For fumonisin analysis, the scan range was moved to *m/z* 530-870 while resolution and max IT were decreased to 35,000 and 128 ms respectively.

3.5 Results and Discussion

3.5.1 LIANA (OTA paper test)

3.5.1.1 Design of LIANA with *A08min*

Linkage-inversion assembled nano-aptasensors (LIANAs) were developed as a generally applicable approach to target molecule detection based on aptamer-mediated recognition resulting in turn-on fluorescence. For the LIANA sensor, *A08min* was used as a 40-nt aptamer that has demonstrated high-affinity binding to OTA.[111] As shown in Figure 3.2, gold nanorods (AuNRs) are used as quenchers of CdSe/ZnS (green-emitting) and CdTe (red-emitting) fluorescent quantum dots (QDs). The AuNRs and QDs are functionalized with *A08min* aptamer through 5'-SH- and 5'-NH_2-modified DNA respectively. Introducing the 5'-5' linker DNA leads to the formation of the nanostructure complex resulting in fluorescence quenching through FRET. Upon the addition of OTA, the aptamer will preferentially bind to its target and release the 5'-5' linker strand resulting in disassembly of LIANA, and fluorescence recovery.

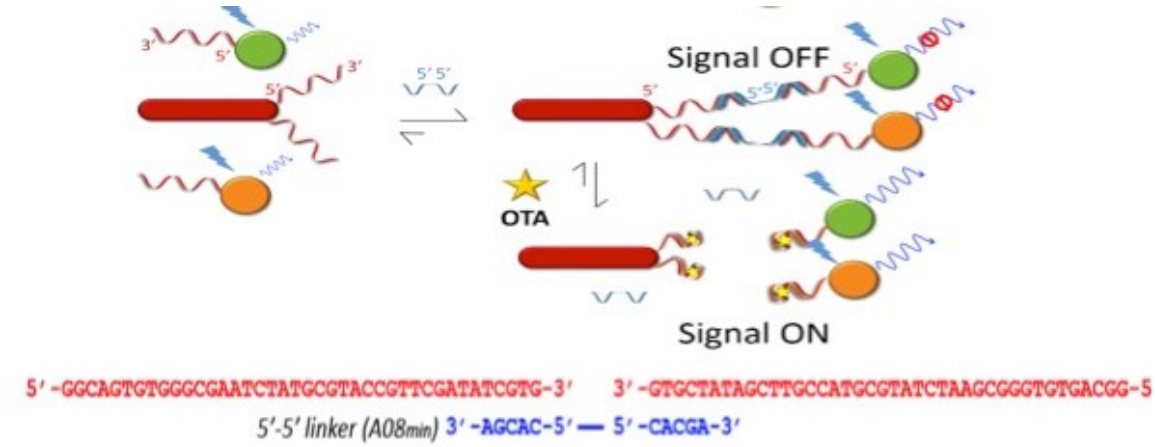

Figure 3.2 Assay design of linkage-inversion assembled nano-aptasensor (LIANA). AuNRs (red rods) and QDs (green and orange circles) are functionalized with *A08min* and assembled by a 5′-5′ linker DNA resulting in the quenching of QD fluorescence "Signal Off". OTA-induced dispersion of the nanostructures leads to a restoration of the fluorescence signals "Signal On". The 5'-5' linker DNA as shown is able to link together two *A08min* aptamers, each conjugated to AuNRs (quenchers) and QDs (fluorophores) at the 5'-termini through short complementary regions with minimal steric hindrance.

The 5'-5' linker is synthesized into the short DNA strand through the use of reverse phosphoramidites during chemical synthesis of DNA. In traditional solid-phase DNA synthesis, proceeding in the 3' to 5' direction, the 3'-OH links the phosphoramidite and the free 5'-OH is protected by a dimethoxytrityl (DMT) protecting group (acid-labile). In a 5'-5' reverse phosphoramidite linker, the position of the 5'-DMT protecting group and the 3'-phosphoramidite are reversed to produce a 5'-5' linker at the desired site within the DNA strand. The advantage of using a 5'-5' linker for the short complementary strand in the LIANA design is to facilitate rapid assembly of the nanostructure while reducing steric hindrance that would be introduced by using a traditional 5'-3' linker strand. A 5'-3' linker strand composed of the same complementary bases without the 5'-5' linker has been shown to be ineffective in assembling the nanostructure (data not shown). A further advantage of the LIANA design

is that in order to disassemble the quenched construct to achieve fluorescence recovery, only one interaction of aptamer-target needs to occur to disrupt the linker interaction, thus increasing overall sensitivity of the construct.

The conjugation of 5'-SH-modified aptamers to AuNRs occurs preferentially at the terminal ends due to the reactive chemistry of AuNRs.[192] AuNRs have two surface plasmon resonances (latitudinal and longitudinal) that overlap well with the emissions of both green-emitting and red-emitting QDs. This lends well to multiplex detection, using a unique aptamer sequence for two targets each conjugated to a unique QD fluorescence emission to detect two targets in a single sample. Alternatively, two aptamers for the same target could be integrated into the same system, possibly expanding the linear range or performance conditions of the system.

It should also be noted that with this design, QD-QD and/or AuNR-AuNR assemblies are also possible. Interestingly, these were seen only rarely and can be mitigated by thorough mixing of the aptamer-modified component prior to linker addition (data not shown).

3.5.1.2 LIANA paper test to detect OTA in a complex matrix

The LIANA construct with *A08min* was applied to a simple, rapid paper-based detection system for OTA. The quenched nano-assembly has no fluorescence in the absence of OTA. OTA was spiked into a complex extract of wheat, barley, corn, oats, and malted barley to stimulate testing conditions in real sample extracts. The paper test was performed on an unmodified filter paper, a low cost and accessible substrate for downstream use (Figure 3.3).

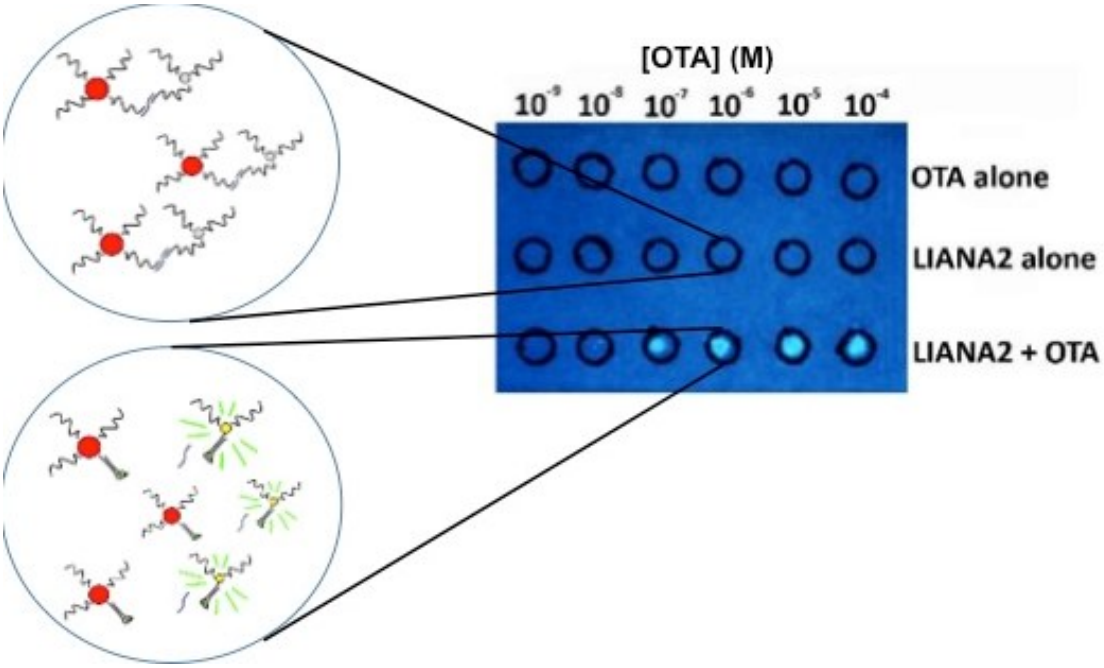

Figure 3.3 LIANA paper test with OTA-spiked complex extract solution. 1 µl of LIANA was spotted onto the bottom two rows of sample zones (black circles). The top row was 1 µl of OTA alone (10^{-4} to 10^{-9} spiked in complex extract) to control for any inherent fluorescence of OTA. The middle row contains 1 µl of complex extract with no OTA, showing the quenched nano-assemblies. The bottom row contains 1 µl of complex extract spiked with OTA (10^{-4} to 10^{-9}) showing dissembly of the nano-construct and "turn on" fluorescence. Paper test was visualized under a hand-held UV light (254 nm) and imaged with a Nikon Camera D7000.

The paper test for OTA using *A08min* demonstrates a rapid, portable sensor on a simple platform for detection. The visual limit of detection for OTA is between 10 nM – 100 nM in a complex extract. The regulatory limits for OTA established by the European Union range between 0.5 µg/kg (1.24 nM) for food intended for infants and young children, and 5 µg/kg (12.4 nM) for unprocessed cereals and coffee beans. A platform such as this can be easily integrated with portable imaging technology to quantify the fluorescence of each sample zone to achieve more quantitative detection. The potential applications for this test involve in-field testing for OTA for screening samples prior to being sent away for confirmatory testing. For OTA, the sensitivity of the test could be modulated to meet a threshold level to get a simple "yes / no" response for regulations.

Sensitivity can be modulated in this design by modifying the aptamer used (selecting an aptamer that binds OTA under the desired conditions within the range of detection), and adapting the length of the 5'-5' linker DNA (a longer linker would decrease sensitivity of the test).

3.5.2 LIANA (FB_1 detection in solution)

3.5.2.1 Aptamer conjugation with AuNPs

Citrate-capped AuNPs were synthesized and quantified by UV-Vis at a concentration of 11.32 nM. 5'-SH-modified aptamers were conjugated to AuNPs using the pH-assisted method, and UV-Vis spectroscopy was used to quantify the amount of aptamer bound to the AuNPs (~ 80 pmol aptamer bound to 100 pmol AuNPs). Aptamer-functionalized AuNPs were resuspended in FB_1 binding buffer and no colour change or aggregation was noted, due to the bound aptamer. Control reactions with no aptamer present aggregated upon suspension in buffer.

Carboxyl-QDs and 5'-NH_2-modified aptamer were conjugated through EDC / Sulfo-NHS coupling chemistry. The EDC crosslinker forms an unstable o-acylisourea intermediate that futher reacts with Sulfo-NHS to form an amine-reactive Sulfo-NHS ester that can then react with a primary amine to form a stable amide bond conjugate (Figure 3.4).

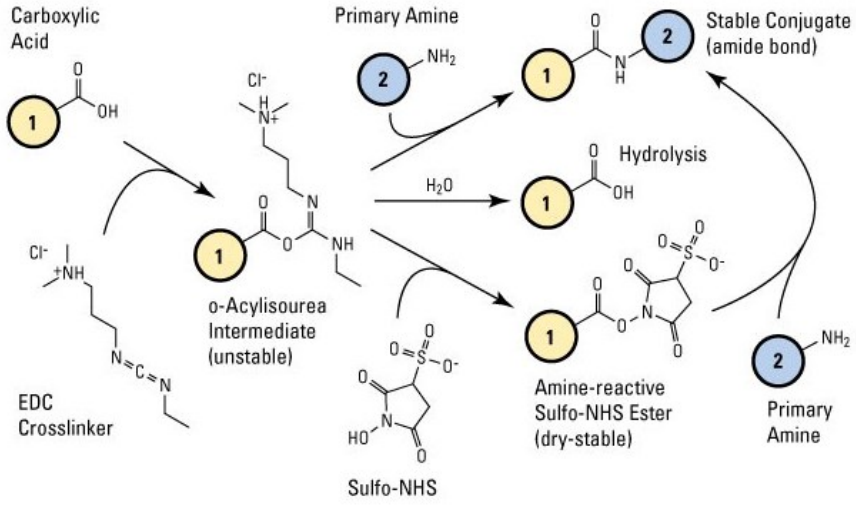

Figure 3.4 EDC / Sulfo-NHS conjugation chemistry to link carboxyl-modified QDs and amine-modified aptamer. Source: www.lifetechnologies.com

For the QD-aptamer conjugation reactions under all conditions, no difference in aptamer concentration was noted between the "before" and "after" conjugation fractions indicating that negligible coupling of aptamer to QDs was achieved. Trials of QD-aptamer conjugation were conducted in a series of buffers to aim to prevent salt-induced charge shielding and subsequent aggregation of QDs. The buffers included in the trials, all with no consistent success in coupling as determined by UV-Vis quantification of aptamer, included: (1) water; (2) FB_1 binding buffer; (3) FB_1 binding buffer with 50 mM NaCl; (4) FB_1 binding buffer with 10 mM NaCl; (5) 10 mM MES buffer for EDC and Sulfo-NHS activation followed by 10 mM Na_2PO_4 buffer for NH_2-modified aptamer coupling; (6) 50 mM borate buffer pH 9. The highest coupling efficiency was noted for *FB1_39t3-5* with buffer conditions (5) as above, with a 10% efficiency of aptamer conjugation to QDs.

An agarose gel monitored the DNA between the fractions. A sample agarose gel from the MES / Na_2PO_4 conjugation reaction is shown in Figure 3.5, with both NH_2-

modified *FB1_39t3* and *A08* aptamer (as a control).

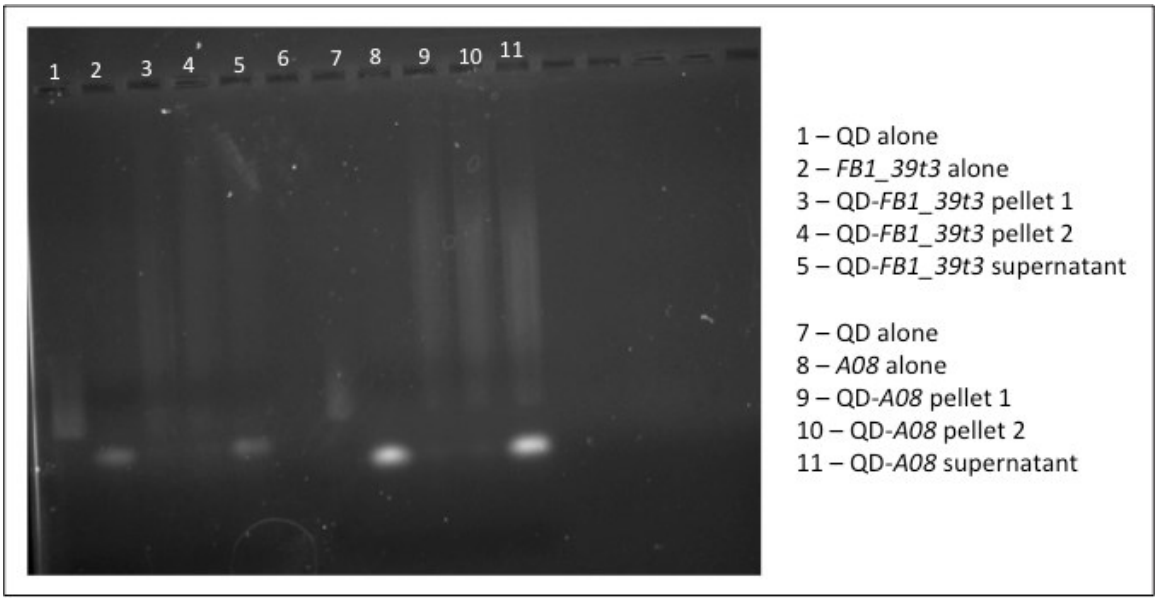

Figure 3.5 Agarose gel of fractions for QD-aptamer conjugation trials visualized with the fluorescence filter, AlphaImager. Pellet fractions include the QDs collected by centrifugation; supernatant fractions were collected directly after centrifugation.

For both *FB1_39t3* and *A08* conjugation reactions, the majority of the aptamer was recovered in the supernatant (Lane 5, Lane 11 Figure 3.5) indicating negligible amounts were coupled to the QDs (Lanes 3, 4, 9, and 10 Figure 3.5). The QDs, both alone and in the 'pellet' fractions, exhibit streaking through the agarose gel, possibly indicating aggregation in the 'pellet' fractions and 'alone' fractions disrupting the separation of QDs into a clear fluorescent band. When stained by EtBr, no DNA was seen in the 'pellet' fractions, further confirming that negligible aptamer coupling to QDs was achieved (data not shown). Troubleshooting efforts including modifying the buffer composition and using fresh conjugation reagents (EDC, Sulfo-NHS) were unsuccessful. Trials were continued in the hope that low amounts of aptamer coupling may have occurred and could maintain a low degree of LIANA assembly.

3.5.2.2 5'-5' linker quenching trials and controls

Assembly of the LIANA is driven by the addition of the short, 5'-5' linker DNA. For *FB1 39*, two linkers were used (Table 3.3); F8 has an 8-nt complementary region linking each aptamer, and F5 has a 5-nt complementary region. For *FB1_39t3* and *FB1_39t3-5*, equivalent linkers were designed to be complementary for the minimized aptamers, designated M8 and M5. Upon addition of the linker DNA, the AuNP-aptamer and QD-aptamer should be assembled into close proximity for FRET quenching of the QD fluorescence by the AuNP. With the longer complementary regions, it would be expected that F8 and M8 quench at a faster rate than F5 and M5.

Initial quenching trials aimed to characterize the quenching efficiency of the 8-nt and 5-nt complementary linker strands with each assembly of *FB1 39*, *FB1_39t3* and *FB1_39t3-5* functionalized QDs and AuNPs. The first set of trials were from an aptamer-QD conjugate reaction (EDC, Sulfo-NHS) performed in water and resuspended in FB_1 binding buffer prior to use. Figure 3.6 shows the quenching for each of *FB1 39*, *FB1_39t3* and *FB1_39t3-5* quenched through sequential addition of linker (F8/F5 and M8/M5).

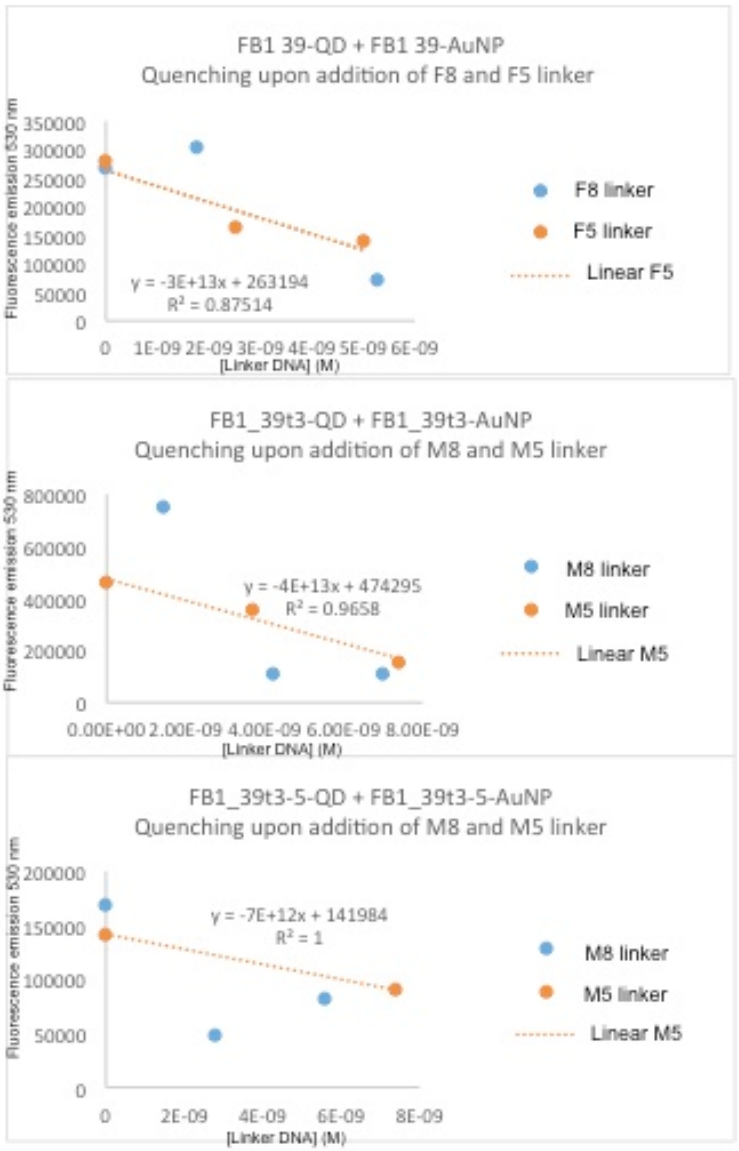

Figure 3.6 Quenching trials of *FB1 39*, *FB1_39t3* and *FB1_39t3-5* with addition of 5'-5' linker DNA

The rate of quenching between M8 and M5 linker was further explored with the *FB1_39t3* assembly (Figure 3.7). For this trial, and the remainder of the trials, the aptamer-QD conjugations were performed in 10 mM MES and 10 mM Na_2PO_4 buffers. It was observed that the rate of quenching for M8 and M5 was relatively similar, which is

counterintuitive to the assumption that a longer region of complementarity in the linker region would result in more efficient quenching.

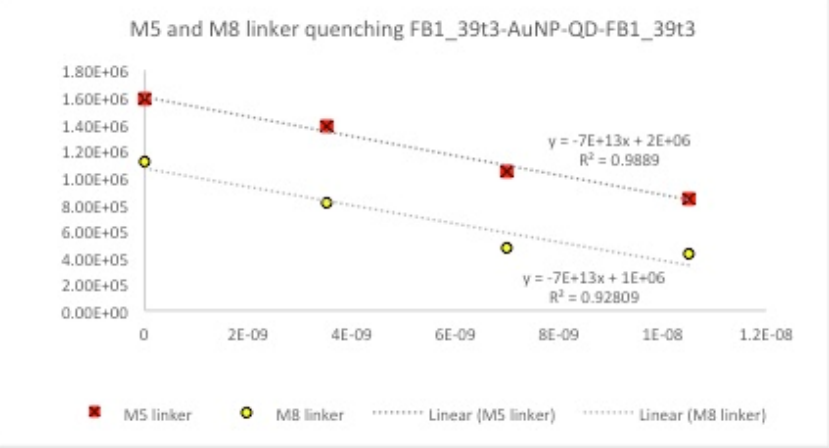

Figure 3.7 Comparison of quenching with M8 and M5 linker for QD-*FB1_39t3*-AuNP LIANA assembly

As the 5'-5' linker quenching was not consistent with what was expected, controls were tested to identify if the quenching observed was due to LIANA assembly or other factors. First, *FB1_39*-QD and unmodified AuNPs were tested with the addition of F8 linker DNA. Secondly, unmodified QDs and *FB1_39*-AuNPs were tested with the addition of F8 linker DNA. In both of these controls, the addition of linker DNA should not result in significant quenching as one of the constructs does not have the aptamer to link together the assembly (Table 3.4)

Table 3.4 Fluorescence emission at 530 nm and the resulting % quenching of *FB1 39*-QD and unmodified AuNPs with the addition of F8 linker DNA, and unmodified QDs and *FB1 39*-AuNPs with the addition of F8 linker DNA

[F8] linker	Em. 530 nm	% quenching
FB1 39-QD, unmodified AuNP		
0	265688	0
1.75 nM	302491	-13.8
5.25 nM	71610	73.0
3.5 μM	65294	75.4
Unmodified QD, *FB1 39*-AuNP		
0	237861	0
3.5 μM	145185	38.9

Both controls, with no aptamer on the QD and no aptamer on the AuNP, exhibited quenching in the presence of M8 linker DNA (Table 3.4). The unmodified AuNP control quenched to ~75% with 3.5 μM M8 linker; unmodified QD control quenched to ~39% with 3.5 μM M8 linker.

Further trials were tested with the *FB1_39t3* LIANA components. Both unmodified AuNPs and QDs, the absence of AuNPs, and the absence of M8 linker DNA were assessed (Table 3.5). All trials with M8 linker used a constant concentration of linker DNA to reduce variables.

Table 3.5 Trials eliminating components of the LIANA construct using *FB1_39t3* as a model, eliminating both the aptamer-functionalization on the QDs and AuNPs, the AuNPs, and the M8 linker DNA and quantifying the amount of fluorescence quenching observed (at 530 nm) under each set of conditions.

LIANA components			% Fluorescence (530 nm)
QD	**AuNP**	**Conc. M8 Linker**	
FB1_39t3-QD	*FB1_39t3*-AuNP	7 nM	83%
FB1_39t3-QD	AuNP	7 nM	61%
FB1_39t3-QD	0	7 nM	38%
QD	0	0 nM	50%
FB1_39t3-QD	*FB1_39t3*-AuNP	0 nM	51%
A08-QD	*FB1_39t3*-AuNP	7 nM	45%

Quenching to 83% fluorescence was observed with the apparent full LIANA construct (*FB1_39t3*-QD, *FB1_39t3*-AuNP, and M8 linker). Removing the aptamer from the AuNPs resulted in quenching to 61% of fluorescence. Removing AuNPs completely quenched further to 38% of the original fluorescence. Unmodified QDs in the absence of AuNPs or linker DNA quenched to 50% fluorescence. Aptamer-modified AuNPs and QDs quenched to 51% in the absence of linker DNA. A control aptamer (*A08*) conjugated to the QDs with *FB1_39*-AuNP quenched to a similar level of 45%. These results confirm that the quenching observed is completely independent of the aptamer-linker mediated LIANA assembly, and is attributed entirely to the QD quenching in FB_1 binding buffer.

3.5.2.3 QD aggregation troubleshooting

FB1_39t3-QD suspended in FB_1 binding buffer show visible aggregation both within the solution and aggregates adhering to the side of the microfuge tube after rounds

of centrifugation (Figure 3.8). Aggregation of water-soluble QDs will result in fluorescence quenching.[190]

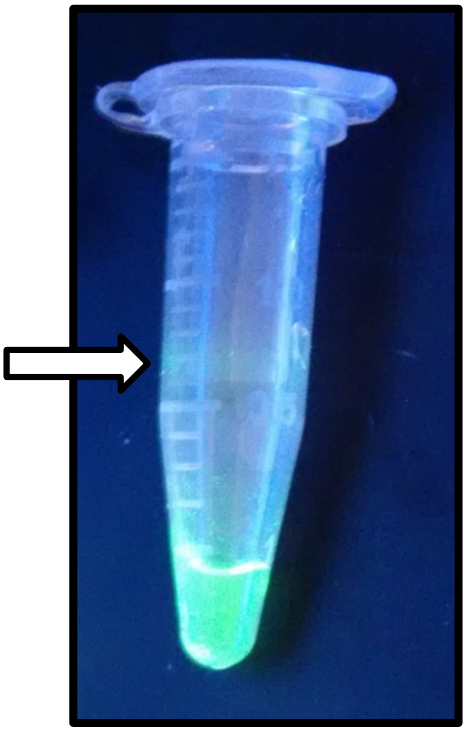

Figure 3.8 *FB1_39t3*-QD exhibiting aggregation in the solution (grainy solution) and on the walls of the microfuge tube (green residue shown with arrow), visualized by illumination with a hand-held UV light (254 nm)

QD aggregation and subsequent fluorescence quenching can be attributed to a number of factors. As the QDs are coated with a carboxyl-capped polymer, conditions of high ionic strength (over 100 mM) can cause charge-shielding effects to reduce the dispersion of the colloids resulting in aggregation. Additionally, surfactant-like molecules can undergo a "wrap and wrest" mechanism to adsorb the polymer coating, causing rapid fluorescence quenching.[191] Approaches used to shield the interactions between QDs that result in aggregation include the addition of Tween, BSA, or inorganic F- ions to the buffer to decrease non-specific surface interactions.[211] A simpler approach that would

have less effect on the matrix that the QDs are being used within is sonication, used to disperse any aggregated QDs back into the solution.

Various treatments of the *FB1_39t3*-QD solution were tested to compare their affect on the aggregation and subsequent quenching of fluorescence in a solution of FB_1 binding buffer. Unmodified QDs were tested as well. Each sample was monitored over five consecutive fluorescence measurements with mixing by pipette 10 times in between.

An aliquot of the *FB1_39t3*-QD solution was sonicated for 20 min at room temperature in an effort to disperse aggregates. A separate aliquot was centrifuged for 60 seconds in an effort to pellet out the aggregates and test the fluorescence stability of the supernatant solution. In the case that any complementarity or inter-strand DNA interactions between *FB1_39t3*-QDs (in the absence of linker DNA) were resulting in aggregation, the same aliquot was heated to 55°C for 10 minutes to disrupt any secondary structure of the aptamer and then measured for the last two time points. Unmodified QDs were measured in comparison (Figure 3.9).

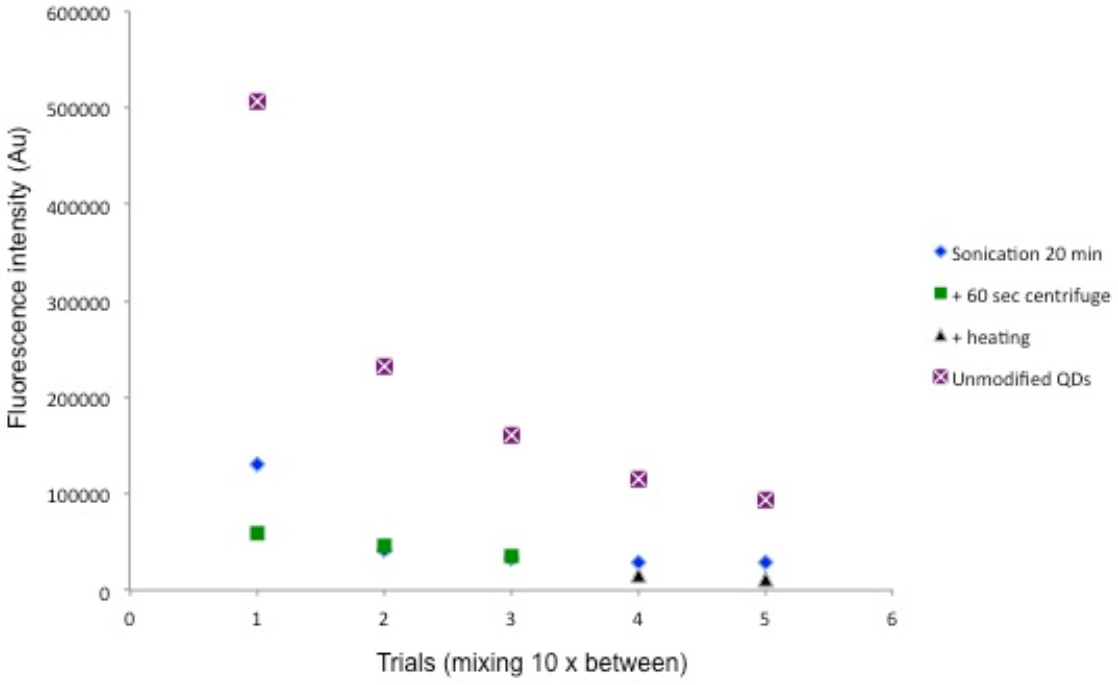

Figure 3.9 *FB1_39t3*-QD aggregation over five measurements with 10 x mixing by pipette between each trial. The effects of sonication, centrifugation, and heating were tested on the rate of aggregation of *FB1_39t3*-QDs. Unmodified QDs were tested as a control. Fluorescence intensity was monitored at 530 nm. All samples were suspended in FB_1 binding buffer.

Unmodified QDs exhibited exponential quenching of fluorescence over consecutive measurements with mixing between (Figure 3.9). Sonication, heating, and measuring the supernatant after centrifugation all had negligible effects on the fluorescence quenching in FB_1 binding buffer.

Lastly, unmodified QDs were tested over multiple consecutive measurements (mixing by pipette 10 times between) to monitor their fluorescence quenching in FB_1 binding buffer that was adjusted to different levels of ionic strength (NaCl concentration at 100 mM, 50 mM, 10 mM). The degree of fluorescence quenching tracked with the NaCl concentration in the buffer (Figure 3.10). In the 100 mM NaCl FB_1 binding buffer, the fluorescence at 530 nm dropped to below 40% of the original intensity after three

consecutive measurements and mixing. The purchased QDs were certified to be stable at a salinity of 100 mM; there were clearly either additional factors resulting in quenching, or the batch of QDs from the manufacturer was faulty.

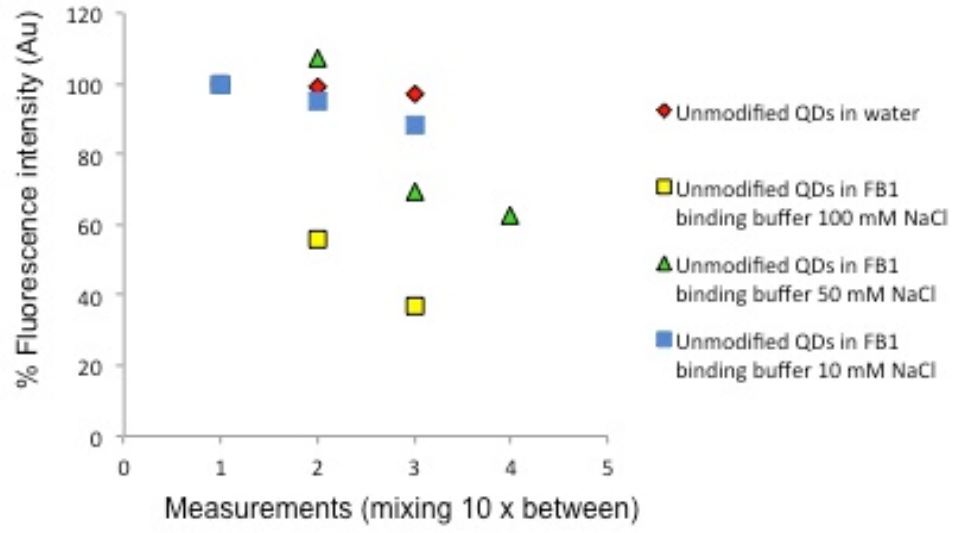

Figure 3.10 Fluorescence quenching (monitored at 530 nm) of unmodified QDs suspended in water and FB_1 binding buffer (100 mM, 50 mM, 10 mM NaCl) over multiple measurements with 10 x mixing by pipette between.

3.5.3 Fluorescent turn-on sensors using carbon-based quenchers

Carbon-based quenchers employing SWCNTs and GO were used to develop simple turn-on fluorescence sensors for FB_1 in solution. The SWCNT quenching studies were conducted with both unmodified and acid-modified SWCNTs. Fluorescence donors were 5'-fluroescein modified *FB_1 39* for the SWCNT studies, and QD-*$FB_1$39* and QD-*FB1_39t3* for the graphene oxide studies.

3.5.3.1 SWCNTs

Unmodified SWCNTs have very low solubility in water, and it is therefore very difficult to ascertain the exact concentration of SWCNTs in solution as the solution generally settles out a dark pellet, leaving a light yellow supernatant to use as the

quencher. This solution was used to quench 5'-fluorescein modified *$FB_1$39* aptamer. As fluorescein is very dependent on pH and ionic strength of the FB_1 binding buffer, adding variable amounts of a FB_1 stock resulted in an inconsistent fluorescence signal with a constant amount of 5'-fluorescein aptamer. To control for this variability, the fluorescence of each sample, incubated with a range of FB_1 concentrations, was quantified by fluorescence spectroscopy before and after the addition of a constant amount of SWCNTs. In the presence of FB_1, the aptamer will interact with FB_1 preferentially over the added SWCNTs, resulting in a protective effect against fluorescence quenching. In the absence of FB_1, the aptamer will adsorb to the surface of the SWCNTs and the fluorescence will be drastically quenched by FRET.

In Figure 3.11 below, the fluorescence emission of fluorescein (520 nm) is monitored for 5'-fluoro-*$FB_1$39* in the presence of FB_1 (0 – 750 nM) both before and after the addition of a constant amount of SWCNTs in solution. Panel A shows the fluorescence spectra of fluorescein-modified aptamer. Panel B shows the fluorescence intensity at 520 nm for each concentration of FB_1 before and after SWCNT addition. Panel C shows the change in fluorescence upon SWCNT addition follows a linear trend. At higher concentrations of FB_1, there is a smaller change in fluorescence upon addition of SWCNT. This demonstrates a protective effect of FB_1 from SWCNT-mediated quenching of fluorescein-modified aptamer (Figure 3.11).

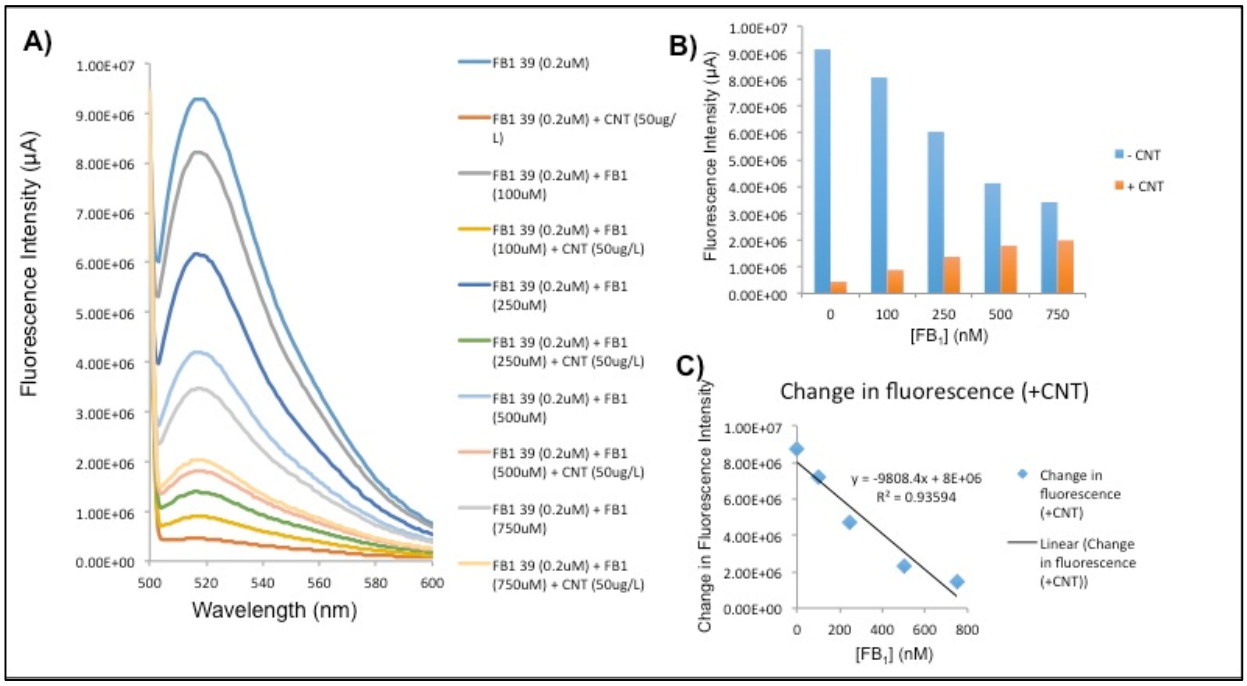

Figure 3.11 Pristine SWCNT addition to 5'-fluorescein-*FB1 39* with a range of FB_1 present, demonstrating a linear trend between FB_1 concentration and the change in fluorescence upon addition of SWCNTs.

3.5.3.2 Acid-modified SWCNTs

The modification and functionalization of SWCNT surfaces have found use in sensor applications, either to increase solubility in aqueous media, conjugate species to the surface, or modify the reactivity of the surface. Acid-modifying the SWCNT surface increases water solubility and develops a pH-dependent negative surface charge. Given the negative charge on DNA due to the phosphate backbone, it would be assumed that the adsorption of ssDNA onto the surface of acid-modified SWCNTs (amSWCNTs) would be lower relative to pristine SWCNTs. For a sensor application where the presence of a

target is aiming to overcome the attractive forces between the aptamer and the quencher, this could be an advantage and could increase sensitivity.

The amSWCNTs were quantified and compared to the pristine (unmodified) SWCNTs by UV-Vis spectroscopy (Figure 3.12). Unmodified SWCNTS both before and after centrifuging down the pellet and testing the supernatant had a small absorption peak around 300 nm. Unmodified SWCNTs after sonication had a more gradual and wide absorption range. The amSWCNTs had a significantly higher absorption with a wide peak around 200 – 300 nm indicating a greater dispersion in solution[196] (Figure 3.12).

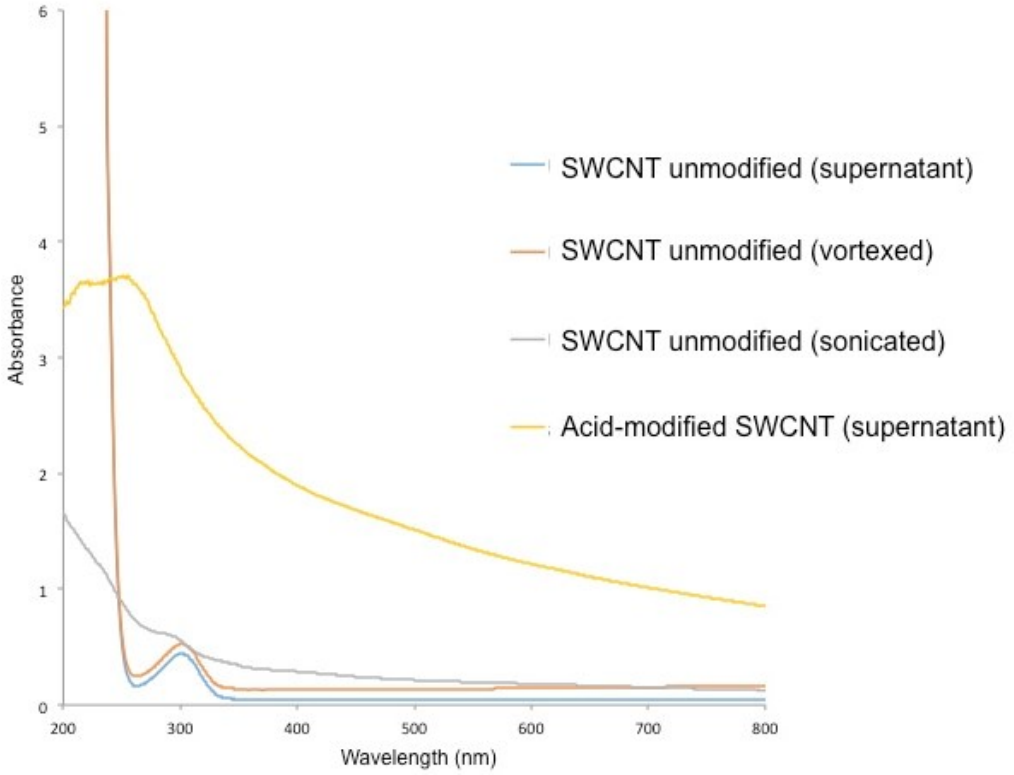

Figure 3.12 UV-Vis absorption spectrum of unmodified (pristine) SWCNTs and amSWCNTs

Further characterization of the amSWCNTs was obtained through HR-TEM images of the solution. In Figure 3.13, it is evident that there are still aggregates of

SWCNTs clustering, but there are many regions of dispersed long strands of amSWCNTs present.

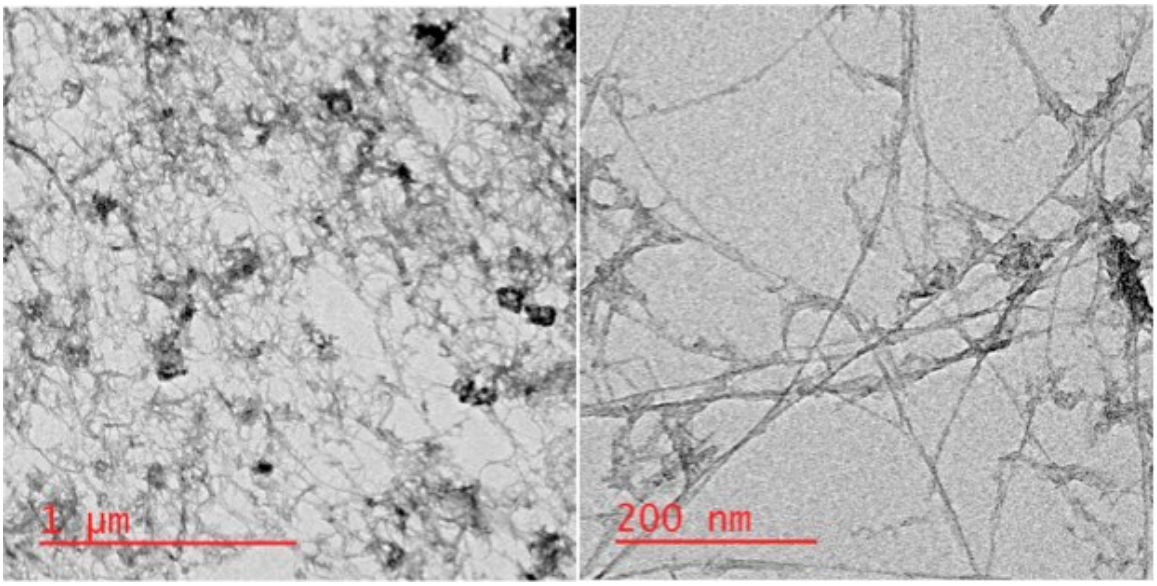

Figure 3.13 HR-TEM images of acid-modified SWCNTs

The fluorescence quenching of 5'-fluorescein-*FB1 39* was monitored with the addition of amSWCNTs (Figure 3.14). Quenching of fluorescein (monitored at 515 nm) upon addition of amSWCNTs was observed to be linear and rapid; incubation of the 16 µl (0.1 mg/ml) sample for an additional 5 min before re-quantifying fluorescence revealed a negligible change in the fluorescence. The rate of quenching of amSWCNTs was compared to the quenching rate of pristine SWCNTs (Figure 3.14). As expected, amSWCNTs quenched the fluorescence of 5'-fluorescein tagged DNA at a slower rate than unmodified SWCNTs, due to the electrostatic repulsion between the negative phosphate backbone and certain negatively charged residues from acid modification (ie: hydroxyl and carboxyl).

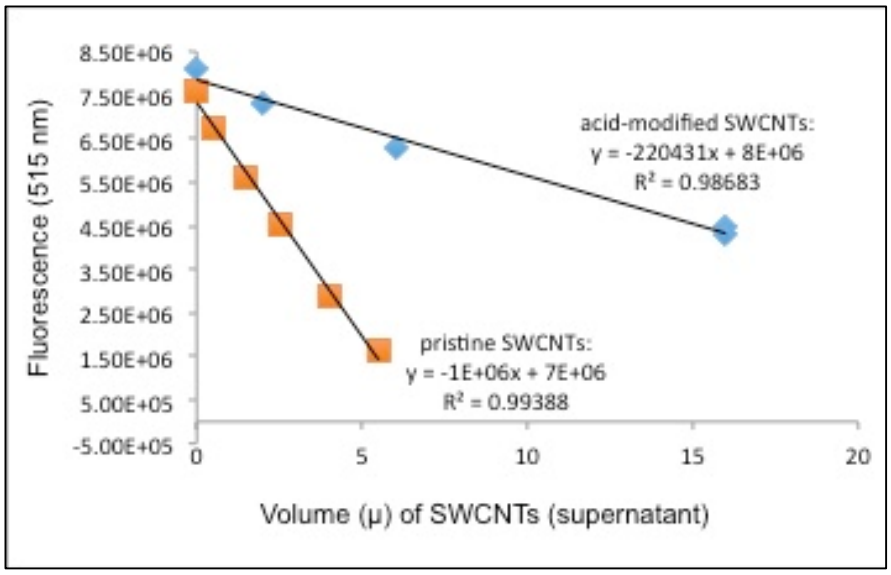

Figure 3.14 Quenching rate of 5'-fluorescein-*FB1 39* with amSWCNT addition (at 0.1 mg/ml) compared to pristine SWCNTs (supernatant)

The amSWCNTs were then integrated into a similar FB_1 sensing assay as previously tested with the pristine SWCNTs (Figure 3.15 below). Fluorescence was measured before and after addition of amSWCNTs to compare the change of fluorescence relative to FB_1 concentration. The range of FB_1 concentrations was between $0 – 1x10^{-5}$ M and the sensor was tested in FB_1 binding buffer. Unlike the results obtained from the pristine SWCNTs, there was not a clear trend between FB_1 concentration and fluorescence quenching. There is a slight negative trend in Figure 3.15 (panel C) between $1x10^{-8}$ and $1x10^{-6}$ M FB_1, indicating that in this range FB_1 binding to 5'-fluroescein-*FB1 39* may be providing a slight protective effect over the quenching induced by addition of amSWCNTs. However, this trend is much less convincing than the previous results obtained with the pristine SWCNTs.

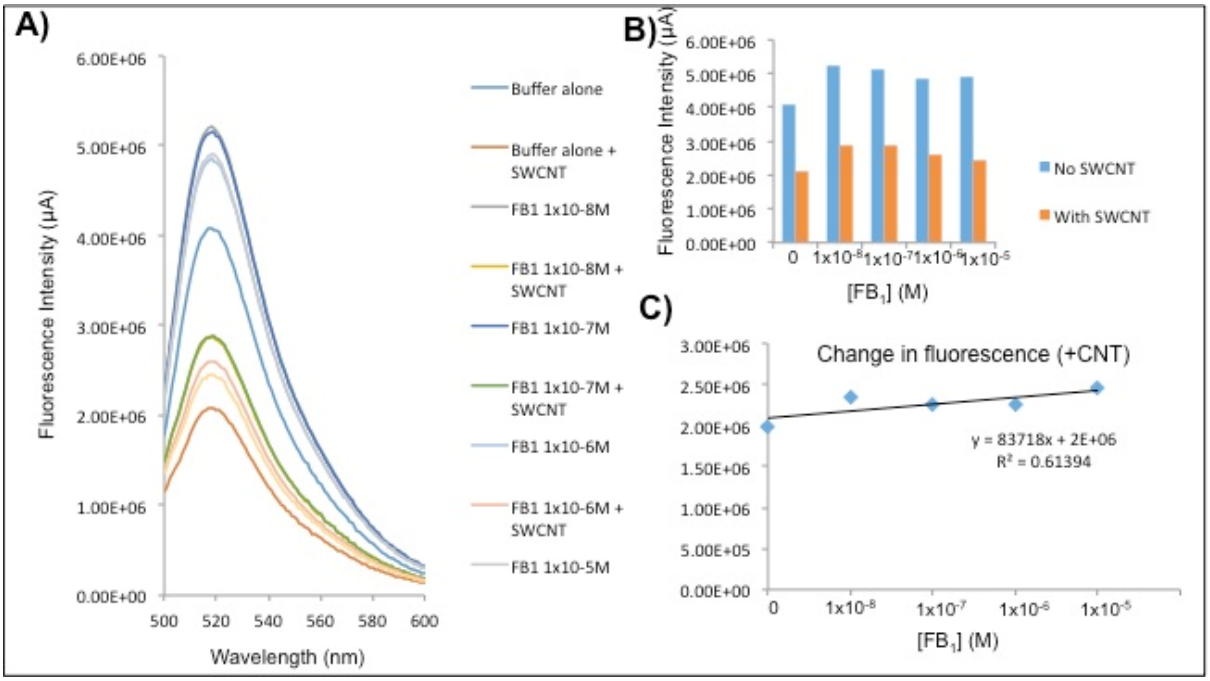

Figure 3.15 amSWCNT addition to 5'-fluorescein-*FB1 39* with a range of FB_1 present, demonstrating a slight linear trend between $1x10^{-8}$ – $1x10^{-6}$ M FB_1 concentration to protect from quenching and decrease the change in fluorescence upon addition of SWCNTs.

One possible contributing factor to the poor performance of the amSWCNT-based FB_1 sensor is the pH of the solution. In FB_1 binding buffer (pH 7.4-7.6), less of the acid-modifying motifs (*i.e.* hydroxyl) would be in their charged ionic state. Performing the quenching in a more acidic pH buffer would theoretically decrease the interactions between the negatively charged DNA and the amSWCNTs. The rate of quenching was monitored at pH 7.4 and pH 6.3 for 5'-fluorescein-*FB1 39* and amSWCNTs in FB_1 binding buffer (Figure 3.16). As expected, at the more acidic pH, the quenching occurred more rapidly than at a neutral pH.

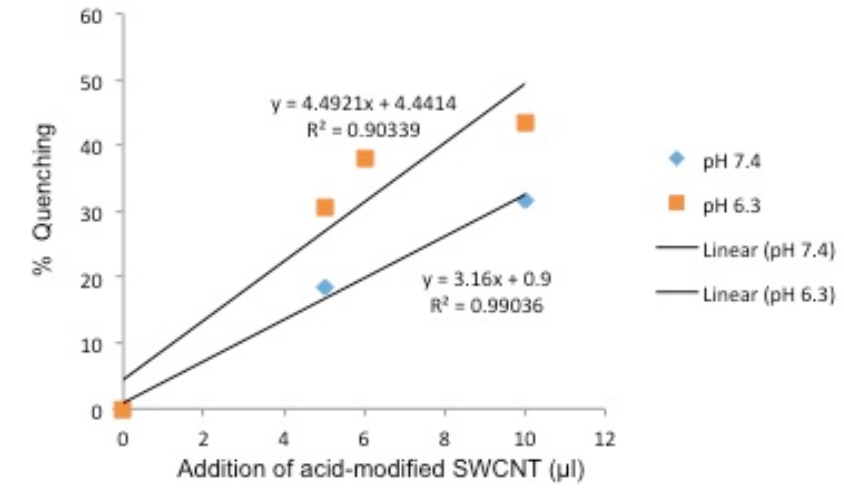

Figure 3.16 The relative rate of fluorescence quenching (517 nm) as % quenching of 5'-fluorescein-*FB$_1$39* and amSWCNTs in FB$_1$ binding buffer at pH 7.4 and pH 6.3

An analogous sensor to previous trials was tried with the amSWCNTs in the lower pH buffer system to see if fluorescence recovery upon FB$_1$ addition was more responsive at pH 6.3 than pH 7.4. Again, the fluorescence of 5'-fluorescein-*FB$_1$39* was monitored at varying concentrations of FB$_1$ ($1x10^{-7}$ to $1x10^{-3}$) before and after amSWCNT addition (Figure 3.17). There was a slight negative trend to the change in fluorescence with increasing FB$_1$ concentration, indicating a mild protective effect of FB$_1$ against amSWCNT quenching due to target-aptamer interaction.

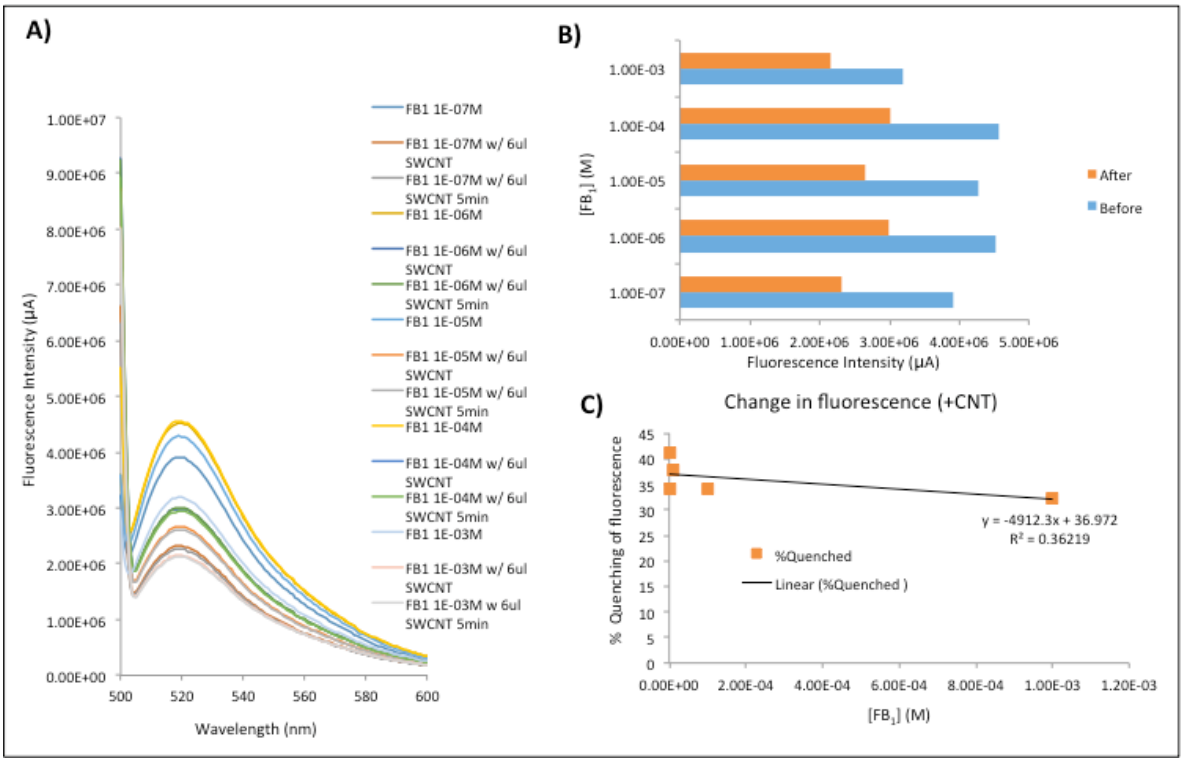

Figure 3.17 Effects of adjusting the pH to 6.3, amSWCNT addition to 5'-fluorescein-*FB1_39* with a range of FB_1 present, demonstrating a slight linear trend between $1x10^{-7}$ – $1x10^{-3}$ M FB_1 concentration to protect from quenching and decrease the change in fluorescence upon addition of SWCNTs.

Further experiments would be needed to optimize and confirm the performance of this sensor. However, efforts were moved on to explore quantum-dot based fluorescence sensors to avoid the interference effects of buffer and salinity and photo quenching associated with fluorescein as a fluorescent source.

3.5.3.3 Graphene oxide

3.5.3.3.1 *FB1_39t3* conjugated to CdSe/ZnS QDs

The graphene oxide sensor trials were performed in parallel to the initial LIANA FB_1 sensor trials (Section 3.5.2), as the same conjugation chemistry was employed to link the 5'-NH_2 modified aptamer sequences with the carboxyl-capped QDs. Experiments to

test the success of the aptamer-QD coupling efficiency and troubleshooting QD aggregation were collaborative between the two applications of the aptamer-QD constructs. Due to the same ongoing issues with QD aggregation and failure of adequate coupling efficiency to obtain significant levels of aptamer-QD conjugates, only preliminary results will be shown here to avoid repetition. With the aptamer-QD coupling performed in the 10 mM MES / 10 mM Na_2PO_4 buffer combination, a small amount of aptamer was likely coupled through the albeit inefficient conjugation chemistry to the QD surface (~10% coupling achieved as highest efficiency measured).

Results from the *FB1_39t3*-QD fluorophore quenched to 50% of fluorescence by an aqueous suspension of graphene oxide (GO) are shown below in Figure 3.18. As the QD fluorescence had been shown to be relatively inconsistent between samples, a single GO-quenched sample of *FB1_39t3*-QD was split into two equal aliquots; one was treated as a control with the addition of water, and the other with the addition of a high concentration of FB_1 dissolved in water. By comparing the water vs. FB_1 samples, and adjusting for the dilution factor, fluorescence recovery to 60% of the original fluorescence was noted for the high concentration FB_1 sample (10 µl of FB_1 at 54 µM into a final volume of 50 µl). The addition of water alone resulted in further quenching of the solution to 25% of the original full fluorescence.

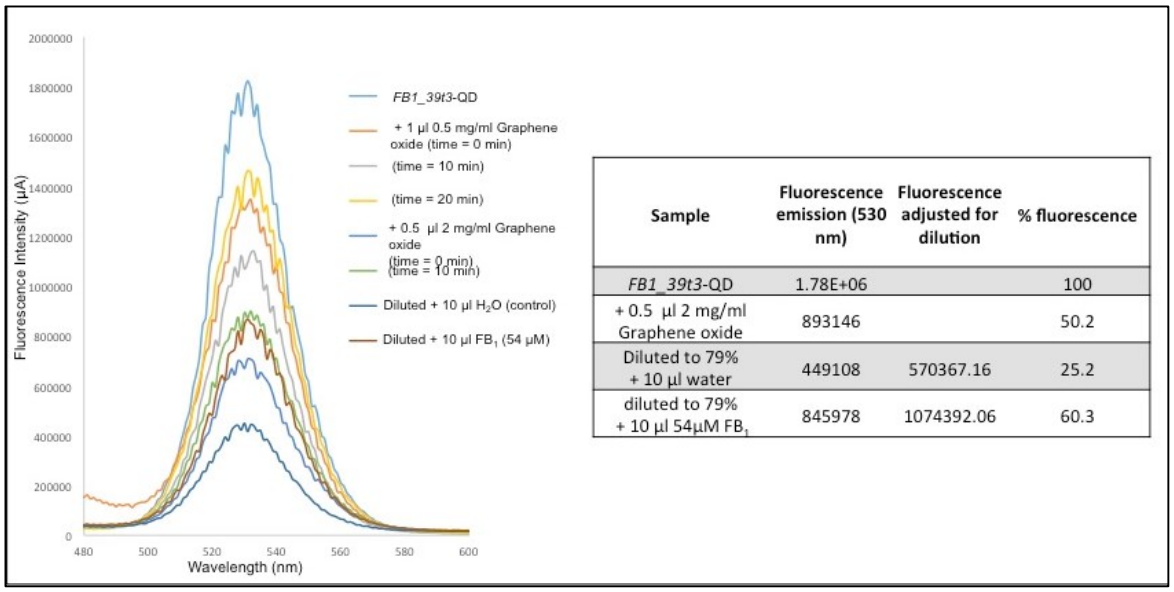

Sample	Fluorescence emission (530 nm)	Fluorescence adjusted for dilution	% fluorescence
FB1_39t3-QD	1.78E+06		100
+ 0.5 µl 2 mg/ml Graphene oxide	893146		50.2
Diluted to 79% + 10 µl water	449108	570367.16	25.2
diluted to 79% + 10 µl 54µM FB_1	845978	1074392.06	60.3

Figure 3.18 Fluorescence of *FB1_39t3*-QD with quenching by graphene oxide monitored over several time points. After quenching was stabilized at 50% of the original fluorescence, the sample was split and diluted with either 10 µl water (control) or 10 µl FB_1 at 54 µM and the fluorescence and subsequent effects of the overall fluorescence recovery were measured. Note that the fluorescence spectra appear jagged due to minor instrumentation malfunction at the time of measurement.

Although this shows slight promise for fluorescence recovery responsive to FB_1, the ongoing concerns with the CdSe/ZnS QDs prevented further experiments from progressing as the results were not as reliable or consistent as would be required for developing a GO and QD based FB_1 sensor.

3.5.3.3.2 *$FB_1$39* conjugated to CdTe QDs

After ongoing concerns with the aptamer-conjugated green-emitting QDs (CdSe/ZnS), the same conjugation chemistry (10 mM MES / 10 mM Na_2PO_4) was applied to conjugating 5'-NH_2-*$FB_1$39* to carboxyl capped red-emitting CdTe QDs. Similarly to previous trials with the green-emitting QDs, UV-Vis analysis of the aptamer fractions before and after coupling revealed negligible amounts of *$FB_1$39* appeared to be conjugated to the QD successfully. Nevertheless, this conjugate was monitored over six

consecutive fluorescence measurements with mixing by pipette between (10 times) in a range of conditions. The *FB139*-QD conjugate was monitored in FB_1 binding buffer, 100 mM Na_2PO_4 buffer, water, and in FB_1 binding buffer with subsequent addition of GO (1 µl of 2 mg/ml solution at each measurement point) (Figure 3.19). Although the GO treated solution did maintain the lowest fluorescence (highest quenching), almost all of the treatments resulted in a very similar quenching profile of the fluorescence emission of CdTe QDs at 655 nm. These results indicate that the quenching upon GO addition is attributed to a critical concern with the QDs not being stable in the reaction conditions resulting in self quenching over repeated measurements.

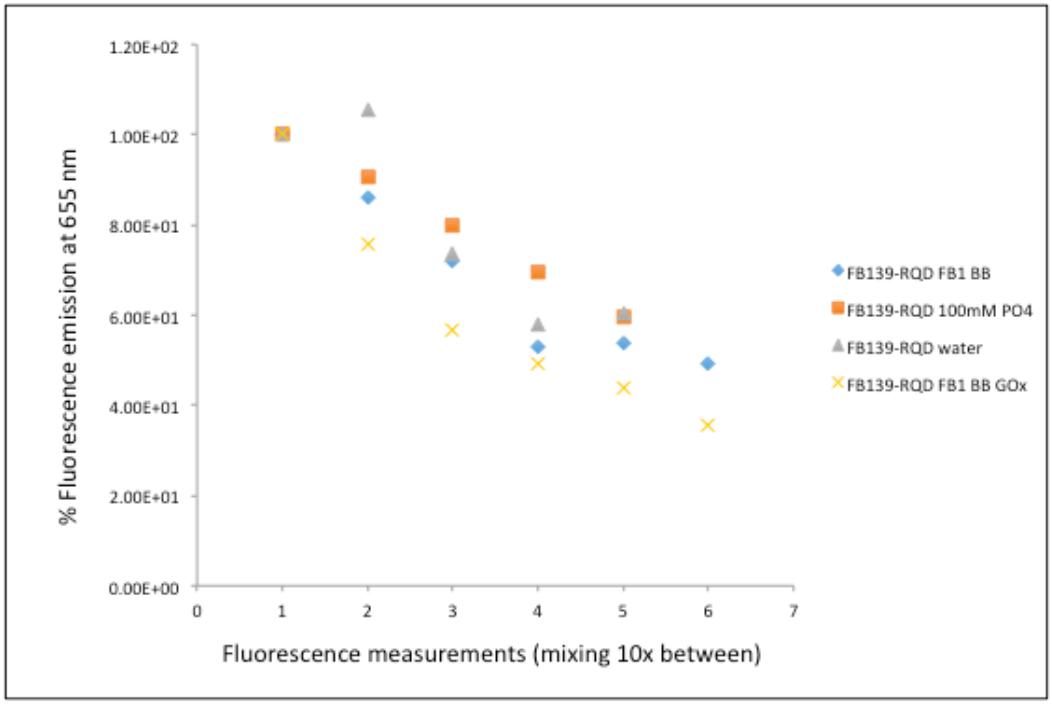

Figure 3.19 Fluorescence emission (655 nm) monitored over 6 consecutive measurements (mixing by pipette 10x between) of *FB139*-QDs (CdTe) in FB1 binding buffer, 100 mM Na_2PO_4 buffer, water, and in FB_1 binding buffer in the presence of 2 mg/ml graphene oxide (addition of 1 µl at each time point)

Due to the ongoing concerns with the aptamer-QD conjugates, further trials were not pursued for this sensor design.

3.5.4 Label-free SYBR Green I sensor for FB_1

SYBR Green I (SG) intercalates into the minor groove of duplex DNA resulting in a dramatic enhancement of fluorescence with a peak ~520 nm upon excitation at 497 nm. SG can be used to develop a label-free binding assay for quantifying small-molecule aptamer interactions.[111] If target binding results in a disruption of the secondary structure of the aptamer and subsequent displacement of SG, the fluorescence of the construct will decrease linearly with target concentration. From the DNase I assay, it is understood that binding of FB_1 to *$FB_1$39* does not result in any dramatic changes in the duplex structure of the aptamer, as changes in the DNase I digestion pattern with target concentration were consistent yet subtle. *$FB_1$39*, *FB1_39t3* and *FB1_39t3-5* were tested with the SG assay and no change in fluorescence was observed between $0 - 1x10^{-5}$ M FB_1 (data not shown). For this reason, a complementary probe to the *FB1_39t3* region (*cFB1_39*) was synthesized (with no modifications) to evaluate the ability of FB_1 binding to displace the probe. As the complementary probe is long (48 nt, half of the length of *$FB_1$39*), there is a noticeable increase in SG fluorescence when it is bound to *$FB_1$39*. Displacement of some of the *cFB1_39t3* will result in a reversion of the fluorescence signal to levels closer to the original *$FB_1$39* SG fluorescence. This assay is illustrated below (Figure 3.20).

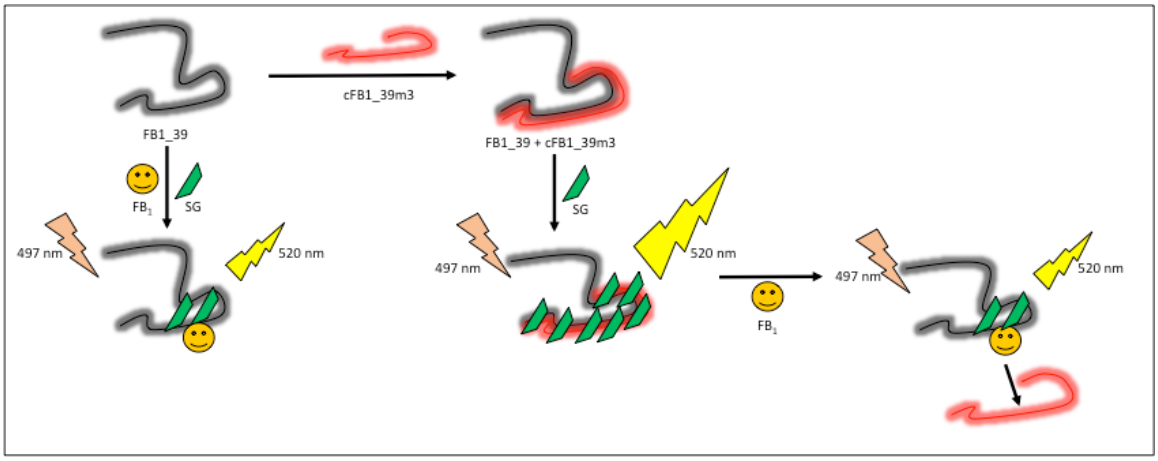

Figure 3.20 Sensing scheme for label-free SYBR Green I (SG) fluorescence assay for detecting FB_1. The fluorescence of *$FB_1$39* in the presence of SG is lower than that of *$FB_1$39 + cFB1_39t3* which is a 48-nt complement strand. With a higher degree of duplex structure, in the presence of SG the fluorescence is increased (indicated by the larger yellow lightning bolt). The presence of target does not affect the secondary structure of *$FB_1$39* enough to change the SG fluorescence. However, when FB_1 is added to the *$FB_1$39 + cFB1_39t3* mixture, FB_1 binding to *$FB_1$39* will kick off some of the bound *cFB1_39t3* and cause the SG fluorescence to drop back to levels closer to the initial *$FB_1$39* baseline levels.

A thermal melting study was conducted to determine the stability of the *cFB1_39t3* probe in the presence of *$FB_1$39*. The T_m of the probe dissociation was 75.6 ± 0.82°C indicating it is very stable relative to the T_m of *$FB_1$39* (41°C) (Figure 3.21).

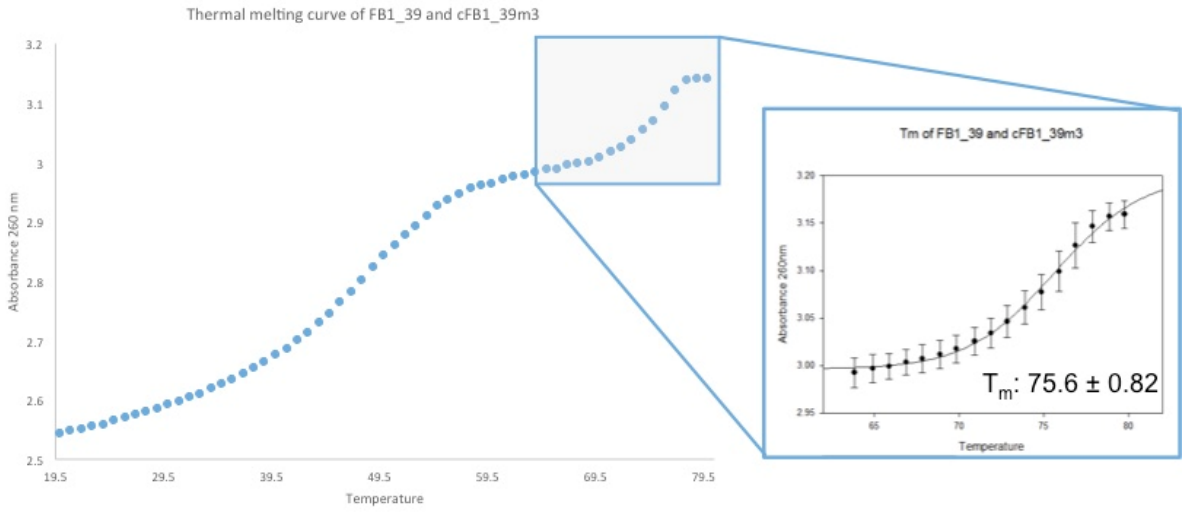

Figure 3.21 T_m curve of *$FB_1$39* and *cFB1_39t3* showing two distinct regions of denaturation. The first T_m corresponds to the *$FB_1$39* aptamer, and the second (inset) corresponds to the denaturation of the *cFB1_39t3* region off of the *$FB_1$39* aptamer. The T_m of this interaction is 75.6 ± 0.82°C indicating that it is very stable (due to its long overlap of complementarity, 48 nt)

The initial trials displayed, as expected, a higher SG fluorescence emission for *$FB_1$39+cFB1_39t3* than for *$FB_1$39* alone. With increasing concentration of FB_1, the difference in fluorescence between *$FB_1$39+cFB1_39t3* and *$FB_1$39* alone decreased, particularly between FB_1 concentrations between $1x10^{-8} – 1x10^{-5}$ M (Figure 3.22).

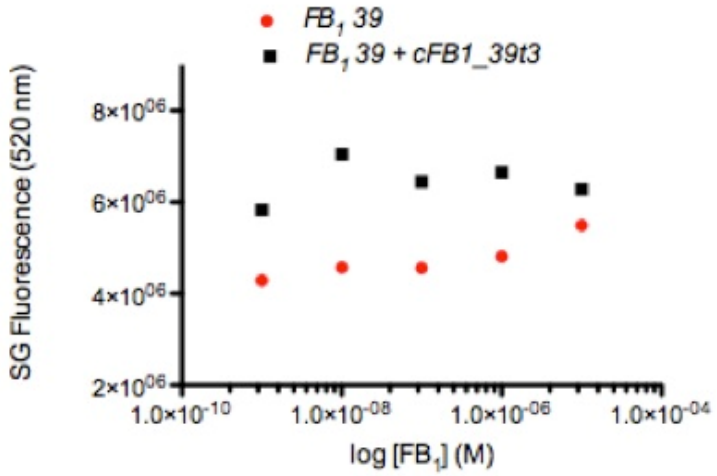

Figure 3.22 SG fluorescence (520 nm) of *FB1 39+cFB1_39t3* and *FB1 39* demonstrating a trend in the *FB1 39+cFB1_39t3* fluorescence towards the *FB1 39* level of fluorescence at high [FB1], indicating that target binding is involved in displacing the *cFB1_39t3* probe from *FB1 39*.

As the trend was not strong, further experiments were not continued with this assay.

3.5.5 Selectivity and performance of fumonisin and ochratoxin aptamers in a sample matrix

Contrary to the FB_1-bound affinity tests used to characterize the K_d of *FB1 39* minimers in Section 2.5.3.2, the design of this test was switched to facilitate testing aptamer performance and selectivity in a real sample matrix. 5'-NH_2-modified *FB1 39*, *FB1_39t3*, *FB1_39t3-5* and *A08* were functionalized onto NH_2-capped magnetic beads. These beads were incubated with a variety of contaminated grape samples with fumonisins and ochratoxins as well as natural matrix components that could interfere with aptamer binding, or could cross-bind with the aptamers causing concern for false positives in a downstream sensor in this matrix (Figure 3.23)

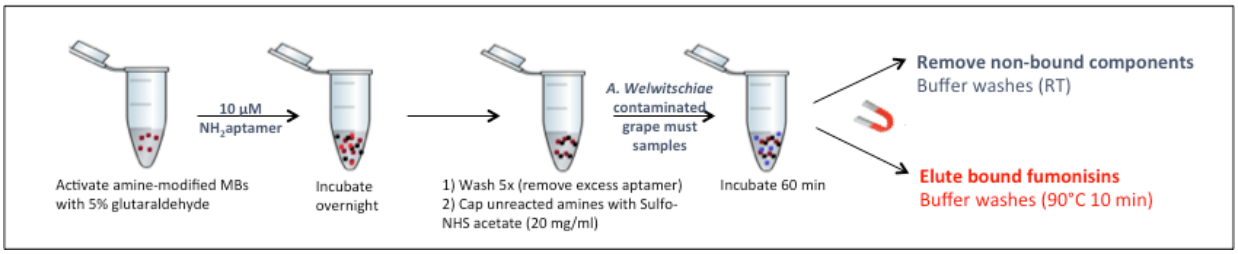

Figure 3.23 Assay design of aptamer-mediated binding to measure selectivity and performance in a contaminated grape matrix. M-270 amine DynaBeads were activated with 5% glutaraldehyde to facilitate coupling with NH_2-modified aptamers. Excess amine groups were capped with Sulfo-NHS Acetate. The contaminated grape matrix (*A. welwitschiae* for fumonisins; *A. carbonarius* for ochratoxin) was incubated with the aptamer-bead matrix for 60 min. The non-bound components were washed off with buffer washes at room temperature, separating by magnet each time. Bound fraction of mycotoxins were heat-eluted off of the aptamer-funcitonalized beads and sent for analysis by HPLC-MS/MS to perform relative quantitation of each toxin from the toxin fraction before and after aptamer-bead extraction.

This test reveals the performance of each of these aptamers in a 'real' sample matrix. Additionally, other non-traditional fumonisins and ochratoxins, or structurally similar endogenous molecules, can be present in these samples. It is of interest to know if the aptamers maintain binding affinity with these species. Firstly, this can be of importance depending on which species are regulated, notably if the aptamer would cross-react and create a false positive result. Secondly, knowing which structurally-similar species are bound by the aptamer *vs.* are not bound by the aptamer can develop evidence for where on the small molecule the aptamer is binding (*i.e.* if the aptamer loses affinity for the modified toxin that is missing one functional group, this would be an indicator that that functional group is important for binding interactions and recognition).

The relative quantitation of fumonisins or ochratoxins found within each fraction (before incubation with aptamer-functionalized beads vs. bound eluted fractions) was achieved by HPLC-MS/MS. A representative extracted chromatograph showing the retention order of FB_2, FB_4, and FB_6 is shown in Figure 3.24.

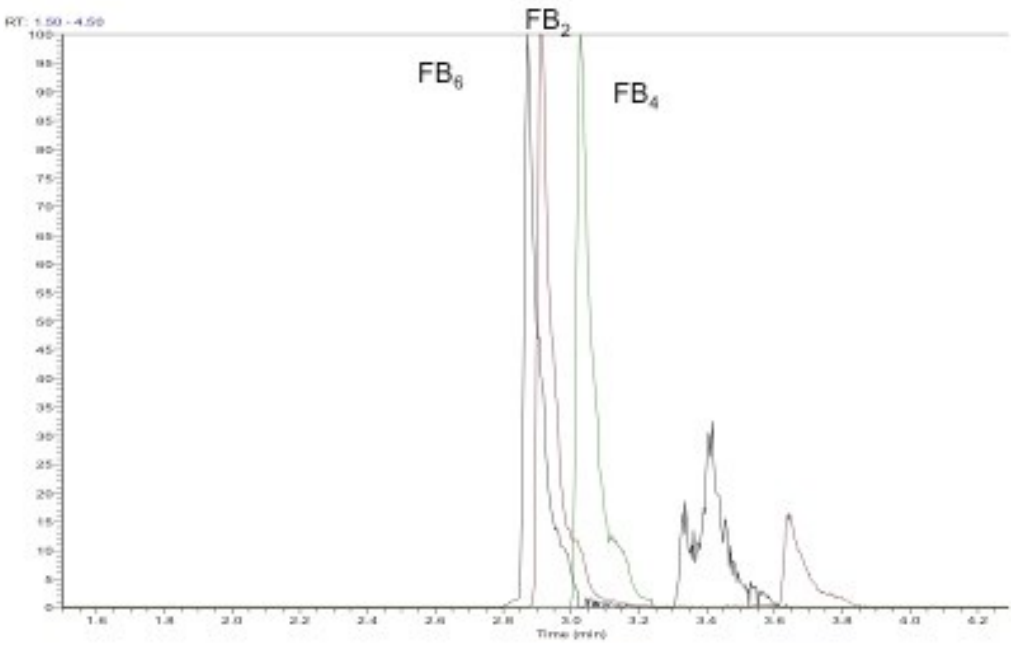

Figure 3.24 Representative extracted chromatograph showing retention order of FB_2, FB_4 and FB_6

HR-MS/MS was then used to confirm the identity of each peak by the characteristic fragmentation pattern of each mycotoxin form (Figure 3.25).

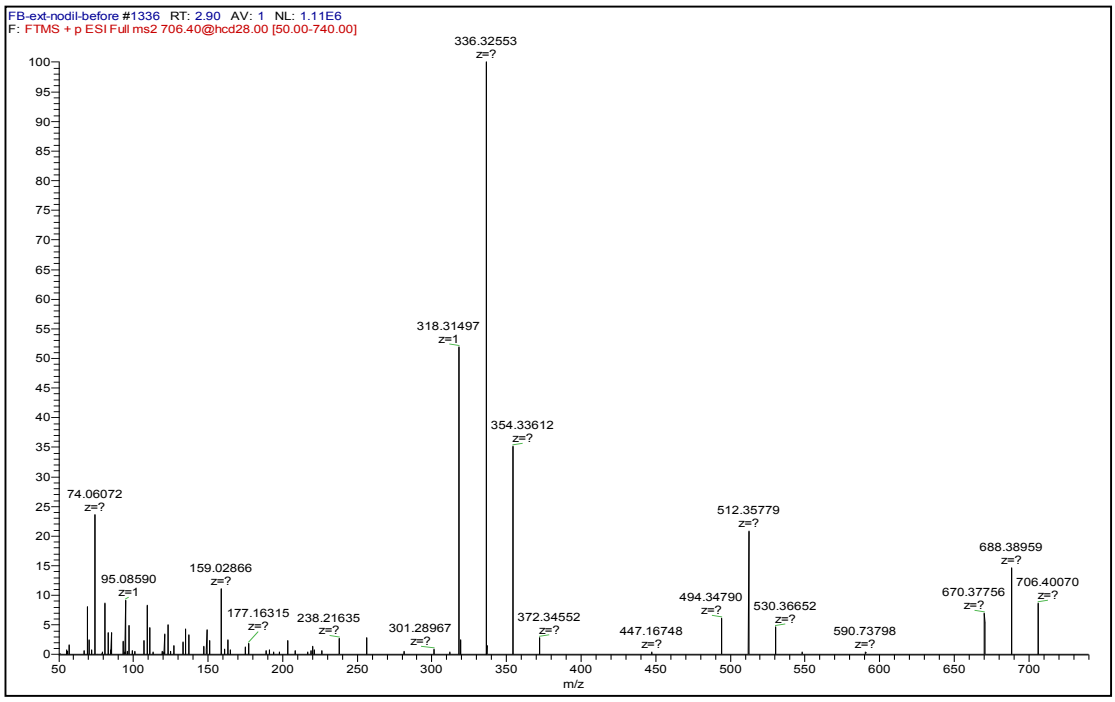

Figure 3.25 MS^2 spectra of FB_2 with a characteristic fragmentation pattern allowing for identification

From the extracted fumonisins, FB_2, FB_4, and FB_6 were found in each bound fractions (*$FB_1$39*, *FB1_39t3* and *FB1_39t3-5*) at low levels. Due to the high amount of fumonisins extracted from the grape matrix, only a low percent of the fumonisins present were bound by the aptamer-functionalized beads. Of the 10x dilute extracted fumonisins, *$FB_1$39* bound the highest percentage of fumonisins, and had some affinity for each of the natural fumonisins produced by the *A. welwitschiae* strain (FB_2, FB_4 and FB_6) (Table 3.6). The binding of *$FB_1$39* and *FB1_39t3* to the extracted fumonisins was not consistent between the 5x diluted and 10x diluted extracted samples. However, *FB1_39t3-5* demonstrated binding at low levels in all of the samples except for FB_2 from the 5x diluted extracted sample (Table 3.6).

Table 3.6 Dilute extracted fumonisins from *A. welwitschiae* producing fumonisins on grapes, showing the bound fractions of each fumonisin (FB_2, FB_4, and FB_6) to each of the FB_1 aptamers (*$FB_1$39*, *FB1_39t3*, and *FB1_39t3-5*).

		% of bound fumonisins (signal recovery), control subtracted		
Fumonisin grape must sample		**FB1_39**	**FB1_39t3**	**FB1_39t3-5**
5x dilute extracted fumonisins	FB_2	0	**0.32**	0
	FB_4	0	**0.73**	**0.24**
	FB_6	0	**0.11**	**0.16**
10x dilute extracted fumonisins	FB_2	**0.23**	0	**0.1**
	FB_4	**1.4**	0	**0.23**
	FB_6	**0.36**	0	**0.19**

Aptamer-mediated extraction of fumonisins directly from the grape matrix (with no extraction procedure) was also tested. The sample preparation for these samples is minimal, involving a simple filtering step prior to the aptamer binding test. Both FB_4 and FB_6 fell below the detection levels in all samples (both bound fractions and the samples before aptamer-bead incubation) suggesting that the extraction procedure is necessary to

release these fumonisins from the matrix components in levels above the detection limit. However, FB_2 was present at detectable levels, and all of the aptamers (*$FB_1$39*, *FB1_39t3* and *FB1_39t3-5*) bound FB_2 from the matrix. The 10x dilute matrix diluted into buffer resulted in >20% binding of FB_2 with *$FB_1$39*- and *FB1_39t3*-bound beads (Table 3.7).

The fractions were also screened for other structurally diverse fumonisins. FA_2, FA_3, FA_4, FC_2, and FC_4 were detected in small amounts in some of the extracted fumonisin samples, but only FA_2 was present in any of the bound aptamer fractions (*FB1_39t3-5* bound 0.6%). Although inconclusive, this could indicate the aptamers selected for FB_1 have a relatively low affinity for some of the other fumonisin compounds. The list of fumonisin compounds measured, their structures, and the detection in each fraction can be found in Appendix A (Figure 5.1 and Table 5.1).

Table 3.7 Dilute fumonisins (no extraction) from an *A. welwitschiae* producing fumonisins on grapes, showing the bound fractions of each fumonisin (FB_2, FB_4, and FB_6) to each of the FB_1 aptamers (*$FB_1$39*, *FB1_39t3*, and *FB1_39t3-5*)

		% of bound fumonisins (signal recovery), control subtracted		
Fumonisin grape must sample		**FB1_39**	**FB1_39t3**	**FB1_39t3-5**
90:10 buffer:grape must no extraction	FB_2	**2.11**	**4.3**	**1.5**
	FB_4	0	0	0
	FB_6	0	0	0
10x dilute 90:10 buffer:grape must no extraction	FB_2	**22.4**	**21.4**	N/A
	FB_4	0	0	N/A
	FB_6	0	0	N/A

5'-NH_2-*A08* was the only aptamer tested for performance and selectivity in the *A. carbonarius* contaminated grape matrix. OTA was not detected in the samples that did not undergo the acidic extraction procedure. In the extracted samples, up to 5.2% of OTA was extracted from the matrix (10x diluted) with *A08*-functionalized beads (Table 3.8).

Table 3.8 Dilute ochratoxin (with and without extraction) from *A. carbonarius* infected grapes, showing the bound fractions of OTA to *A08* aptamers.

		% of bound ochratoxin A (signal recovery), control subtracted
Ochratoxin grape must sample		**A08 aptamer**
5x dilute extracted ochratoxin	OTA	2.4
10x dilute extracted ochratoxin	OTA	5.2
90:10 buffer:grape must no extraction	OTA	0
10x dilute 90:10 buffer:grape must no extraction	OTA	0

3.6 Conclusions

The LIANA turn-on fluorescent sensor was able to detect OTA with a visual LOD between 10 – 100 nM in a complex matrix on a simple, rapid, user-friendly and portable paper-based platform. Progress was made towards developing an analogous LIANA sensing platform for FB_1 (in solution) but unfortunately issues with QD aggregation and subsequent fluorescence quenching as well as aptamer-QD coupling efficiency stalled any major progress. In a fluorescent turn-on sensor, fluorescein-modified *$FB_1$39* was quenched by unmodified SWCNTs and fluorescence recovery was relatively linear between 100 – 750 nM FB_1. Acid-modified SWCNTs were less consistent and sensitive in a similar sensor design. Aptamer-labelled QDs were used in a fluorescent turn-on sensor using graphene oxide as a quencher for FB_1 detection; unfortunately results were inconsistent due to low efficiency in aptamer-QD coupling and QD aggregation. Lastly, *$FB_1$39*, *FB1_39t3*, *FB1_39t3-5*, and *A08* were tested for their capacity to bind naturally

contaminated samples (*Aspergillus* contaminated grapes) in a real sample matrix, demonstrating performance and selectivity against other similar compounds and matrix components. For the ochratoxin-contaminated samples, *A08* bound approximately 5% of the OTA from the extracted samples (diluted). For the fumonisin-contaminated samples, the highest binding recovery was noted for *FB139* and *FB1_39t3* binding FB_2 from the non-extracted diluted fumonisin extract. These results demonstrate the ability of these aptamers to selectively bind their targets in a complex matrix with a low degree of sample preparation. As the source of the low percent of fumonisin binding to the aptamer-modified beads could be from many sources (overloading binding capacity, matrix effects, low affinity of aptamers for non-FB_1 fumonisins) it would be useful to evaluate the binding of a spiked FB_1 sample into a matrix to determine the binding efficiency of each aptamer in a future study.

4.0 Contributions to knowledge and future studies

Mycotoxins are naturally-occurring fungal secondary metabolites that contaminate staple food crops around the world. The most dramatic human health and economic effects of mycotoxin contamination are in developing areas of the world, where there are limited resources allocated to monitoring and regulating mycotoxin levels to mitigate the health risks upon consumption. The use of aptamer-mediated molecular recognition in mycotoxin biosensors aligns well with the inherent advantages of aptamers: stability and long shelf life amenable to use in field, affinity and selectivity of binding to small molecule targets, cost-effective chemical synthesis and low variability in production.

In Chapter 2, aptamers for two important mycotoxins, FB_1 and OTA, were screened using a novel DNase I footprinting assay. This simple assay measures the in-solution binding affinity of aptamers to targets without requiring expensive equipment or reagents. The duplex structure of aptamers can also be mapped by DNase I digestion. This assay is generally applicable for aptamers for small molecule and protein targets, excluding previously minimized aptamers. It would be useful to analyze a well-characterized aptamer using the DNase I assay to align the derived structural information with NMR and X-ray crystallography data. Putative minimer sequences for *$FB_1$39* were identified that retained high affinity binding to FB_1 in solution and bound to a solid support. These minimers range between 38 – 78 nt in length. Future studies would be

valuable to further characterize the affinity of these aptamers for FB_1 to confirm the K_d and conformation with techniques such as SPR, CD, and ITC.

Chapter 3 examined various applications of mycotoxin aptamers in sensing applications. Ongoing challenges with aggregation and coupling efficiency of aptamers to carboxyl-QDs limited the success of FB_1 fluorescent aptasensors. A rapid and sensitive paper-based fluorescent test was developed for OTA detection. Using a simple hand-held UV light, OTA was detected with an LOD between 10 - 100 nM in a complex sample extract. This represents a promising application of aptamer-mediated recognition for mycotoxin detection on a transportable and accessible platform. Further work to develop an analogous test for FB_1 would be valuable. Additionally, the use of fluorescent semi-conductor QDs makes these tests amenable to multiplex mycotoxin detection. Other promising applications for aptamers include lateral flow tests, and replacing antibodies with aptamers in immunoaffinity columns used in conjunction with confirmatory testing methods. Although progress made in these fields for OTA detection, there is a wide gap to fill for FB_1 detection with similar or novel aptasensor technologies.

Appendix A: Additional fumonisins tested for in grape matrix

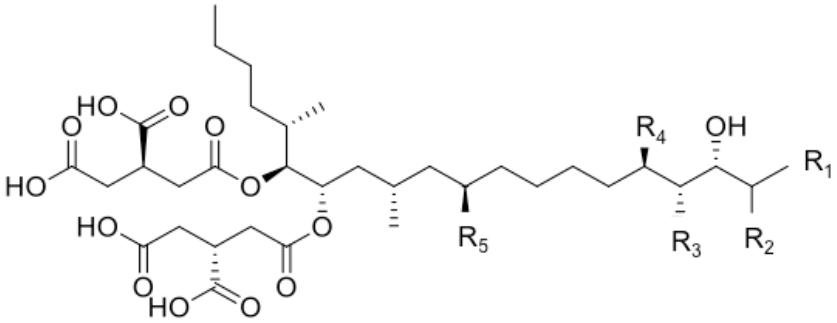

	R_1	R_2	R_3	R_4	R_5
FB_1	CH_3	NH2	H	OH	OH
FB_3	CH_3	NH2	H	H	OH
FA_1	CH_3	$NHCOCH_3$	H	OH	OH
FA_2	CH_3	$NHCOCH_3$	H	OH	H
FA_3	CH_3	$NHCOCH_3$	H	H	OH
FA_4	CH_3	$NHCOCH_3$	H	H	H
FC_1	H	H	H	OH	OH
FC_2	H	H	H	OH	H
FC_3	H	H	H	H	OH
FC_4	H	H	H	H	H
FPy_2	H	=O	H	OH	H
FPy_4	H	=O	H	H	H
FLa_2	H	OH	H	OH	H
FLa_4	H	OH	H	H	H

Figure A-1 Structures of fumonisins tested for in *A. welwitschiae* infected grapes

Table A-1 Dilute 'extracted' and 'direct' fumonisins from *A. welwitschiae* on grapes, showing the fractions (percent bound, control subtracted) of each compound bound to each of the FB_1 aptamers (*$FB_1$39*, *FB1_39t3*, and *FB1_39t3-5*), NP = no peak detected, *compound present in 'before' fraction but not in eluted fractions, **compound present in eluted fraction but not in 'before' fraction

Direct grape must samples					Extracted grape must samples				
		$FB_1$39	FB1_39t3	FB1_39t3-5			$FB_1$39	FB1_39t3	FB1_39t3-5
no dilut'n	FB_1	NP	NP	NP	5x dilute	FB_1	NP	NP	NP
	OH-FB_1	NP	NP	NP		OH-FB_1	NP	NP	NP
	FB_3	NP	NP	NP		FB_3	NP	NP	NP
	FA_1	NP	NP	NP		FA_1	NP	NP	NP
	FA_2	NP	NP	NP		FA_2	NP	NP	0.633
	FA_3	NP	NP	NP		FA_3*	NP	NP	NP
	FA_4	NP	NP	NP		FA_4*	NP	NP	NP
	FC_1	NP	NP	NP		FC_1	NP	NP	NP
	FC_2	NP	NP	NP		FC_2*	NP	NP	NP
	FC_3	NP	NP	NP		FC_3	NP	**	NP
	FC_4	NP	NP	NP		FC_4*	NP	NP	NP
	FLa_2	NP	NP	NP		FLa_2	NP	NP	NP
	Fla_4	NP	NP	NP		Fla_4	NP	NP	NP
	FPy_2*	NP	NP	NP		FPy_2	NP	NP	NP
	FPy_4	NP	NP	NP		FPy_4	NP	NP	NP
10x dilute	FB_1	NP	NP	NP	10x dilute	FB_1	NP	NP	NP
	OH-FB_1	NP	NP	NP		OH-FB_1	NP	NP	NP
	FB_3	NP	NP	NP		FB_3	NP	NP	NP
	FA_1	NP	NP	NP		FA_1	NP	NP	NP
	FA_2	NP	NP	NP		FA_2*	NP	NP	NP
	FA_3	NP	NP	NP		FA_3	NP	NP	NP
	FA_4	NP	NP	NP		FA_4*	NP	NP	NP
	FC_1	NP	NP	NP		FC_1	NP	NP	NP
	FC_2	NP	NP	NP		FC_2*	NP	NP	NP
	FC_3	NP	NP	NP		FC_3	NP	NP	**
	FC_4	NP	NP	NP		FC_4*	NP	NP	NP
	FLa_2	NP	NP	NP		FLa_2	NP	NP	NP
	Fla_4	NP	NP	NP		Fla_4	NP	NP	NP
	FPy_2	NP	NP	NP		FPy_2	NP	NP	NP
	FPy_4	NP	NP	NP		FPy_4	NP	NP	NP

*Compound present in "before" fraction but not eluted fractions
**Compound present in eluted fractions but not "before" fractions

References

[1] Pitt J.I., Wild C.P., Baan R.A., Gelderblom W.C.A., Miller J.D., Riley R.T., Wu, F. (2012) Improving public health through mycotoxin control, *IARC Agency for Research on Cancer, Lyon, France, IARC Scientific Publication No 158,* ISBN:978-832-2158-6.

[2] Haliburton J.C., Buck W.B. (1986) Equine leukoencophalomalacia: a historical review, *Diagnosis of Mycotoxicoses: Dordrecht Martinus Nijhoff Publishers* p75-80.

[3] Miller J.D., Schaafsma A.W., Bhatnagar D., Bondy G., Carbone L., Harris L.J., Harrison G., Munkvold G.P., Oswald L.P., Pestka J.J., Sharpe L., Sumarah M.W., Tittlemier S.A., Zhou T. (2013) Mycotoxins that affect the North American agri-food sector: state of the art and directions for the future, *World Mycotoxin Journal*, **1**:63-82.

[4] Rheeder J.P., Marasas W.F.O., Thiel P.G., Sydenham E.W., Shephard G.S., van Schalkwyk D.J. (1992) *Fusarium moniliforme* and fumonisins in corn in relation to human esophageal cancer in Transkei, *Postharvest Pathology and Mycotoxins,* **3**:353-357

[5] Suga H., Kitajima M., Nagumo R., Tsukiboshi T., Uegaki R., Nakajima T., Kushiro M., Nakagawa H., Shimizu M., Kageyama K., Hyakumachi M. (2014) A single nucleotide polymorphism in the translation elongation factor 1α gene correlates with the ability to produce fumonisin in Japanese *Fusarium fujikuroi*, *Fungal Biology*, **118**:402-412.

[6] Uegaki R., Tohona M., Yamamura K., Tsukiboshi T. (2014) Changes in the concentration of fumonisins in forage rice during the growing period, differences among cultivars and sites, and identification of the causal fungus, *J Ag Food Chem,* **62**:3356-3362.

[7] Miller J.D. (2001) Factors that affect the occurrence of fumonisin, *Env Health Perspec,* **109**:321-324.

[8] Miler J.D. (2008) Mycotoxins in small grains and maize: old problems, new challenges, *Food Addit Contam Part A Chem Anal Control Expo Risk Assess,* **25**:219-230.

[9] Knudsen P.B., Mogensen J.M., Larsen T.O., lsen K.F. (2011) Occurrence of fumonisins B_2 and B_4 in retail raisins, *J Agric Food Chem,* **59**:772-776.

[10] Somma S., Perrone G., Logrieco A.F. (2012) Diversity of black *Aspergilli* and mycotoxin risks in grape, wine and dried vine fruits, *Phytopatho Mediterranea,* **51**:131-147.

[11] Heperkan D., Karbancioglu Güler F., Oktay H.I. (2012) Mycoflora and natural occurrence of aflatoxin, cyclopiazonic acid, fumonisin and ochratoxin A in dried figs, *Food Addit Contam:Part A,* **29**:227-286.

[12] Moretti A., Ferracane L., Somma S., Ricci V., Mule G., Susca A., Ritieni A., Logrieco A.F. (2010) Identification, mycotoxin risk and pathogenicity of *Fusarium* species associated with fig endosepsis in Apulia, Italy, *Food Addit Contam: Part A*, **27**:718-728.

[13] Logrieco A., Ferracane R., Visconti A., Ritieni A. (2010) Natural occurrence of fumonisin B_2 in red wine from Italy, *Food Addit Contam: Part A,* **27**:1136-1141.

[14] Mogensen J.M., Frisvad J.C., Thrane U., Nielsen K.F. (2010) Production of fumonisin B_2 and B_4 by *Aspergillus niger* on grapes and raisins, *J Agric Food Chem,* **58**:954-958.

[15] Gelderblom W.C.A., Jaskiewicz K., Marasas W.F.O., Thiel P.G., Horak R.M., Vleggaar R., Kriek N.P.J. (1988) Fumonisins – Novel mycotoxins with cancer-promoting activity produced by *Fusarium moniliforme*, *Appl Environ Microbiol*, **54**:1806-1811.

[16] Bowers E., Hellmich R., Munkvold G. (2014) Comparison of fumonisin contamination using HPLC and ELISA methods in *Bt* and near-isogenic maize hybrids infested with European Corn Borer or Western Bean Cutworm, *J Agric Food Chem,* **62**:6463-6472.

[17] Shephard G.S., Thiel P.G., Sydenham E.W., Snijman P.W. (1995) Toxicokinetics of the mycotoxin fumonisin B_2 in rats, *Food Chem Toxicol,* **33**:591-595.

[18] Martinez-Larranaga M.R., Anadon A., Diaz M.J., Fernandez-Cruz M.L., Martinez M.A., Frejo M.T., Martinez M., Fernandez R., Anton R.M., Marales M.E., Tafur M. (1999) Toxicokinetics and oral bioavailability of fumonisin B_1, *Vet Hum Toxicol,* **41**:357-362.

[19] Riley, R.T., Torres O., Showker J.L., Zitomer N.C., Matute J., Voss K.A., Gelineau-van Waes, J., Maddox J.R., Gregory S.G., Ashley-Koch A.E. (2012) The kinetics of urinary fumonisin B_1 excretion in humans consuming maize-based diets, *Mol Nutr Food Res,* **56**:1445-1455.

[20] Schroeder J.J., Crane H.M., Xia J., Liotta D.C., Merrill Jr. A.H. (1994) Disruption of sphingolipid metabolism and stimulation of DNA synthesis by fumonisin B_1, *J Biol Chem,* **269**:3475-3481.

[21] Riley R.T., Wang, E., Schroeder J.J., Smith E.R., Plattner R.D., Abbas H., Yoo H.S., Merrill Jr. A.H. (1996) Evidence for disruption of sphingolipid metabolism as a contributing factor in the toxicity and carcinogenicity of fumonisins, *Natural Toxins,* **4**:3-15.

[22] Merrill Jr. A.H., Cameron Sullards M., Wang E., Voss K.A., Riley R.T. (2001) Sphingolipid metabolism: roles in signal transduction and disruption by fumonisins, *Env Health Perspec,* **109**:283-289.

[23] Marasas W.F.O., Riley R.T., Hendricks K.A., Stevens V.L., Sadler T.W., Gelineau-van Waes J., Missmer S.A., Cabrera J., Torres O., Gelderblom W.C.A., Allegood J., Martinez C., Maddox J., Miller J.D., Starr L., Cameron Sullards S., Victoria Roman A., Voss K.A., Wang E., Merrill Jr. A.H. (2004) Fumonisins disrupt sphingolipid metabolism, folate transport, and neural tube development in embryo culture and in vivo: a potential risk factor for human neural tube defects among populations consuming fumonisin-contaminated maize, *J Nutr,* **134**:711-716.

[24] Riley R.T., Enongene E., Voss K.A., Norred W.P., Meredith F.I., Sharma R.P., Spitsbergen J., Williams D.E., Carlson D.B., Merrill Jr. A.H. (2001) Sphingolipid perturbations as mechanisms for fumonisin carcinogenesis, *Env Health Perspec,* **109**:301-308.

[25] Voss K.A., Smith G.W., Haschek W.M. (2007) Fumonisins: toxicokinetics, mechanism of action and toxicity, *Animal Feed Science and Technology*, **137**:299-325.

[26] Wang E., Norred W.P., Bacon C.W., Riley R.T., Merrill Jr. A.H. (1991) Inhibition of sphingolipid biosynthesis by fumonisins, *J Biol Chem,* **266**:14486-14490.

[27] Riboni L., Viani P., Bassi R., Prinetii A., Tettamanti G. (1997) The role of sphingolipids in the process of signal transduction, *Prog Lipid Res,* **36**:153-195.

[28] Merrill Jr. A.H., Schmelz E.M., Dillehay D.L., Spiegel S., Shayman J.A., Schroder J.J., Riley R.T., Wang E. (1997) Sphingolipids, the enigmatic lipid class: biochemistry physiology and pathophysiology, *Toxicol Appl Pharmacol,* **142**:208-225.

[29] Delongchamp R.R., Young J.F. (2001) Tissue sphinganine as a biomarker of fumonisin-induced apoptosis, *Food Addit Contam,* **18**:225-261.

[30] Hahn, I., Nagl V., Schwartz-Zimmermann H.E., Varga E., Schwarz C., Slavik V., Reisinger N., Malachova A., Cirlini M., Generotti S., Dall'Asta C., Krska R., Moll W.D., Berthiller F. (2015) Effects of orally administered fumonisin B_1 (FB_1), partially hydrolysed FB_1, hydrolysed FB_1 and *N*-(1-deoxy-D-fructos-1-yl) FB_1 on the sphingolipid metabolism in rats, *Food and Chem Toxicol,* **76**:11-18.

[31] Harrer H., Humpf H.U., Voss K.A. (2015) In vivo formation of *N*-acyl-fumonisin B_1, *Mycotoxin Res,* **31**:33-40.

[32] Ross P.F., Ledet A.E., Owens D.L., Rice L.G., Nelson H.A., Osweiler G.D., Wilson T.M. (1993) Experimental equine leukoencephalomalacia, toxic hepatosis, and encephalopathy caused by corn naturally contaminated with fumonisins, *J Vet Diagn Invest,* **5**:69-74.

[33] Marasas W.F.O., Kellerman T.S., Gelderblom W.C.A., Coetzer J.A.W., Thiel P.G., van der Lugt J.J. (1988) Leukoencephalomalacia in a horse induced by fumonisin B_1 isolated from *Fusarium moniliforme*, *Onderstepoort J Vet Res,* **55**:197-203.

[34] Wilson T.M., Ross P.R., Owens D.L., Rice L.G., Green S.A., Jenkins S.I. (1992) Experimental reproduction of ELEM, *Mycopathologia,* **117**:115-120.

[35] Kellerman T.S., Marasas W.F., Thiel P.G., Gelderblom W.C., Cawood M., Coetzer J.A. (1990) Leukoencephalomalacia in two horses induced by oral dosing of fumonisin B_1, *Onderstepoort J Vet Res,* **57**:269-275.

[36] WHO. Fumonisin B_1 (Environmental Health Criteria 219) International programme on chemical safety. Geneva:WHO:2000

[37] Haschek W.M., Motelin G., Ness D.K., Horlin K.S., Hall W.F., Vesoden R.F. (1992) Characterization of fumonisin toxicity in orally and intravenously dosed swine, *Mycopathologia,* **117**:83-96.

[38] Smith G.W., Constable P.D., Tumbleson M.E., Rottinghaus G.E., Haschek W.M. (1999) Sequence of cardiovascular changes leading to pulmonary edema in swine fed culture material containing fumonisin, *Am J Vet Res,* **60**:1292-1300.

[39] Bondy G., Mehta R., Caldwell D., Coady L., Armstrong C., Savard M., Miller J.D., Chomyshyn E., Bronson R., Zitomer N., Riley R.T. (2012) Effects of long term exposure to the mycotoxin fumonisin B_1 in p53 heterozygous and p53 homozygous transgenic mice, *Food Chem Toxicol,* **50**:3604-3613.

[40] Hard G.C., Howard P.C., Kovatch R.M., Bucci T.J. (2001) Rat kidney pathology induced by chronic exposure to fumonisin B_1 includes rare variants of renal tubule tumor, *Toxicologic Pathology,* **29**:379-386.

[41] Howard P.C., Eppley R.M., Stack M.E., Warbritton A., Voss K.A., Lorentzen R.J., Kovach R.M., Bucci T.J. (2001) Fumonisin B_1 carcinogenicity in a two-year feeding study using F344 rats and $B6C3F_1$ mice, *Environ Health Perspec,* **109**:277-282.

[42] Lemmer E.R., Vessey C.J., Gelderblom W.C.A., Shephard E.G., Van Schalkwyk D.J., Van Wijk R.A., Marasas W.F.O., Kirsch R.E., Hall P.M. (2004) Fumonisin B_1-induced hepatocellular and cholangiocellular tumors in male Fischer 344 rats: potentiating effects of 2-acetylaminofluorene on oval cell proliferation and neoplastic development in a discontinued feeding study, *Carcinogenesis,* **25**:1257-1264.

[43] Riedel S., Abel S., Swanevelder S., Gelderblom W.C.A. (2015) Induction of an altered lipid phenotype by two cancer promoting treatments in rat liver, *Food Chem Toxicol,* **78**:96-104.

[44] NTP Technical report on the toxicology and carcinogenesis studies of fumonisin B_1 (Cas No. 116355-83-0) in F344 rats and B6C3F1 mice (feed studies). National Toxicology Program, Research Triangle Park, NC. NTP Technical Report 496. 2001.

[45] Farber E. (1990) Clonal adaptation during carcinogenesis, *Biochem Pharmacol,* **39**:1837-1846.

[46] IARC, International Agency for Research on Cancer (2002) Fumonisin B_1. In: Some traditional herbal medicines, some mycotoxins, naphthalene and styrene. In WHO IARC monographs on the evaluation of carcinogenic risks to humans, Vol 82 (p301-366) Lyon, France:IARC.

[47] Sydenham E.W., Thiel P.G., Marasas W.F.O., Shephard G.S., Van Schalkwyk D.J., Koch K.R. (1990) Natural occurrence of some *Fusarium* mycotoxins in corn from low and high esophageal cancer prevalence areas of the Transkei, South Africa, *J Agric Food Chem,* **38**:1900-1903.

[48] Rose E.F., McGlashan N.D. (1975) The spatial distribution of oesophageal carcinoma in the Transkei, South Africa, *Br J Cancer,* **31**:197-206.

[49] Hendricks K. (1999) Fumonisins and neural tube defects in South Texas, *Epidemiology,* **10**:198-200.

[50] Missmer S.A., Suarez L., Felkner M., Wang E., Merrill Jr.A.H., Rothman K.J., Hendricks K.A. (2006) Exposure to fumonisins and the occurrence of neural tube defects along the Texas-Mexico border, *Environ Health Perspec,* **114**:237-241.

[51] Sadler T.W., Merrill Jr.A.H., Stevens V.L., Sullards M.C., Wang E., Wang P. (2002) Prevention of fumonisin B_1-induced neural tube defects by folic acid, *Teratology,* **66**:167-176.

[52] Gelineau-van Waes J., Starr L., Maddox J., Aleman F., Voss K.A., Wilberding J., Riley R.T. (2005) Maternal fumonisin exposure and risk for neural tube defects: mechanisms in an *in vivo* mouse model, *Birth Defects Res (Part A),* **73**:487-497.

[53] Antonissen G., Martel A., Pasmans F., Ducatelle R., Verbrugghe E., Vandenbroucke V., Li S., Haesebrouck F., Immerseel F.V., Croubels S. (2014) The impact of *Fusarium* mycotoxins on human and animal host susceptibility to infection diseases, *Toxins,* **6**:430-452.

[54] Minervini F., Garbetta A., D'Antuno I., Cardinali A., Martino N.A., Debellis L., Visconti A. (2014) Toxic mechanisms induced by fumonisin B_1 mycotoxin on human intestinal cell line, *Arch Environ Contam Toxicol,* **67**:115-123.

[55] Wang S.K., Wang, T.T., Huang G.L., Shi R.F., Yang L.G., Sun G.J. (2014) Stimulation of the proliferation of human normal esophageal epithelial cells by fumonisin B_1 and its mechanism, *Experimental and Therapeutic Medicine,* **7**:55-60.

[56] Cabañes J., Bragualt M.R., Castella G. (2010) Ochratoxin A producing species in the genus *Penicillium*, *Toxins,* **2**:1111-1120.

[57] Sonjak S., Licen M., Frisvad J.C., Gunde-Cimerman N. (2011) Salting of dry-cured meat – A potential cause of contamination with the ochratoxin A-producing species *Penicillium nordicum*, *Food Microbiology,* **28**:1111-1116.

[58] Visagie C.M., Varga J., Houbraken J., Meijer M., Kocsube S., Yilmaz N., Fotedar R., Seifert K.A., Frisvad J.C., Samson R.A. (2014) Ochratoxin production and taxonomy of the yellow aspergilla (*Aspergillus* section *Circumdati*), *Stud Mycol,* **78**:1-61.

[59] Alborch L., Bragulat M.R., Abarca M.L., Cabanes F.J. (2011) Temperature and incubation time effects on growth and ochratoxin A production by *Aspergillus sclerotinoniger* and *Aspergillus lacticoffeatus* on culture media, *Lett Appl Microbiol,* **52**:208-212.

[60] Mally A. (2012) Ochratoxin A and mitotic disruption: mode of action analysis of renal tumor formation by ochratoxin A, *Toxicol Sci,* **127**:315-330.

[61] Zanic-Grubisic T., Zrinski R., Cepelak I., Petrik J., Radic B., Pepeljnjak S. (2000) Ochratoxin A-induced inhibition of phenylalanine hydroxylase and its reversal by phenylalanine, *Toxicol Appl Pharmacol,* **167**:132-139.

[62] el Khoury A., Atoui A. (2010) Ochratoxin A: General overview and actual molecular status, *Toxins,* **2**:461-493.

[63] Wagacha J.M., Muthomi J.W. (2008) Mycotoxin problem in Africa: Current status, implications to food safety and health and possible management strategies, *Int J Food Microbiol,* **124**:1-12.

[64] Cicoňová P., Laciaková A., Maté D. (2010) Prevention of ochratoxin A contamination of food and ochratoxin A detoxification by microorganisms – A review, *Czech J Food Sci,* **28**:465-474.

[65] IARC Monographs on the evaluation of carcinogenic risks to humans, Volume 56: Some naturally occurring substances: Some food items and constituents, heterocyclic aromatic amines and mycotoxins, IARC, Lyon France, 1993.

[66] Pfohl-Leszkowicz A., Manderville R.A. (2007) Ochratoxin A: An overview on toxicity and carcinogenicity in animals and humans, *Mol Nutr Food Res,* **51**:61-99.

[67] Joint FAO/WHO Expert Committee on Food Additives (JECFA) Safety evaluation of certain mycotoxins in food. In WHO (ed) Food Additives Series. (2001) **47**:103-279.

[68] Krska R., Schubert-Ullrich P., Molinelli A., Sulyok M., MacDonald S., Crews C. (2008) Mycotoxin analysis: An update, *Food Addit Contam: Part A,* **25**:152-163.

[69] Anklam E., Stroka J., Boenke A. (2002) Acceptance of analytical methods for implementation of EU legislation with a focus on mycotoxins, *Food Control*, **13**:173-183.

[70] von Holst C., Stroka J. (2014) Performance criteria for rapid screening methods to detect mycotoxins, *World Mycotoxin Journal,* **7**:439-447.

[71] Daško L., Rauová D., Belajová E. (2006) Comparison of the suitability of derivatisation agents in HPLC – fluorescence detection analysis of fumonisins, *J Food Nutr Res,* **45**:127-133.

[72] Berthiller F., Burdaspal P.A., Crews C., Iha M.H., Krska R., Lattanzio V.M.T., MacDonald S., Malone R.J., Maragos C., Solfrizzo M., Stroka J., Whitaker T.B. (2014) Developments in mycotoxin analysis: an update for 2012-2013, *World Mycotoxin Journal,* **7**:3-33.

[73] Hadj Ali W., Pichon V. (2014) Characterization of oligosorbents and application to the purification of ochratoxin A from wheat extracts, *Anal Bioanal Chem,* **406**:1233-1240.

[74] De Girolamo A., McKeague M., Miller J.D., DeRosa M.C., Visconti A. (2011) Determination of ochratoxin A in wheat after clean-up through a DNA aptamer-based solid phase extraction column, *Food Chemistry,* **127**:1378-1384.

[75] Maragos C.M. (2009) Recent advances in the development of novel materials for mycotoxin analysis, *Anal Bioanal Chem,* **395**:1205-1213.

[76] Gelderblom W.C.A., Marasas W.F.O. (2012) Controversies in fumonisin mycotoxicology and risk assessment, *Human and Experimental Toxicology,* **31**:215-235.

[77] Evaluations of the Joint FAO/WHO Expert Committee on Food Additives (JECFA) WHO Technical Report Series 966. (2001) JECFA Report 74: Fumonisins 4.2

[78] Shephard G.S., Kimanya M.E., Kpodo K.A., Gnonlonfin G.J.B., Gelderblom W.C.A. (2013) The risk management dilemma for fumonisin mycotoxins, *Food Control,* **34**:596-600.

[79] Kimanya M.E., De Meulenaer B., Van Camp J., Baert K., Kolsteren P. (2011) Strategies to reduce exposure of fumonisins from complementary foods in rural Tanzania, *Maternal and Child Nutrition,* **8**:503-511.

[80] Shephard G.S., Gelderblom W.C.A. (2014) Rapid testing and regulating for mycotoxin concerns: a perspective from developing countries, *World Mycotoxin Journal,* **7**:431-437.

[81] Russell R., Paterson M., Lima N. (2010) How will climate change affect mycotoxins in food? *Food Res Int,* **43**:1902-1914.

[82] Ellington A.D., Szostak J.W. (1990) *In vitro* selection of RNA molecules that bind specific ligands, *Nature,* **346**:818-822.

[83] Turek C., Gold L. (1990) Systematic evolution of ligands by exponential enrichment: RNA ligands to bacteriophage T4 DNA polymerase, *Science,* **249**:505-510.

[84] Robertson D.L., Joyce G.F. (1990) Selection *in vitro* of an RNA enzyme that specifically cleaves single-stranded DNA, *Nature*, **344**:467-468.

[85] Mayer G. (2009) The chemical biology of aptamers, *Angewandte Chemie Int Ed,* **48**:2672-2689.

[86] Mullis K.B. (1994) The polymerase chain reaction (Nobel lecture), *Angew Chem Int Ed Engl,* **33**:1209-1213.

[87] McBride J.J., Caruthers M.H. (1983) An investigation of several deoxynucleoside phosphoramidites useful for synthesizing deoxyoligonuclotides, *Tetrahedron Lett,* **24**:245-248.

[88] Wilson D.S., Szostak J.W. (1999) *In vitro* selection of functional nucleic acids, *Annu Rev Biochem,* **68**:611-647.

[89] McKeague M., DeRosa M.C. (2012) Challenges and opportunities for small molecule aptamer development, *J Nucleic Acids,* **2012**:748913.

[90] Wu J., Zhu Y., Xue F., Mei Z., Yao L., Wang X., Zheng L., Liu J., Liu G., Peng C., Chen W. (2014) Recent trends in SELEX technique and its application to food safety monitoring, *Microchim Acta,* **181**:479-491.

[91] Famulok M., Mayer G. (2011) Aptamer modules as sensors and detectors, *Acc Chem Res,* **44**:1349-1358.

[92] Mairal T., Özalp C.V., Sánchez P.L., Mir M., Katakis I., O'Sullivan C.K. (2008) Aptamers: molecular tools for analytical applications, *Anal Bioanal Chem,* **390**:989-1007.

[93] Ozer A., Pagano J.M., Lis J.T. (2014) New technologies provide quantum changes in the scale, speed and success of SELEX methods and aptamer characterization, *Mol Ther Nucleic Acids,* **3**:e183.

[94] Dong Y., Xu Y., Yong W., Chu X., Wang D. (2013) Aptamer and its potential applications for food safety, *Crit Rev Food Sci Nutrn,* **54**:1548-1561.

[95] Cruz-Toledo J., McKeague M., Zhang X., Giamberardino A., McConnell E., Francis T., DeRosa M.C., Dumontier M. (2012) Aptamer base: a collaborative knowledge base to describe aptamers and SELEX experiments, *Database,* **2012**:bas006.

[96] Luo X., McKeague M., Pitre S., Dumontier M., Green J., Golshani A., DeRosa M.C., Dehne F. (2010) Computational approaches toward the design of pools for the in vitro selection of complex aptamers, *RNA,* **16**:2252-2262.

[97] McKeague M., DeRosa M.C. (2014) Aptamers and SELEX: Tools for the development of transformative molecular recognition technology, *Aptamers and Synthetic Antibodies,* **1**:12-16.

[98] Famulok M., Mayer G., Blind M. (2000) Nucleic acid aptamers – from selection *in vitro* to applications *in vivo*, *Acc Chem Res,* **33**:591-599.

[99] Jayasena S.D. (1999) Aptamers: an emerging class of molecules that rival antibodies in diagnostics, *Clin Chem,* **45**:1628-1650.

[100] Steele F.R., Gold L. (2012) The sweet allure of XNA, *Nature Biotechnology,* **30**:624-625.

[101] Geiger A., Burgstaller P., von der Eltz H., Roeder A., Famulok M. (1996) RNA aptamers that bind L-arginine with sub-micromolar dissociation constants and high enantioselectivity, *Nucleic Acids Res,* **24**:1029-1036.

[102] Jenison R.D., Gill S.C., Pardi A., Polisky B. (1994) High-resolution molecular discrimination by RNA, *Science,* **263**:1425-1429.

[103] Levy-Nissenbaum E., Radovic-Moreno A.F., Wang A.Z., Langer R., Farokhzad O.C. (2008) Nanotechnology and aptamers: applications in drug delivery, *Trends in Biotechnology,* **26**:442-449.

[104] Chen A., Yang S. (2015) Replacing antibodies with aptamers in lateral flow immunoassay, *Biosens Bioelectron,* **71**:230-242.

[105] Schoukroun-Barnes L.R., White R.J. (2015) Rationally designing aptamer sequences with reduced affinity for controlled sensor performance, *Sensors,* **15**:7754-7767.

[106] Reuter J.S., Mathews D.H. (2010) RNAstructure: software for RNA secondary structure prediction and analysis, *BMC Bioinformatics,* **41**:471-474.

[107] Jiang L., Patel D.J. (1998) Solution structure of the tobramycin-RNA aptamer complex, *Nature Struct Biol,* **5**:769-774.

[108] Edwards A.L., Garst A.D., Batey R.T. (2009) Determining structures of RNA aptamers and riboswitches by X-Ray crystallography, *Methods in Molec Biol,* **535**:135-163.

[109] Lin P.H., Chen R.H., Lee C.H., Chang Y., Chen C.S., Chen W.Y. (2011) Studies of the binding mechanism between aptamers and thrombin by circular dichroism, surface plasmon resonance and isothermal titration calorimetry, *Colloids and Surfaces B: Biointerfaces,* **88**:552-558.

[110] Cruz-Aguado J.A., Penner G. (2008) Determination of ochratoxin A with a DNA aptamer, *J Agric Food Chem,* **56**:10456-10461.

[111] McKeague M., Velu R., Hill K., Bardoczy V., Mesaros T., DeRosa M.C. (2014) Selection and characterization of a novel DNA aptamer for label-free fluorescence biosensing of ochratoxin A, *Toxins,* **6**:2435-2452.

[112] Barthelmebs L., Jonca J., Hayat A., Prieto-Simon B., Marty J.L. (2011) Enzyme-linked aptamer assays (ELAAs) based on a competition format for a rapid and sensitive detection of ochratoxin A in wine, *Food Control,* **22**:737-743.

[113] McKeague M., Bradley C.R., DeGirolamo A., Visconti A., Miller J.D., DeRosa M.C. (2010) Screening and initial binding assessment of fumonisin B_1 aptamers, *Int J Mol Sci,* **11**:4864-4881.

[114] Chen X., Huang Y., Duan N., Wu S., Xia Y., Ma X., Zhu C., Jiang Y., Ding Z., Wang Z. (2014) Selection and characterization of single stranded DNA aptamers recognizing fumonisin B_1, *Microchim Acta,* **181**:1317-1324.

[115] Ma X., Wang W., Chen X., Xia Y., Wu S., Duan N., Wang Z. (2014) Selection, identification, and application of aflatoxin B_1 aptamer, *Eur Food Res Technol,* **238**:919-925.

[116] Malhotra S., Pandey A.K., Rajput Y.S., Sharma R. (2014) Selection of aptamers for aflatoxin M_1 and their characterization, *J Mol Recognit,* **27**:493-500.

[117] Ma X., Wang W., Chen X., Xia Y., Duan N., Wu S., Wang Z. (2015) Selection, characterization and application of aptamers targeted to Aflatoxin B_2, *Food Control,* **47**:545-551.

[118] Chen X., Huang Y., Duan N., Wu S., Ma X., Xia Y., Zhu C., Jiang Y., Wang Z. (2013) Selection and identification of ssDNA aptamers recognizing zearalenone, *Anal Bioanal Chem,* **405**:6573-6581.

[119] Chen X., Huang Y., Duan N., Wu S., Xia Y., Ma X., Zhu C., Jiang Y., Wang Z. (2014) Screening and identification of DNA aptamers against T-2 toxin assisted by graphene oxide, *J Ag Food Chem,* **62**:10368-10374.

[120] Song S., Wang L., Li J., Zhao J., Fan C. (2008) Aptamer-based biosensors, *Trends in Anal Chem,* **27**:108-117.

[121] Zhou J., Battig M.R., Wang Y. (2010) Aptamer-based molecular recognition for biosensor development, *Anal Bioanal Chem,* **398**:2471-2480.

[122] Han K., Liang Z., Zhou N. (2010) Design strategies for aptamer-based biosensors, *Sensors,* **10**:4541-4557.

[123] Zhu Z., Feng M., Zuo L., Zhu Z., Wang F., Chen L., Li J., Shan G., Luo S.Z. (2015) An aptamer based surface plasmon resonance biosensor for the detection of ochratoxin A in wine and peanut oil, *Biosens Bioelectron,* **65**:320-326.

[124] Osypova A., Thakar D., Dejeu J., Bonnet H., Van der Heyden A., Dubacheva G.V., Richter R.P., Defrancq E., Spinelli N., Coche-Guerente L., Labbe P. (2015) A sensor based on aptamer folding to detect low-molecular-weight analytes, *Anal Chem,* DOI:10.1021/acs.analchem.5b01736.

[125] Chen X., Bai X., Li H., Zhang B. (2015) Aptamer-based microcantilever array biosensor for detection of fumonisin B_1, *RSC Adv,* **5**:35448-35452.

[126] Chen X., Huang Y., Ma X., Jia F., Guo X., Wang Z. (2015) Impedimetric aptamer-based determination of the mold toxin fumonisin B_1, *Microchim Acta,* **182**:1709-1714.

[127] Yue S., Jie X., Wei L., Bin C., Dou W.D., Yi Y., QingXia L., JianLin L., TieSong Z. (2014) Simultaneous detection of ochratoxin A and fumonisin B_1 in cereal samples using an aptamer-photonic crystal encoded suspension array, *Anal Chem,* **86**:11797-11802.

[128] Chen J., Fang Z., Liu J., Zeng L. (2012) A simple and rapid biosensor for ochratoxin A based on a structure-switching signaling aptamer, *Food Control,* **25**:555-560.

[129] Wu S., Duan N., Ma X., Xia Y, Wang H., Wang Z., Zhang Q. (2012) Multiplexed fluorescence resonance energy transfer aptasensor between upconversion nanoparticles and graphene oxide for the simultaneous determination of mycotoxins, *Anal Chem,* **84**:6263-6270.

[130] Wei Y., Zhang J., Wang Z., Duan Y. (2015) Amplified fluorescent aptasensor through catalytic recycling for highly sensitive detection of ochratoxin A, *Biosens Bioelectron,* **65**:16-22.

[131] Kuang H., Chen W., Xu D., Xu L., Zhu Y., Liu L., Chu H., Peng C., Xu C., Zhu S. (2010) Fabricated aptamer-based electrochemical "signal off" sensor of ochratoxin A, *Biosens Bioelectron,* **26**:710-716.

[132] Yang C., Wang Y., Marty J.L., Yang X. (2011) Aptamer-based colorimetric biosensing of ochratoxin A using unmodified gold nanoparticles indicator, *Biosens Bioelectron,* **26**:2724-2727.

[133] Li F., Zhang H., Wang Z., Newbigging A.M., Reid M.S., Li X.F., Le X.C. (2014) Aptamers facilitate amplified detection of biomolecules, *Anal Chem,* doi:10.1021/ac5037236.

[134] Jiang L., Peng J., Yuan R., Chai Y., Yuan Y., Bai L., Wang Y. (2013) An aptasensing platform for simultaneous detection of multiple analytes based on the amplification of exonuclease-catalyzed target recycling and DNA concatemers, *Analyst,* **138**:4818-4822.

[135] Guo X., Wen F., Zheng N., Luo Q., Wang H., Wang H., Li S., Wang J. (2014) Development of an ultrasensitive aptasensor for the detection of aflatoxin B1, *Biosens Bioelectron,* **56**:340-344.

[136] Huang J., Chen Y., Yang L., Zhu Z., Zhu G., Yang X., Wang K., Tan W. (2011) Amplified detection of cocaine based on strand-displacement polymerization and fluorescence resonance energy transfer, *Biosens Bioelectron,* **28**: 450-453.

[137] Hayat A., Yang C., Rhouati A., Marty J.L. (2013) Recent advances and achievements in nanomaterial-based, and structure switchable aptasensing platforms for ochratoxin A detection, *Sensors,* **13**:15187-15208.

[138] Nutiu R., Li Y. (2004) Structure-switching signaling aptamers: transducing molecular recognition into fluorescence signaling. *Chem Eur J,* **10**:1868-1876.

[139] Li N., Ho C.M. (2008) Aptamer-based optical probes with separated molecular recognition and signal transduction modules, *J Am Chem Soc,* **130**:2380-2381.

[140] Nie J., Deng Y., Deng Q.P., Zhang D.W., Zhou Y.L., Zhang X.X. (2013) A self-assemble aptamer fragment/target complex based high-throughput colorimetric aptasensor using enzyme linked aptamer assay, *Talanta,* **106**:309-314.

[141] Baldrich E., Restrepo A., O'Sullivan C.K. (2004) Aptasensor development: elucidation of critical parameters for optimal aptamer performance, *Anal Chem,* **76**:7053-7063.

[142] Li S., Chen D., Zhou Q., Wang W., Gao L., Jiang J., Liang H., Liu Y., Liang G., Cui H. (2014) A general chemiluminescence strategy for measuring aptamer-target binding and target concentration, *Anal Chem,* doi.org/10.1021/ac501061c

[143] Sato K., Hosokawa K., Maeda M. (2007) Colorimetric biosensors based on DNA-nanoparticle conjugates, *Analytical Sciences,* **23**:17-20.

[144] Liu J., Lu Y. (2006) Fast colorimetric sensing of adenosine and cocaine based on a general sensor design involving aptamers and nanoparticles, *Angew Chem Int Ed,* **45**:90-94.

[145] Liu J., Lu Y. (2006) Preparation of aptamer-linked gold nanoparticle purple aggregates for colorimetric sensing of analytes, *Nature Protocols,* **1**:246-252.

[146] Lee J., Kim J.H., Lee S.H., Kim J.Y., Mah S.J., Gu M.B. (2013) In-situ on-fabric one-touch colorimetric detection using aptamer-conjugated gold nanoparticles, *BioChip J,* **7**:180-187.

[147] Peng Y., Li L., Mu X., Guo L. (2013) Aptamer-gold nanoparticle-based colorimetric assay for the sensitive detection of thrombin, *Sensors and Actuators B: Chemical,* **177**:818-825.

[148] Gopinath S.C.B., Lakshmipriya T., Awazu K. (2014) Colorimetric detection of controlled assembly and disassembly of aptamers on unmodified gold nanoparticles, *Biosens Bioelectron,* **51**:115-123.

[149] Smith J.E., Griffin D.K., Leny J.K., Hagen J.A., Chavez J.L., Kelley-Loughnane N. (2014) Colorimetric detection with aptamer-gold nanoparticle conjugates coupled to an android-based color analysis application for use in the field, *Talanta,* **121**:247-255.

[150] Wang L., Ma W., Chen W., Liu L., Ma W., Zhu Y., Xu L. Huang H., Xu C. (2011) An aptamer-based chromatographic strip assay for sensitive toxin semi-quantitative detection, *Biosens Bioelectron,* **26**:3059-3062.

[151] Shim W.B., Kim M.J., Mun H., Kim M.G. (2014) An aptamer-based dipstick assay for the rapid and simple detection of aflatoxin B_1, *Biosens Bioelectron,* **62**:288-294.

[152] Wang Y., Gao D., Zhang P., Gong P., Chen C., Gao G., Cai L. (2013) A near infared fluorescence resonance energy transfer based aptamer biosensor for insulin detection in human plasma, *Chem Commun,* **50**:811

[153] Deng W., Goldys E.M. (2014) Chemical sensing with nanoparticles as optical reporters: from noble metal nanoparticles to quantum dots and upconverting nanoparticles, *Analyst,* DOI: 10.1039/c4an01272k.

[154] Pons T., Medintz I.L., Sapsford K.E., Higashiya S., Grimes A.F., English D.S., Mattoussi H. (2007) On the quenching of semiconductor quantum dot photoluminescence by proximal gold nanoparticles, *Nano Letters,* **7**:3157-3164.

[155] Kim Y.S., Jurng J. (2011) Gold nanoparticle-based homogenous fluorescent aptasensor for multiplex detection, *Analyst,* **136**:3720-3724.

[156] Liu J., Lee J.H., Lu Y. (2007) Quantum dot encoding of aptamer-linked nanostructures for one-pot simultaneous detection of multiple analytes, *Anal Chem,* **79**:4120-4125.

[157] Wang C., Qian J., Wang K., Wang K., Liu Q., Dong X., Wang C., Huang X. (2015) Magnetic-fluorescent-targeting multifunctional aptasensor for highly sensitive and one-step rapid detection of ochratoxin A, *Biosens Bioelectron,* **68**:783-790.

[158] Liu J., Lee J.H., Lu Y. (2007) Quantum dot encoding of aptamer-linked nanostructures for one-pot simultaneous detection of multiple analytes, *Anal Chem,* **79**:4120-4125.

[159] Ueno Y., Furukawa K., Matsuo K., Inoue S., Hayashi K., Hibino H. (2013) Molecular design for enhanced sensitivity of a FRET aptasensor built on the graphene oxide surface, *Chem Commun,* **49**:10346-10348.

[160] Wu S., Duan N., Li X., Tan G., Ma X., Xia Y., Wang Z., Wang H. (2013) Homogenous detection of fumonisin B_1 with a molecular beacon based on fluorescence resonance energy transfer between $NaYF_4$:Yb, Ho upconversion nanoparticles and gold nanoparticles, *Talanta,* **116**:611-618.

[161] Vidal J.C., Bonel L., Ezquerra A., Hernandez S., Bertolin J.R., Cubel C., Castillo J.R. (2013) Electrochemical affinity biosensors for detection of mycotoxins: a review, *Biosens Bioelectron,* **49**:146-158.

[162] Yang M., Jiang B., Xie J., Xiang Y., Yuan R., Chai Y. (2014) Electrochemiluminescence recovery-based aptasensor for sensitive ochratoxin A detection via exonuclease-catalyzed target recycling amplification, *Talanta,* **125**:45-50.

[163] Wang R., Xiang Y., Zhou X., Liu L. Shi H. (2015) A reusable aptamer-based evanescent wave all-fiber biosensor for highly sensitive detection of ochratoxin A, *Biosens Bioelectron,* **66**:11-18.

[164] Wang L., Ma W., Chen W., Liu L., Ma W., Zhu Y., Xu L., Kuang H., Xu C. (2011) An aptamer-based chromatographic strip assay for sensitive toxin semi-quantitative detection, *Biosens Bioelectron,* **26**:3059-3062.

[165] Wang L., Chen W., Ma W., Liu L., Ma W., Zhao Y., Zhu Y., Xu L., Kuang H., Xu C. (2011) Fluorescent strip sensor for rapid determination of toxins, *Chem Commun,* **47**:1574-1576.

[166] Lv Z., Chen A., Liu J., Guan Z., Zhou Y., Xu S., Yang S., Li C. (2014) A simple and sensitive approach for ochratoxin A detection using a label-free fluorescent aptasensor, *PLoS ONE,* **9**:eB5968.

[167] Miyachi Y., Ogino C., Kondo . (2014) Structural evaluation of the DNA aptamer for ATP DH25.42 by AFM, *Nucleosides, Nucleotides and Nucleic Acids,* **33**:31-39.

[168] Lin P.H., Chen R.H., Lee C.H., Chang Y., Chen C.S., Chen W.Y. (2011) Studies of the binding mechanism between aptamers and thrombin by circular dichroism, surface plasmon resonance and isothermal titration calorimetry, *Colloids and Surfaces B: Biointerfaces,* **88**:552-558.

[169] Reinstein O., Yoo M., Han C., Palmo T., Beckham S.A., Wilce M.C.J., Johnson P.E. (2013) Quinine binding by the cocaine-binding aptamer. Thermodynamic and hydrodynamic analysis of high-affinity binding of an off-target ligand, *Biochemistry,* **52**:8652-8662.

[170] Ding Y., Zhang X., Tham K.W., Qin P.Z. (2014) Experimental mapping of DNA duplex shape enabled by global lineshape analyses of a nucleotide-independent nitroxide probe, *Nucleic Acids Research,* **42**:e140.

[171] Zhou J., Battig M.R., Wang Y. (2010) Aptamer-based molecular recognition for biosensor development, *Anal Bioanal Chem,* **398**:2471-2480.

[172] Katilius E., Flores C., Woodbury N.W. (2007) Exploring the sequence space of a DNA aptamer using microarrays, *Nucleic Acids Research,* **35**:7626-7635.

[173] Kwon Y.S., Raston N.H.A., Gu M.B. (2014) An ultra-sensitive colorimetric detection of tetracyclines using the shortest aptamer with highly enhanced affinity, *Chem Commun,* **50**:40-42.

[174] Tseng C.Y., Ashrafuzzaman M., Mane J.Y., Kapty J., Mercer J.R., Tuszynski J.A. (2011) Entropic fragment-based approach to aptamer design, *Chem Biol Drug Des,* **78**:1-13.

[175] Ruigrok V.J.B., Levisson M., Hekelaar J., Smidt H., Dijkstra B.W., van der Oost J. (2012) Characterization of aptamer-protein complexes by X-ray crystallography and alternative approaches, *Int J Mol Sci,* **13**:10537-10552.

[176] McGrath B.M., Walsh G. (2005) Directory of therapeutic enzymes, *CRG Press,* 2005, ISBN 978-0-8493-2714-8.

[177] Connaghan-Jones K.D., Moody A.D., Bain D.L. (2008) Quantitative DNase footprint titration: a tool for analyzing the energetics of protein-DNA interaction, *Nat Protoc,* **3**:900-914.

[178] Brenowitz M., Senear D.F., Kingston R.E. (1989) DNase I footprint analysis of protein-DNA binding, *Current Protocols in Molecular Biology,* 12.4.1-12.4.16.

[179] Tullius T.D. (1989) Physical studies of protein-DNA complex by footprinting, *Annu Rev Biophys Biophys Chem,* **18**:213-237.

[180] Zianni M., Tessanne K., Merighi M., Laguana R., Tabita F.R. (2006) Identification of the DNA bases of a DNase I footprint by the use of dye primer sequencing on an automated capillary DNA analysis instrument, *J of Biomolecular Techniques,* **17**:103-113.

[181] Wongphatcharachai M., Wang P., Enomoto S., Webby R.J., Gramer M.R., Amonsin A., Sreevatsan S. (2012) Neutralizing DNA aptamers against swine influenza H3N2 viruses, *J Clinical Microbiology,* **51**:46-54.

[182] Walters R.D., McSwiggen D.T., Goodrich J.A., Kugel J.F. (2014) Selection and characterization of a DNA aptamer that can discriminate between cJun/cJun and cJun/cFos, *PLoS ONE,* **9**:e101015.

[183] Joshi R., Janagama H., Dwivedi H.P., Senthil Kumar T.M.A., Jaykus L.A., Schefers J., Sreevatsan S. (2009) Selection, characterization, and application of DNA aptamers for the capture and detection of *Salmonella enterica* serovars, *Molecular and Cellular Probes,* **23**:20-28.

[184] White R.J., Rowe A.A., Plaxco K.W. (2010) Re-engineering aptamers to support reagentless, self-reporting electrochemical sensors, *Analyst,* **135**:589-594.

[185] Burgstaller P., Kochoyan M., Famulok M. (1995) Structural probing and damage selection of citrulline- and arginine-specific RNA aptamers identify base positions required for binding, *Nucleic Acids Research,* **23**:4769-4776.

[186] McKeague M., De Girolamo A., Valenzano S., Pascale M., Ruscito A., Velu R., Frost N.R., Hill K., Smith M., McConnell E.M., DeRosa M.C. (2015) Comprehensive analytical comparison of strategies used for small molecule aptamer evaluation, *Anal Chem,* DOI:10.1021/acs.analchem5b02102.

[187] Michalet X. (2005) Quantum dots for live cells, in vivo imaging, and diagnostics, *Science,* **307**:538-544.

[188] Chiu T.C., Huang C.C. (2009) Aptamer-functionalized nano-biosensors, *Sensors,* **9**:10356-10388.

[189] Clapp A.R., Medintz I.L., Uyeda H.T., Fisher B.R., Goldman E.R., Bawendi M.G., Mattoussi H. (2005) Quantum dot-based multiplexed fluorescence resonance energy transfer, *J Am Chem Soc,* **127**:18212-18221.

[190] Noh M., Kim T., Lee H., Kim C.K., Joo S.W., Lee K. (2010) Fluorescence quenching caused by aggregation of water-soluble CdSe quantum dots, *Colloids and Surfaces A: Physiochemical and Engineering Aspects,* **359**:39-44.

[191] Kalwarczyk E., Ziebacz N., Kalwarczy, T., Holyst R., Fialkowski M. (2013) A "wrap-and-wrest" mechanism of fluorescence quenching of CdSe/ZnS quantum dots by surfactant molecules, *Nanoscale,* **5**:9908-9916.

[192] Caswell K.K., Wilson J.N., Bunz U.H.F., Murphy C.J. (2003) Preferential end-to-end assembly of gold nanorods by biotin-streptavidin connectors, *J Am Chem Soc Comm,* **125**:13814-13915.

[193] Iijima S. (1991) Helical microtubes of graphite carbon, *Nature,* **354**:56-58.

[194] Belin T., Epron F. (2005) Characterization methods of carbon nanotubes: a revew, *Materials Science and Engineering: B,* **119**:105-118.

[195] Kim S.W., Kim T., Kim Y.S., Choi H.S., Lim H.J., Yang S.J., Park C.R. (2012) Surface modifications for the effective dispersion of carbon nanotubes in solvents and polymers, *Carbon,* **50**:3-33.

[196] Jeong S.H., Kim K.K., Jeong S.J., An K.H., Lee S.H., Lee Y.H. (2007) Optical absorption spectroscopy for determining carbon nanotube concentration in solution, *Synthetic Metals,* **157**:570-574.

[197] Park J.S., Goo N.I., Kim D.E. (2014) Mechanism of DNA adsorption and desorption on graphene oxide, *Langmuir,* **30**:12587-12595.

[198] Wu M., Kempaiah R., Huang P.J., Maheshwari V., Liu J. (2011) Adsorption and desorption of DNA on graphene oxide studied by fluorescently labeled oligonucleotides, *Langmuir,* **27**:2731-2738.

[199] Kong L., Xu J., Xu Y., Xiang Y., Yuan R., Chai Y. (2013) A universal and label-free aptasensor for fluorescent detection of ATP and thrombin based on SYBR Green I dye, *Biosens Bioelectron,* **42**:193-197.

[200] Sarpong K., Datta B. (2012) Nucleic-acid-binding chromphores as efficient indicators of aptamer-target interactions, *J Nucleic Acids,* **2012**:1-7

[201] Pelton R. (2009) Bioactive paper provides a low-cost platform for diagnostics, *Trends in Analytical Chemistry,* **28**:925-945.

[202] Parolo C., Merkoci A. (2013) Paper-based nanobiosensors for diagnostics, *Chem Soc Rev,* **42**:450-457.

[203] Xu H., Mao X., Zeng Q., Wang S., Kawde A.N., Liu G. (2009) Aptamer-functionalized gold nanoparticles as probes in a dry-reagent strip biosensor for protein analysis, *Anal Chem,* **81**:669-675.

[204] Guo Z., Duan J., Yang F., Li M., Hao T., Wang S., Wei D. (2012) A test strip platform based on DNA-functionalized gold nanoparticles for on-site detection of mercury (II) ions, *Talanta*, **93**: 49-54.

[205] Zhu W.J., Feng D.Q., Chen M., Chen Z.D., Zhu R., Fang H.L., Wang W. (2014) Bienzyme colorimetric detection of glucose with self-calibration based on tree-shaped paper strip, *Sensors and Actuators B: Chemical,* **190**:414-418.

[206] He M., Liu Z. (2013) Paper-based microfluidic device with upconversion fluorescence assay, *Anal Chem,* **85**:11691-11694.

[207] Carrasquilla C., Little J.R.L., Li Y., Brennan J.D. (2015) Patterned paper sensors printed with long-chain DNA aptamers, *Chem Eur J,* **21**:7369-7373.

[208] Zhao W., Ali M.M., Aguirre S.D., Brook M.A., Li Y. (2008) Paper-based bioassays using gold nanoparticles colorimetric probes, *Anal Chem,* **80**:8431-8437.

[209] Smiley S., DeRosa M., Blais B. (2013) Immobilization of DNA aptamers on polyester cloth for antigen detection by dot blot immunoenzymatic assay (Aptablot), *J Nucleic Acids,* **2013**:936542.

[210] Hu J., Wang S., Wang L., Li F., Pingguan-Murphy B., Lu T.J., Xu F. (2014) Advances in paper-based point-of-care diagnostics, *Biosens Bioelectron,* **54**:585-597.

[211] Liu J., Yang X., Wang K., He X., Wang Q., Huang J., Liu Y. (2012) Aggregation control of quantum dots through ion-mediated hydrogen bonding shielding, *ACS Nano,* **6**:4973-4983.